AD NUMBER

AD876681

LIMITATION CHANGES

TO:

Approved for public release; distribution is unlimited.

FROM:

Distribution authorized to U.S. Gov't. agencies and their contractors; Critical Technology; JUL 1970. Other requests shall be referred to Air Force Technical Applications Center, VSC, Alexandria, VA 22313. This document contains export-controlled technical data.

AUTHORITY

teleddyne geotech ltr via AFTAC, 1 may 1972

ESTIMATION OF P-WAVES USING VERTICAL AND SMALL APERTURE HORIZONTAL ARRAYS

15 July 1970

Prepared For

AIR FORCE TECHNICAL APPLICATIONS CENTER
Washington, D. C.

By

R. L. Sax

SEISMIC DATA LABORATORY

Under

Project VELA UNIFORM

Sponsored By

ADVANCED RESEARCH PROJECTS AGENCY
Nuclear Monitoring Research Office
ARPA Order No. 624

DISCLAIMER NOTICE

THIS DOCUMENT IS THE BEST QUALITY AVAILABLE.

COPY FURNISHED CONTAINED A SIGNIFICANT NUMBER OF PAGES WHICH DO NOT REPRODUCE LEGIBLY.

ESTIMATION OF P-WAVES USING VERTICAL AND SMALL APERTURE HORIZONTAL ARRAYS

SEISMIC DATA LABORATORY REPORT NO. 257

AFTAC Project No.:	VELA T/0706
Project Title:	Seismic Data Laboratory
ARPA Order No.:	624
ARPA Program Code No.:	9F10
Name of Contractor:	TELEDYNE GEOTECH
Contract No.:	F33657-70-C-0941
Date of Contract:	01 April 1970
Amount of Contract:	$ 1,785,000
Contract Expiration Date:	30 June 1971
Project Manager:	Royal A. Hartenberger (703) 836-7647

P. O. Box 334, Alexandria, Virginia

This research was supported by the Advanced Research Projects Agency, Nuclear Monitoring Research Office, under Project VELA-UNIFORM and accomplished under technical direction of the Air Force Technical Applications Center under Contract F33657-70-C-0941.

ABSTRACT

In estimating signals as P-waves, without regard to distinguishing the P-waves in ambient noise from those which are added by a teleseismic signal, the comparative performance of a thirteen element small aperture horizontal array and a seven element vertical array favors the vertical array. Analysis of the variance of the residual noise under the estimate of signal on the vertical array results in a signal estimation error which is 31 db down on the vertical array estimate of signal, and 15 db down on the horizontal array. Some preliminary indications, using the estimate of signal on the horizontal array to compute residuals on the horizontal array and using estimates of signal on the vertical array to compute residuals on the vertical array, are 31 db on the vertical array and 23 db on the horizontal array. Most of this difference in the two arrays is in the low frequency noise (less than 0.8 Hz) as band pass filtering tends to remove the difference in estimation error between the two arrays.

From the point of view of using the arrays to remove ambient noise, the results of a single P-wave signal estimation favors the horizontal array over the vertical array, 4.1 db to 1.8 db. This results because the ambient noise at this site can be characterized as a single dominant P-wave plus uncorrelated noise. As a horizontal array element is displaced from a reference element, the relative amount of uncorrelated noise increases much more rapidly than on a vertical array. This suggests a Markovian P-wave noise model for quiet sites such as the one considered here. Thus small horizontal arrays can be expected to contain substantially more uncorrelated noise despite the much larger stepout aperture of the vertical array.

The processor used here is iterative and allows for amplitude anomalies in the teleseismic P-wave model and allows for variable uncorrelated noise under each channel. Both the amount of uncorrelated noise and the amplitude anomalies differ significantly for events from different regions. It is conceivable that a processor can be designed which distinguishes the ambient P-wave model from the teleseismic P-wave model with amplitude anomalies. Such a processor would involve a double P-wave estimation with the two P-wave modes distinguishable by their amplitude anomalies. This contrasts with the single P-wave estimation considered in this report.

TABLE OF CONTENTS

LIST OF TABLES

INTRODUCTION

The purpose of this study is to develop an advanced signal estimation technique and to use it to make a comparative evaluation of a vertical array and a small aperture horizontal array centered over the vertical array. Such a technique should reduce the noise level, and lead to more accurate measurements of P-waves for detection and discrimination.

The methods used basically follow those used by Dean (1966) and Shumway and Dean (1968). The particular method applied here is the single P-wave signal estimation. Our signal models are more general in that the amplitude of both the incident and reflected plane waves can vary from sensor to sensor to account for amplitude anomalies. Time anomalies were not accounted for in our model, but perhaps should be accounted for in advanced models.

Shumway and Husted (1970) carried out a signal estimation and detection procedure based on the assumption that signal estimation errors have common statistical properties on each channel. In our estimation procedure, the variance of the noise on each channel is a quantity to be estimated. An iterative procedure is used to estimate the signal gain due to amplitude anomalies and to estimate the variance of the residual noise on each channel.

Analysis of variance from a prescribed signal model was used by Booker (1965) as a means of measuring array performance. In this analysis, the estimation error was computed in a similar fashion over a time window starting at the expected signal arrival time.

Shumway and Husted (1970) extended the analysis of variance to frequency dependent signal and noise by using power spectral densities.

Spatial correlation measurements of ambient noise were used as a basis for designing multi-channel filter estimates of teleseismic P-waves, using small aperture horizontal arrays and vertical arrays, by Backus et al (1964) and Rodin (1965). Some apparent reduction of noise occurring before signals was obtained. Since only modest gains were shown, on the order of 1 db over beamed sums, the present study does not use these techniques and is limited to simple weighted beaming. Weighted beaming is optimum under the assumption that the errors on each channel are independent with different variances. Another interesting application uses multi-channel correlation measurements of ambient noise to detect the first motion of signals by plotting the noise estimation error wnich should be large at the onset of an event. This has been illustrated for small aperture horizontal arrays by Claerbout (1964) and for vertical arrays by Douze and Mack (1970).

Time varying filters were applied to the estimation of signals on small aperture horizontal arrays with some modest improvement over time invariant filters by Lintz (1969). Sax and Hawkins (1966) used time varying multiplicative filters to detect weak signals using a vertical array. This method showed some increased detection over band pass filtering.

Broding et al (1964) made an application for the detection of P-waves of three dimensional arrays utilizing five abandoned oil wells. In our configuration one deepwell array was used approximately 2 1/2 times deeper than theirs, and with

six seismometers instead of three.

Broding et al, obtained $\sqrt{n}$ reduction in ambient noise by simple beaming. They indicated however that their ambient noise was a dominant fundamental mode Rayleigh wave. In the present case, with ambient P-waves, such a reduction cannot be anticipated. Broding's result, however, suggests that the present technique should be applied to a site where fundamental Rayleigh modes are significant.

PROCEDURES

The short-period data used in this study were recorded by vertical component sensors operating in a deep well and in a surface array centered over the vertical array. The vertical array contains six elements spaced at nearly equal intervals over 2.9 km; the horizontal array has a diameter of about 3.5 km and contains 13 sensors. On the vertical array teleseismic P-waves are distinguishable on f-k spectra at frequencies greater than 0.6 Hz. By scaling these results, the horizontal array can distinguish between two uncorrelated teleseismic P-waves propagating from opposite directions at frequencies greater than 3.0 Hz, and can distinguish opposite traveling fundamental mode Rayleigh waves at frequencies greater than 0.5 Hz.

The gradient of propagation slowness at the earth's surface is typically -- .0069 sec/km^2, with downward sense taken positive. The propagation slowness at the earth's surface is taken as 0.204 sec/km, which is a typical value for limestone, metamorphics, or granite. Taking, s_o, as the slowness at the surface and, a, as the gradient of slowness with depth, the slowness can be obtained as a function of depth:

$$s = s_o + az$$

The ray parameter, p, for teleseismic P-waves, depends on the distance between source and receiver, and is given by Richter (1958) for teleseimsic P-waves. Given p, s_o, a, and the coordinates of the array, the components of stepout due to displacement from the origin are as follows:

$$T_x = -px \sin\theta \quad T_y = -py \cos\theta$$
$$T_z = z\left[(s_o + az)^2 - p^2\right]^{\frac{1}{2}}. \tag{1}$$

The angle, θ, is the back azimuth of the event measured clockwise from North. The total stepout associated with each horizontally displaced sensor is

$$T = T_x + T_y. \tag{1a}$$

The uphole time associated with each vertical array sensor is T_z.

The model used to represent signals propagating across the array neglects most of the complications arising from the heterogeneity of the earth except to the extent that such effects are lumped into amplitude anomalies. The model neglects all conversions, and is as follows:

Horizontal Array:

$$U(t,x,y,o) = C(x,y,o)\, h(t-T_x-T_y) \tag{2a}$$

Vertical Array:

$$U(t,o,o,z) = C(o,o,z)\left[h(t-T_z) + R(z)\, h(T-T_z)\right] \tag{2b}$$

General Array:

$$U(t,x,y,z) = C(x,y,z)\left[h(t-T_x-T_y+T_z) + R(x,y,z)h(t-T_x-T_t-T_z)\right] \tag{2c}$$

No a-priori assumptions are made about the amplitude anomalies $C(x,y,z)$ or about the apparent change in the nominal half-space reflection coefficient, R, due either to gradients in propagation slowness or to inadequacies in the model.

A summary outline of the analysis procedure is as follows:

1. The horizontal (surface) array traces are aligned according to the expected arrival time of an event. The result is shown in the horizontal array sensor traces, Appendix 1.

2. The vertical array traces are match filtered with the operator $1/2\ [\delta(t-T_j) + \delta(t+T_j)]$ which assumes a unit reflection coefficient. They are naturally aligned on the raw data traces so that the principal pulses in the output are vertically above one another. The result is shown in the vertical array sensor traces, Appendix 1.

3. The horizontal array traces are then summed with equal weights. The result is trace H in Appendix 1.

4. The vertical array traces are summed and the result is operated on by the process described by Shumway and Dean (1968) to remove side-lobes. The result is trace V in Appendix 1.

5. Both the horizontal and vertical array data are beamed with their appropriate operators as in (3) and (4) above. The result is trace H+V in Appendix 1.

6. Trace V in Appendix 1 is taken as a preliminary estimate of the true signal. The gain coefficient between it and each of the horizontal array traces is estimated by least-squares. The results, properly gained are plotted in Appendix 2.

7. With the new gain coefficients the surface array is re-beamed, and the result is found in trace H in Appendix 2.

8. Each channel recorded in the vertical array is hypothesized to consist of a direct wave of the form of Trace V in Appendix 1, plus a reflected wave of the same form delayed by a known time. Each wave has an arbitrary incident and reflected amplitude which is determined by fitting the model to the original data trace using least-squares.

9. Trace V of Appendix 1 is delayed and subtracted from the raw data traces according to the values determined in (8) above. The results are plotted as the vertical traces in Appendix 2.

10. The vertical array traces in Appendix 2 are summed. The result is trace V in Appendix 2.

11. Both the horizontal and vertical array traces are beamed with their appropriate operators as in (6) and (9) above. The result is trace H+V in Appendix 2.

12. Trace V in Appendix 2 was then subtracted with the proper delay and gain from each raw trace in Appendix 2 of the horizontal and vertical arrays. The residual is plotted on the horizontal array traces in Appendix 3.

13. The raw horizontal array data traces are then beamed, weighted both by the gains and by the inverse mean square residual noise under the region being beamed. The result is trace H in Appendix 3.

14. Similarly, the vertical traces shown in Appendix 2 are beamed with weights obtained from the appropriate gains and the inverse residual noise. The result is trace V in Appendix 3.

15. Both the horizontal and vertical array data are beamed with their appropriate operators as in (14) and (15) above. The result is trace H+V in Appendix 3.

It should be strongly emphasized that anomalous time delays across the array can severely influence the residual noise figure; no information on anomalous time delays is included in any of the models used in this study. The importance of such anomalies in tracking wavefronts across small horizontal arrays is shown by H. Mack (1969) and such information may eventually be required to estimate teleseismic P-waves effectively on small horizontal arrays. The neglect of these effects may prejudice the comparison between horizontal and vertical arrays, and since this information is in principle obtainable, any unfavorable comparison should not be taken as final. It is perhaps more useful to think of the two arrays as complementary configurations where the horizontal array provides information on direction and distance of the source, while the vertical array may be a sensitive discriminant between wave modes.

The total array consists of 19 short period instruments designed to record high frequency signals such as P-waves at teleseismic distance. The co-ordinates in kilometers of each sensor are listed in Table I.

Seven events are used to demonstrate the array as a P-wave estimator. A list of quantities of interest are tabulated for each event. Most descriptors are self-evident; the quantity called signal contrast is used as a quantitative measure of the size of the signal. It is the ratio of the peak power spectral density after the expected signal arrival time to that before the expected signal arrival time. The list of event parameters is found in Table II.

A set of channel gain estimates, obtained in Step (6) above are tabulated on TableIII. These are applied to the horizontal array channels after correcting for system response. These

TABLE I

East, North, and distance down are taken positive

Array Element		E-W	N-S	Depth
1	U1	0.000 km	0.000 km	0.000 km
2	U2	0.025	0.834	0.000
3	U3	0.830	0.352	0.000
4	U4	-0.062	-.0615	0.000
5	U5	-0.700	-1.139	0.000
5	U6	-0.749	0.797	0.000
7	U7	-0.012	1.510	0.000
8	U8	0.944	1.544	0.000
9	U9	1.723	0.052	0.000
10	U10	1.658	-0.728	0.000
11	U11	0.404	-1.411	0.000
12	U12	-1.283	-0.527	0.000
13	U13	-1.658	0.201	0.000
14	D6	0.000	0.000	0.610
15	D5	0.000	0.000	1.067
16	D4	0.000	0.000	1.524
17	D3	0.000	0.000	1.981
18	D2	0.000	0.000	2.438
19	D1	0.000	0.000	2.896

Distances are measured from the vertical array at the earth's surface.

TABLE II

Event Data

Event No.	Seismogram Number	Time (GMT)	Back Azimuth	Ray Parameter	Magnitude	Focus (km)	Signal Contrast (db)
1	14007	11/25 0329	212.8	.045	4.9	67	06.6
2	14008	11/25 2040	324.4	.056	5.1	33	-00.2
3	14009	11/29 2227	224.0	.045	5.2	161	21.5
4	14010	12/05 0246	127.0	.054	4.4	0	07.0
5	14010	12/05 0246	127.0	.054	4.8	33	02.0
6	14011	11/26 0328	9.3	.077	4.7	33	08.0
7	14012	11/29 1935	104.7	.053	3.9	0	10.8

Propagation Slowness: .204

Gradient: -.0069

TABLE III

Signal Gain Equalization Factors
Horizontal Array

Event Number

Channel	1	2	3	4	5	6	7
U1	.861	.878	.719	.760	.852	1.066	.734
U2	.709	.697	.545	.636	.696	.912	.482
U3	.911	.828	.741	.850	.917	1.041	.640
U4	.724	.690	.498	.702	.808	.942	.562
U5	.794	.686	.723	.729	.778	1.013	.641
U6	.731	.781	.583	653	.739	.979	.601
U7	.607	.609	.409	.492	.552	.678	.424
U8	.731	.618	.631	.677	687	.933	.524
U9	.652	.601	.514	.583	.746	.865	.367
U10	.708	.574	.524	.516	.659	.771	.317
U11	.408	.372	.313	.385	.351	.503	.263
U12	.615	.558	.483	.596	.705	.899	.398
U13	.591	.548	.556	.563	.705	.932	.446

channel gains represent estimates of the gain required to equalize the amplitude anomaly, $C(x_i, y_i, o)$, to a mean value, where the subscript i designates the horizontal array channel at position (x_i, y_i) and at $z = 0$. The amplitude anomaly is the apparent gain of the signal on the i^{th} channel compared to the average over all channels. In the case of the channel gains given in Table III, the mean of all the channels was used as an estimate to h(t) in equation 2a; and a least squares estimate of the constant times the estimate of h(t) which equal $U(t, x_i, y_i, o)$ is the ith channel gain estimate. Independent estimates are obtained for each event.

A set of channel gain estimates for the vertical array are tabulated in Table IV. These utilize the signal model in equation (2b). Least squares estimates were obtained by a procedure similar to that used on the horizontal array. However, since the signal model on the vertical array consists of a reflected wave with unknown echo amplitude as well as incident amplitude, least squares estimates of C(o, o, z) and R(z) were computed for the vertical array channels.

All of the quantities estimated by least squares procedures were determined independently on each channel, and were estimated in a time window of approximately one half minute following the expected arrival time of the signal.

The arbitrary one half minute time window was adequate for the high S/N ratio, the channel gain should be computed with a smaller window with a provision to search within limits for the maximum cross-correlation between the signal estimate and the channel to obtain the record where the added teleseismic energy is most apparent. Also pre-filtering of the channels to emphasize the added teleseismic energy should be considered for low S/N cases.

After estimating the amplitude anomalies on the horizontal and vertical arrays, and the echo amplitude anomaly for the vertical array, the channels were gain equalized. For the horizontal array this amounts to dividing each channel by its apparent amplitude anomaly, thus reducing the apparent signals on each channel to equal size. In addition to dividing each vertical array channel by its apparent amplitude anomaly, the effects of echo distortion were removed. Since we have (1) an initial estimate of the signal based on the assumption of equal channel gains, (2) an estimate of the channel gain on each vertical array channel, (3) an estimate of the echo amplitude on each channel, and (4) an estimate of the echo time on each channel

TABLE IV

Signal Gain Equalization Factors
Vertical Array

Channel	Event Number 1	2	3	4	5	6	7
D6	.769	.795	.862	.767	.717	.863	.854
D5	.918	.932	.934	.948	.963	1.174	.959
D4	1.028	1.015	1.111	1.153	1.086	1.390	1.048
D3	1.062	.968	1.036	1.318	1.205	.412	.950
D2	1.056	.930	.987	.963	.887	1.255	.896
D1	1.010	.941	1.036	.923	.919	1.296	.944

based on the given wave velocity model; we can remove the echos b, appropriately delaying ard scaling the signal estimate to nominally null out the components due to the apparent reflection coefficient, $R(z_i)$. After applying the above mentioned signal equalization procedures, steps (6) and (9), new estimates were made of the signal on the horizontal array, vertical array, and combined horizontal and vertical array, steps (7), (10) and (11). For the purpose of channel gain equalization, and all other feedback operations in the signal estimation procedure, we have selected the vertical array estimate of signal as the estimated signal.

For display purposes, the main output of the program are plots of each channel, plus beams based on the sum of horizontal array channels, vertical array channels, and combined horizontal and vertical array channels. The channels are plotted after shifting to remove time delays associated with equation (1) using the quantities in Table II. For the vertical array, a weight of unity represents the signal as seen at the surface, where it is the sum of the overlaid incident and reflected waveform. Below the surface the incident wave is lined up with the surface seismogram by adding one half of the echo time (up-hole time) and the reflected wave is lined up with the surface seismogram by subtracting one-half the echo time (down-hole time). Each of these are weighted by one half and added so that the total weight of the incident plus reflected wave is one for all of the sensors in the vertical array. Thus we convolve with the filter $1/2\ [\delta(t+T_z) + \delta(t-T_z)]$.

The first set of plots, Appendix 1, shows the beamed traces for array co-ordinates given on Table I and signal propagation parameters given in Table II. The estimates of signal on the three types of arrays (horizontal: H, vertical: V, combined: H+V) assume equal channel gains, reflection coefficients of unity, and equal residual noise variance on each channel. In these plots the contribution of the echos have not been removed from the matched filtered single sensor vertical array plots.

The second set of plots, Appendix 2, shows the beamed sensors using the same time-delays as in Appendix 1. Each channel is multiplied by a least squares gain factor to equalize the gain to the vertical array estimate of signal shown in Appendix 1. The estimates of signal on the three types of array (H, V, and H+V) are based on the sum of the gain equalized

channels. The vertical array channels are not only gain equalized, but the signal estimate from Appendix 1 has been subtracted from each channel with the appropriate weights and delays to remove echo distortion.

The third set of plots in Appendix 3 shows the residual noise on each of tne beamed sensors as the difference between the data on each sensor and the vertical array signal estimate shown in Appendix 2. The estimates of signal in Appendix 3 are weighted proportionally to the inverse variance of residual noise shown in Appendix 3, with the sum of the channel weights equal to one. The channel weights in estimating the signal on the horizontal array are shown on Table V; on the vertical array on Table VI; and on the combined vertical and horizontal array on Table VII.

TABLE V

Noise Equalization - Channel Weights

Horizontal Array

Event Number

Channel	1	2	3	4	5	6	7
U1	.190	.196	.150	.183	.206	.205	.131
U2	.119	.066	.068	.088	.074	.061	.071
U3	.092	.102	.049	.074	.126	.102	.104
U4	.075	.105	.054	.082	.083	.085	.085
U5	.095	.092	.139	.104	.074	.086	.091
U6	.051	.059	.052	.056	.077	.080	.088
U7	.051	.040	.022	.040	.046	.031	.056
U8	.053	.042	.049	.056	.046	.057	.073
U9	.053	.061	.026	.042	.052	.049	.052
U10	.057	.063	.055	.051	.052	.049	.052
U11	.049	.063	.061	.056	.033	.053	.064
U12	.063	.062	.128	.080	.065	.078	.065
U13	.050	.048	.144	.088	.065	.074	.067

TABLE VI

Noise Equalization - Channel Weights

Vertical Array

Channel	Event Number 1	2	3	4	5	6	7
D6	.057	.089	.069	.088	.105	.114	.129
D5	.285	.203	.359	.201	.206	.247	.208
D4	.284	.263	.150	.279	.256	.200	.193
D3	.155	.178	.113	.184	.180	.163	.211
D2	.084	.136	.106	.120	.126	.115	.123
D1	.069	.084	.159	.064	.073	.098	.097

TABLE VII

Noise Equalization - Channel Weights
Total Array

Channel	Event Number 1	2	3	4	5	6	7
U1	.051	.040	.035	.051	.044	.050	.034
U2	.033	.014	.016	.025	.016	.015	.018
U3	.025	.021	.011	.021	.027	.025	.027
U4	.020	.021	.012	.023	.018	.021	.022
U5	.026	.019	.032	.029	.016	.021	.023
U6	.014	.012	.012	.016	.017	.020	.022
U7	.014	.008	.005	.011	.010	.007	.014
U8	.015	.009	.011	.015	.010	.011	.019
U9	.015	.013	.006	.011	.011	.012	.013
U10	.016	.013	.013	.014	.011	.012	.013
U11	.013	.013	.014	.016	.008	.013	.016
U12	.017	.013	.030	.023	.014	.019	.017
U13	.014	.010	.033	.025	.014	.018	.017
D6	.044	.074	.055	.067	.087	.090	.100
D5	.222	.170	.289	.54	.171	.199	.162
D4	.222	.220	.120	.214	.212	.161	.149
D3	.121	.148	.091	.141	.149	.131	.164
D2	.065	.113	.086	.092	.105	.093	.095
D1	.053	.070	.128	.045	.060	.079	.073

Appendix 4 shows plots of the power spectral density of the residual noise on each channel. The residual noise, $\ell_i(t)$, on the i^{th} channel is the difference between the data measured on the channel, $x_i(t)$, and the vertical array estimate of signal, $S(t)$.

$$\ell_i(t) = X_i(t) - S(t)$$

The spectrum of $\ell_i(t)$ is computed as $E_i(\omega)$; the unsmoothed estimate of the power spectral density is $P_i(\omega) = E_i(\omega)^* E_i(\omega)$. The final values plotted in Appendix 4 were smoothed with equal weighting over eleven neighboring frequencies resulting is estimates of the residual power of 22 degrees of freedom (eleven complex frequency points).

Appendix 5 shows plots of the power spectral density of the signal estimates shown in Appendix 3. These are for signal estimates on the horizontal, vertical, and combined array labelled as H, V, and H+V. The P-wave estimates are obtained as a weighted beamed sum, $S(t) = \sum_i q_i X_i(t)$, of the channels, $X_i(t)$.

The complex Fourier analysis of $S(t)$, $\hat{S}(\omega)$; was used to compute the unsmoothed signal power spectrum estimate $P_s(\omega) = \hat{S}^*(\omega)\ \hat{S}(\omega)$. The final values shown on the signal estimate plots in Appendix 5 were smoothed over eleven neighboring frequencies to produce spectral estimates of the signal with 22 degrees of freedom.

The spectrum of the signal estimation error is shown in Appendix 5 in the last three columns. Assuming no correlation in the channel residuals (Appendix 4) between channels the P-wave estimation error power spectral density is the linear sum of the channel residuals shown in Appendix 4. The weights used to obtain the estimate of P-waves, $S(\omega)$, is q_i as shown above. Assuming that residual on the channels is uncorrelated

between channels and the spectral matrix of the residual is diagonal, then the power spectral density of the error of the signal estimate is the weighted sum of the residuals.

$$P_E(\omega) = \sum_i q_i^2 \, P_i(\omega)$$

This is the spectrum shown in the last three columns of Appendix 5 with the residual defined as the difference of the channel and the vertical array signal estimate. If the beam involves N channels, the number of degrees of freedom in the estimate of signal error is 22*(N-1) for noise uncorrelated between channels. If the residual is correlated between channels, then the number of degrees of freedom is less than 22*(N-1).

Appendix 6 is a summary of statistics derived from measurements of signal and noise power spectral density. The tables cover the expected energy band of teleseismic signals. The ambient P-wave statistics are obtained using samples before the seven events. Signal statistics are from a time window of 30 seconds after the expected arrival time of the observed teleseismic events. Detection is considered from two points of view; (1) spectral energy in the signal band vs the ambient noise samples before the arrival time of the signal and (2) spectral energy of the P-wave estimate to the spectral energy of non P-wave energy in the given time window. The non P-wave energy is considered equivalent to the P-wave estimation error.

RESULTS

In Appendix 1, the beamed horizontal array channels appear to be fairly uniform in the apparent gain of each channel except for channel 11 which appears elevated for all seven events. The apparent signal amplitude variation (highest to lowest) range from 1.2:1.0 to 1.4:1.0 for channels other than channel 11. The apparent range of signal amplitudes on the vertical array varies from 1.1:1.0 to 1.25:1.0. One very high signal amplitude occurred on channel D3, event No. 6, which is probably due to a calibration error.

It may seem, upon cursory inspection of the deep well traces, that the depth of the sensors has been reversed. The fact that D1, the deepest trace looks like a surface trace is due to zero's in the Fourier transform of the matched filter which, at this depth, reduces the amplitude of the low-frequency energy thus enhancing the high-frequency energy. The side-lobes of this filter have been removed in the V trace estimate in Appendix 1.

In Appendix 2, the gain equalization and echo removal operations were applied to each channel. Generally, the signal amplitudes appear to be uniform on all channels indicating for these high S/N cases, excellent performance of the signal gain equalization and deghosting algorithms. The algorithms may have to be modified to handle low S/N cases, since the least square technique estimates low gains for these cases. Horizontal array channel U1 is situated directly over the vertical array and is thus comparable with the deghosted vertical array and is thus comparable with the deghosted vertical array channels. In all cases, the result of deghosting on the ambient noise is to make every channel on the vertical array practically identical. This was expected for the teleseismic P-wave signals but was

somewhat of a surprise for the ambient noise. In some (e.g., events 2, 5, 6) of the events there is significantly more high frequency noise on the horizontal array channels than on the vertical array. One might note in particular that this is true for U1 just above the vertical array. This suggests intermittent high frequency noise which damps out very rapidly with depth. Channel D6 is buried only 0.6 km from the surface indicating that much of the intermittent high frequency noise decays with depth in less than 0.6 km. Note that this source of "noise" could not be removed by a band-pass filter. It is, however removed by beaming the horizontal array alone as shown by e.g., trace H in Appendices 1 and 2, Event 5.

In Appendix 3, the estimates of signal are based on gain-equalized channels which are further weighted in inverse proportion to the variance of the residual noise under each channel. The estimate of the P-wave on the vertical array was subtracted from each channel. Both the amount of noise and the apparent frequency content of the noise change markedly after the arrival of the signal. The noise after the arrival of signal was used in computing the channel weights for estimating the signal. In all cases, the residual noise is much lower on the vertical array, particularly at intermediate depths. The range from lowest to highest residual noise is from 4 to 8 db for the horizontal array; from 4 to 7 db for the vertical array; and from 11 to 17 db on the combined vertical and horizontal array. Note that the residual noise is high-frequency and generally uncorrelated on the horizontal array. See, e.g., event 5. This shows why the noise is eliminated by the horizontal beam. It is eliminated by the vertical array because it is not present at depth. The natural hypothesis is high frequency Rayleigh waves scattered at the

surface from both the ambient P and the signal. An objection to this hypothesis is the slightly greater residual noise level on the bottom seismometers. This might possibly be due to a less satisfactory reduction of echo distortion at these depths.

After calculating the signal gain equalization factors for the vertical array, the gains were applied to each channel as correction factors. In addition, the first signal estimate from the vertical array was fed back with the fixed model echo time and subtracted to remove the echo distortion in the vertical array. To obtain the first signal estimate a reflection coefficient of unity was used. For the second estimate, the program automatically calculated a reflection coefficient for each channel. This could compensate for the oversimplified model of a nearly vertically incident halfspace echo. The nearness of the apparent reflection coefficient to unity is a check on the adequacy of the nearly vertical halfspace echo model. On each channel, for the seven events, the apparent reflection coefficient is shown on Table VIII. The range of values, 0.66 to 1.16 shows that the deghosting could not have succeeded so perfectly had unit reflection coefficients been assumed. The almost perfect copy on the vertical array of both the P-wave signal and ambient field estimates, show P-waves to be an adequate model for both the teleseismic signal and ambient noise field.

The least squares weights for the contribution of each of the channels to the beamed sum are calculated from the residual noise on each channel. If the channel weight is small there is much noise under the signal; if the weight is large, there is little noise under the signal. The weights are computed as proportional to the inverse variance of the residual noise on

TABLE VIII

Apparent Reflection Coefficient -

Vertical Array

Event Number

Channel	1	2	3	4	5	6	7
D6	1.00	1.13	1.07	0.93	0.93	1.12	1.16
D5	0.91	0.87	0.92	0.82	0.81	0.91	1.01
D4	0.81	0.81	0.77	0.89	0.78	0.79	0.87
D3	0.95	0.79	0.89	0.72	0.75	0.77	0.84
D2	0.95	0.85	0.81	0.66	0.82	0.78	0.92
D1	0.78	0.93	1.02	0.66	0.89	0.81	1.11

the channel which occurs after the expected arrival time of the teleseismic signal. Since the channels have already been gain equalized, the sum of the weights is equal to one.

The initial assumption for computing the weights was that the variance of non P-wave noise added to the signal was equal on each channel, therefore the weight for each channel was initially taken as 1/19 after the proper gain corrections had been applied. Each sensor of the array was evaluated by dividing the least squares weight for the beamed sum into the expected weight, 1/19. The result is a measure of the ratio of the expected noise power to the observed noise power. The resultant individual channel performance figures are shown in Table IX.

The weights for the weighted beam sum estimate of teleseismic P-waves are based on a-posteriori estimates of non P-wave noise occurring after the expected first arrival time of the teleseismic P-wave. This is a departure from methods utilizing the apparent ambient noise before the signal to design estimators of teleseismic P-waves. Such a method applied here would yield approximately equal weights.

Much of the added noise occurring after the arrival of the signal is expected to be proportional to the energy of the teleseismic P-wave. Further, we might speculate that the non P-wave noise before the expected arrival time of the teleseismic P-wave was generated by a dominant ambient P-wave and is thus proportional to the energy of the ambient P-wave. Table X shows the apparent S/N ratio (Ambient P-wave/Non P-wave) before the teleseismic signal arrived. Table XI shows the apparent S/N ratio (teleseismic P-wave/Non P-wave under teleseismic P-wave) after the expected arrival time of the teleseismic P-wave. Table XII shows the difference between the

TABLE IX

Comparative Channel Performance (Decibels)
$10 \log_{10}$ (Expected Noise/Observed Noise)

	Event Number						
Channel	1	2	3	4	5	6	7
U1	-0.0	-1.2	-1.7	-0.1	-0.8	-0.2	-2.0
U2	-2.2	-6.2	-5.4	-3.3	-5.2	-5.6	-4.5
U3	-3.1	-3.9	-6.7	-4.0	-3.0	-3.3	-3.0
U4	-4.2	-3.9	-6.3	-3.6	-4.8	-4.1	-4.0
U5	-3.0	-5.5	-2.2	-2.6	-5.2	-4.1	-3.6
U6	-5.4	-6.4	-6.4	-4.8	-5.4	-4.3	-3.7
U7	-5.4	-8.1	-10.2	-6.6	-7.4	-8.5	-5.7
U8	-5.5	-8.0	-6.6	-5.2	-7.4	-6.7	-4.9
U9	-5.5	-6.2	-9.4	-6.4	-6.8	-6.4	-5.2
U10	-5.2	-6.1	-8.1	-5.7	-6.8	-6.4	-5.2
U11	-4.1	-6.1	-5.7	-5.3	-8.7	-6.1	-4.5
U12	-5.1	-6.2	-2.6	-3.7	-5.7	-4.4	-4.7
U13	-4.3	-7.6	-2.0	-3.2	-5.7	-4.6	-4.4
D6	-0.7	1.4	0.2	1.2	2.2	2.5	2.9
D5	6.3	5.0	7.1	4.7	5.0	5.9	4.9
D4	6.3	6.2	3.4	6.1	6.0	4.8	4.5
D3	3.6	4.6	2.3	4.2	4.5	4.0	4.9
D2	1.0	3.4	2.1	2.4	2.0	2.4	2.8
D1	0.2	1.3	2.4	-0.6	0.6	1.8	1.4

TABLE X

S/N Ratio Before Signal 10 Log_{10} (P-Wave/Non P-Wave)

DB

Event Number

Channel	1	2	3	4	5	6	7
U1	11.1	8.8	7.8	9.6	7.7	10.4	8.8
U2	6.1	3.1	4.4	6.2	3.3	4.1	5.4
U3	6.2	5.3	7.8	7.1	6.3	4.6	5.9
U4	7.8	5.9	5.3	5.4	6.1	6.8	5.8
U5	8.2	4.3	6.0	4.0	5.3	5.0	5.9
U6	6.2	2.3	3.3	4.9	2.8	4.7	7.9
U7	5.3	2.1	2.3	4.1	1.5	2.6	4.7
U8	6.1	2.8	3.1	3.5	1.6	1.5	3.7
U9	5.0	3.1	3.9	3.5	3.6	2.7	2.8
U10	3.6	2.8	3.3	2.2	3.0	2.4	2.3
U11	4.4	2.5	3.7	1.1	2.3	1.8	3.6
U12	6.4	3.2	4.3	2.6	3.5	4.0	4.7
U13	4.2	2.4	3.0	2.1	1.5	2.8	3.9
D6	12.8	11.8	8.6	12.1	12.3	13.0	15.0
D5	18.7	17.6	15.3	15.3	17.7	17.7	18.2
D4	19.4	20.1	14.2	15.5	19.7	17.8	18.4
D3	13.6	18.3	14.6	15.7	18.3	14.9	19.7
D2	11.0	15.1	11.9	10.7	12.7	12.5	16.5
D1	11.5	11.7	9.5	7.8	9.7	12.3	13.6
Hor. Sum	17.1	14.9	14.3	15.0	14.7	15.3	16.0
Ver. Sum	30.6	32.2	30.8	29.1	30.7	31.1	33.4
Total Sum	27.8	28.4	26.6	25.5	27.7	27.2	27.7

TABLE XI

S/N Ratio After Signal 10 Log_{10} (P-Wave/Non P-Wave)

DB

Event Number

Channel	1	2	3	4	5	6	7
U1	10.7	8.1	9.6	10.2	9.8	11.3	5.1
U2	9.0	4.0	6.9	7.3	5.8	6.[illegible]	2.8
U3	8.1	5.8	5.7	6.7	8.0	8.4	4.6
U4	7.3	6.0	5.9	7.2	6.4	7.9	3.6
U5	8.3	5.6	10.0	8.4	6.0	8.0	4.2
U6	5.5	3.7	5.8	5.8	6.1	7.5	3.9
U7	5.6	2.0	2.2	4.1	3.8	3.4	1.8
U8	5.7	2.1	5.8	5.3	3.8	5.3	3.0
U9	5.7	3.8	2.9	4.2	4.4	5.6	1.5
U10	5.9	3.8	5.8	5.0	4.3	5.5	1.6
U11	5.3	3.9	6.4	5.7	2.6	5.9	2.5
U12	6.4	3.8	9.4	7.2	5.5	7.5	2.7
U13	5.4	2.8	9.9	7.5	5.5	7.3	2.8
D6	10.5	11.0	11.9	11.9	13.3	14.1	9.9
D5	18.9	16.1	21.5	16.6	17.3	18.9	14.1
D4	21.3	19.8	17.5	20.0	20.5	19.0	13.7
D3	16.1	16.7	15.7	16.3	17.3	17.1	14.1
D2	12.1	13.9	14.8	13.0	14.3	14.1	10.8
D1	10.9	11.3	16.4	9.9	11.4	13.3	9.3
Hor. Sum	18.0	15.4	18.1	17.6	16.7	18.1	14.0
Ver. Sum	29.8	31.4	33.3	29.8	32.4	32.2	29.1
Total Sum	28.3	28.6	30.3	27.8	29.6	29.7	25.5

TABLE XII

Ratio of Scattering Cross-Sections $10 \log_{10} (K_{signal}/K_{Ambient})$

$\overline{N}^2$ (Non P-Wave) = $K\ \overline{S}^2$ (P-Wave)

DB

Event Number

Channel	1	2	3	4	5	6	7
U1	0.4	0.7	-1.8	-0.6	-2.1	-0.9	3.7
U2	-2.9	-0.9	-2.5	-0.9	-2.5	-2.3	2.6
U3	-1.9	-0.5	-0.4	1.1	-1.7	-3.8	1.3
U4	0.5	-0.1	0.0	-1.8	-0.3	-1.1	2.2
U5	-0.1	-1.3	-4.0	-4.4	-0.7	-3.0	1.7
U6	0.7	-1.4	-2.0	-0.9	-3.3	-1.8	4.0
U7	-0.3	0.1	0.1	0.0	-2.3	-0.8	2.9
U8	0.4	0.7	-2.7	-1.8	-2.2	-3.8	0.7
U9	-0.7	-0.7	1.0	-0.7	-0.8	-2.9	1.3
U10	-2.3	-1.0	-2.5	-2.8	-.13	-3.1	0.7
U11	-0.9	-1.4	-2.7	-4.6	-0.3	-4.1	1.1
U12	0.0	-0.6	-4.9	-4.6	-2.0	-2.5	2.0
U13	-1.0	-0.4	-6.9	-5.4	-4.0	-4.5	1.1
D6	2.3	0.8	-3.3	0.2	-1.0	-1.1	5.1
D5	-0.2	1.5	-6.2	-1.3	0.4	-1.2	4.1
D4	-1.9	0.3	-3.3	-4.5	-0.8	-1.2	4.7
D3	-2.5	1.5	-1.1	-0.6	1.0	-2.3	5.6
D2	-1.1	1.2	-2.9	-2.3	-1.6	-1.6	2.8
D3	0.6	0.4	-6.9	-2.1	-1.7	-1.0	6.7
Hor. Sum	-0.9	-0.5	-3.8	-2.6	-2.0	-2.8	2.0
Ver. Sum	0.8	0.8	-2.5	-0.7	-1.7	-1.1	4.3
Total Sum	-0.5	-0.2	-3.7	-2.3	-1.9	-2.5	2.2

two cases and should be zero for similar P- Non P scattering cross-sections or constant for different scattering cross-sections.

In Appendix 6, Table F-1 verifies in the frequency domain that the multichannel spectrum of noise is dominated by a coherent P-wave energy at all frequencies up to 1.95 Hz. Considerable variability between events is indicated in the relative magnitude of the P-wave component compared to the non P-wave component. Comparison of teleseismic events on Table F-2 with ambient P-waves on F-1 indicates that in the signal band, 98 Hz, a single dominant P-wave is a better model for teleseismic P-waves than for the ambient P-waves.

In Appendix 6, Table E-1 shows modest gains in the small aperture horizontal array in the signal band. The maximum gain in power is 6 compared to 13 which would be obtained for 13 sensors under $\sqrt{N}$ amplitude improvement. For the vertical array, from Table E-2, the maximum gain was 2 compared to 7 for $\sqrt{N}$ amplitude improvement. As expected, both arrays are inefficient on a per sensor basis unless the dominant ambient P-waves can be distinguished from teleseismic P-waves and removed.

CONCLUSIONS

The ratio of the estimated P-wave energy to residual noise before the expected signal arrival time, averaged over the seven events, is 15.5 db on the horizontal array, 31.0 db on the vertical array and 27.0 on the combined array. The same figures computed after the signal arrival time are 16.0, 31.0, and 28.0. This indicates practically no difference in residual noise figures between ambient and a significant range (3.9 to 5.2 magnitude) of teleseismic events, suggesting that any non P-wave noise is proportional to the single dominant P-wave whether ambient or teleseismic. These figures however, are heavily weighted for ambient noise on the .3 Hz microseism band and it can be seen that the apparent S/N, (residual non P-wave taken as noise) is highly frequency dependent. In Appendix 6,Table F-1 and F-2 show that the S/N is much greater for teleseismic events in the teleseismic signal band (.8-2.00 Hz) indicating much less signal generated residual non P-wave type noise. Much of the difference between the horizontal array and the vertical array residual noise figures disappears if the residuals are computed with horizontal array signal estimates and vertical array signal estimates, respectively. Preliminary indications are that half of the difference between the db estimation error on the two types of array is reduced by this mode of comparison. If, in addition, the data is band limited between .8 and 3.0 Hz, no significant difference is observed between the estimation error on the vertical and horizontal array.

The vertical array, partly because of its greater aperture and partly because of the remarkably low residual noise in the middle of the vertical array is a far superior device for estimating broad-band P-waves by means of the weighted beamed sum.

The use of channel weights appears to be required for anywhere near optimum P-wave estimation on both the horizontal and vertical array. This is indicated by ranges from the lowest to highest weights of 7 to 8 db for each type of array. The indicated variations in amplitude anomalies and residual noise from channel to channel are based on measurements from data and are therefore estimates subject to estimation error. Signal gain adjustment for amplitude anomalies also appears to be necessary for optimum estimation of signals on both types of arrays with expected signal gain anomalies ranging to 1.4:1 for horizontal arrays and 1.25:1 for vertical arrays.

Any advantage of the vertical array on small aperture horizontal arrays as detectors or estimators of teleseismic P-waves must surmount the problem of distinguishing teleseismic P-waves from the apparently Markovian ambient P-wave. In horizontally separating sensors, the fraction of ambient P-wave or coherent noise drops and the fraction of incoherent noise increases in proportion to the distance between sensors. For comparable separations and indeed for much larger separations in terms of P-wave step-out times, the vertical array coherent noise fraction remains nearly unity and the incoherent component negligible.

RECOMMENDATIONS

Sufficient information was obtained from this signal and noise study to make several recommendations. At this site, the ambient noise as well as coda noise is dominated by nearly vertically incident P-waves. The signal estimation error is negligible (approximately -31 db -24 db with horizontal beam reference, -Udb prefiltered 0.8-6.0 Hz) using the vertical array. The major problem in applying the combined vertical and horizontal array as a detector and estimator of teleseismic P-waves hinges on discriminating between a dominant ambient P-wave which is nearly vertically incident and teleseismic P-waves. This suggests that the horizontal array at this site should be of sufficient aperture to distinguish teleseismic P-waves from the ambient P-wave. It may be necessary to increase the aperture of the horizontal array, although this has by no means been demonstrated yet.

Five possible paths for future research are suggested

1) It is noted that a propagation single mode system composed of a dominant P-wave with amplitude anomalies adequately describes both teleseismic signals and ambient noise. The single P-wave models used to estimate teleseismic P-waves should be replaced by two P-wave signal models to distinguish teleseismic signals from ambient noise on the basis of significantly different amplitude anomalies.

2) The accurate estimate of ambient P-waves on the vertical array should be used as desired output of operators on the horizontal array to obtain propagation operators (spike seismograms) for each horizontal array channel.

3) Given an ambient P-wave propagation model determine amplitude anomalies of teleseismic events as an additive P-wave

to ambient P-waves rather than as a single P-wave as in this report.

4) Use estimates of the horizontal array propagation operators for analysis into discrete traveling wave components; either for f-k analysis or simply ray parameter analysis as in program WABBIT.

5) The present design is only adequate for high S/N measurements of signal. By appropriately filtering each channel, and using smaller time windows to compute apparent signal gains on each channel and using a different gain estimation algorithm the processor can be made applicable to lower S/N measurements. Lower S/N events should be used to test the modified processor.

REFERENCES

Backus, M.M., Burg, I.P., Baldwin, R.G., Bryan, E., 1964, Extraction of mantle P-waves from ambient noise: Geophysics, v. 29, p. 672-692.

Booker, A.H., 1965, Analysis of variance as a method for seismic signal detection: Seismic Data Laboratory Report No. 116, Teledyne Geotech.

Broding, R., Bentley-Llewellyn, N., Hearn, D., 1964, A study of a three dimensional detection system: Geoph. v. 29, p. 221-250.

Claerbout, J.F., 1964, Detection of P-waves from weak sources at great distances: Geoph. v. 29, p. 197-211.

Dean, W.C., 1966, Rayleigh waves rejection by optimum filtering of vertical arrays: Seismic Data Laboratory Report No. 166, Teledyne Geotech.

Douze, E.J., Mack, H., 1970, publication pending.

Lintz, P.R., 1969, Principles of Wiener auto-adaptive filter, 19th International Symposium of the M.R.I.: Polytechnic Institute of Brooklyn. (Also Seismic Data Laboratory Report No. 224, Teledyne Geotech.)

Mack, H., 1960, Nature of short period P-wave signal variation at LASA: JGR, v. 74, p. 3161-3170.

Richter, C.F., 1958, Elementary seismology: San Francisco W. H. Freeman.

Sax, R.L., 1968, Response of several vertical array processors: Seismic Data Laboratory Report No. 212, Teledyne Geotech.

Sax, R.L., Hawkins, R., 1966, Vertical array teleseismic signal measurements: Seismic Data Laboratory Report No. 170, Teledyne Geotech.

Shumway, R.H., and Husted, H.L., 1970, Frequency dependent estimation and detection for seismic arrays: Seismic Data Laboratory Report No. 242, Teledyne Geotech.

Shumway, R.H., and Dean, W.C., 1968, Best linear unbiased estimation for multivariate stationary processes: Technometrics 16, p. 523-534.

APPENDIX 1

DATA BEAMED TO U1 (OVER VERTICAL ARRAY)

U1-U13	Horizontal Array Channels
D6-D1	Vertical Array Channels (Shallowest to Deepest)
H	Signal Estimate on Horizontal Array
V	Signal Estimate on Vertical Array
H+V	Signal Estimate on Combined Array

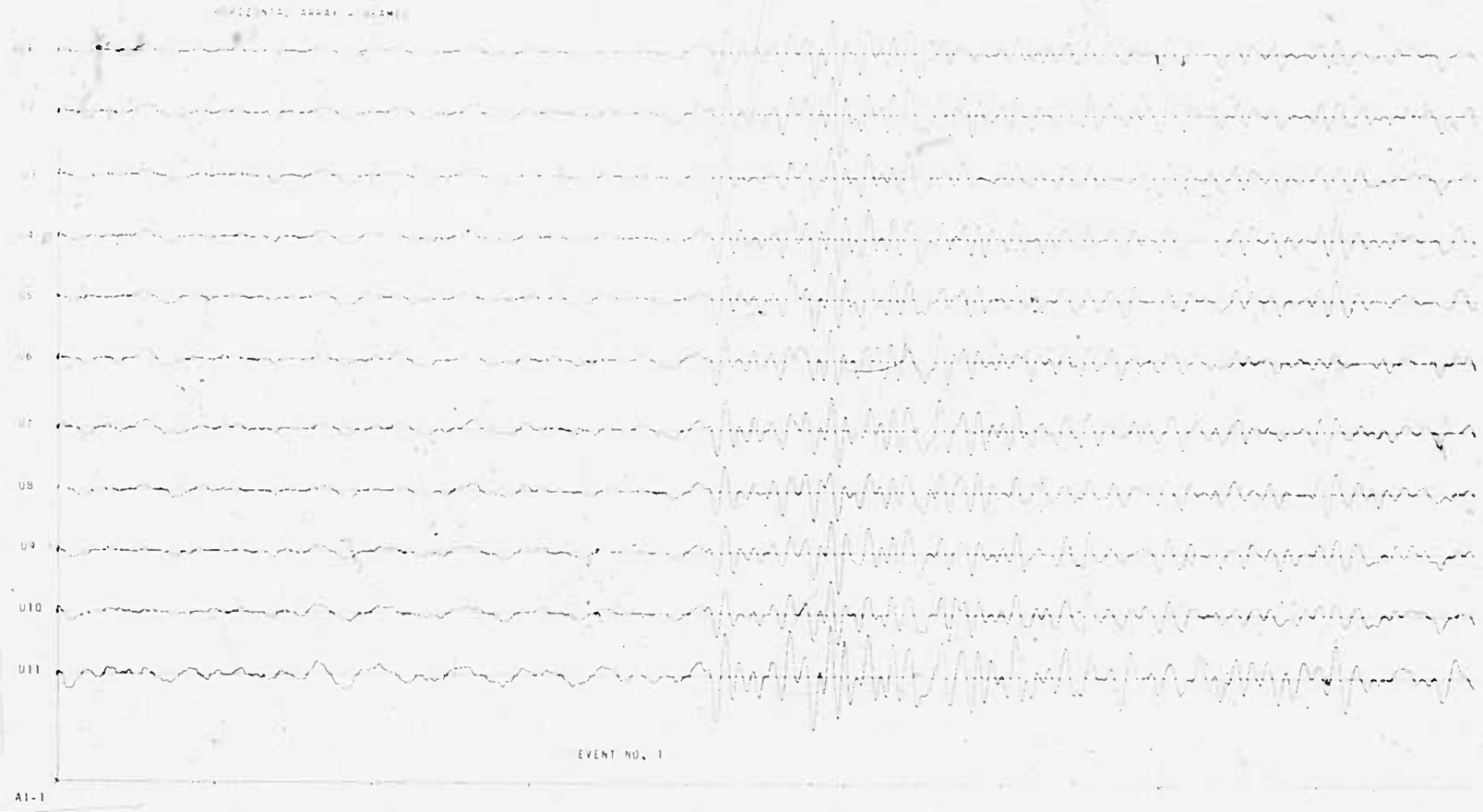
U8
U9
U10
U11
EVENT NO. 1
A1-1

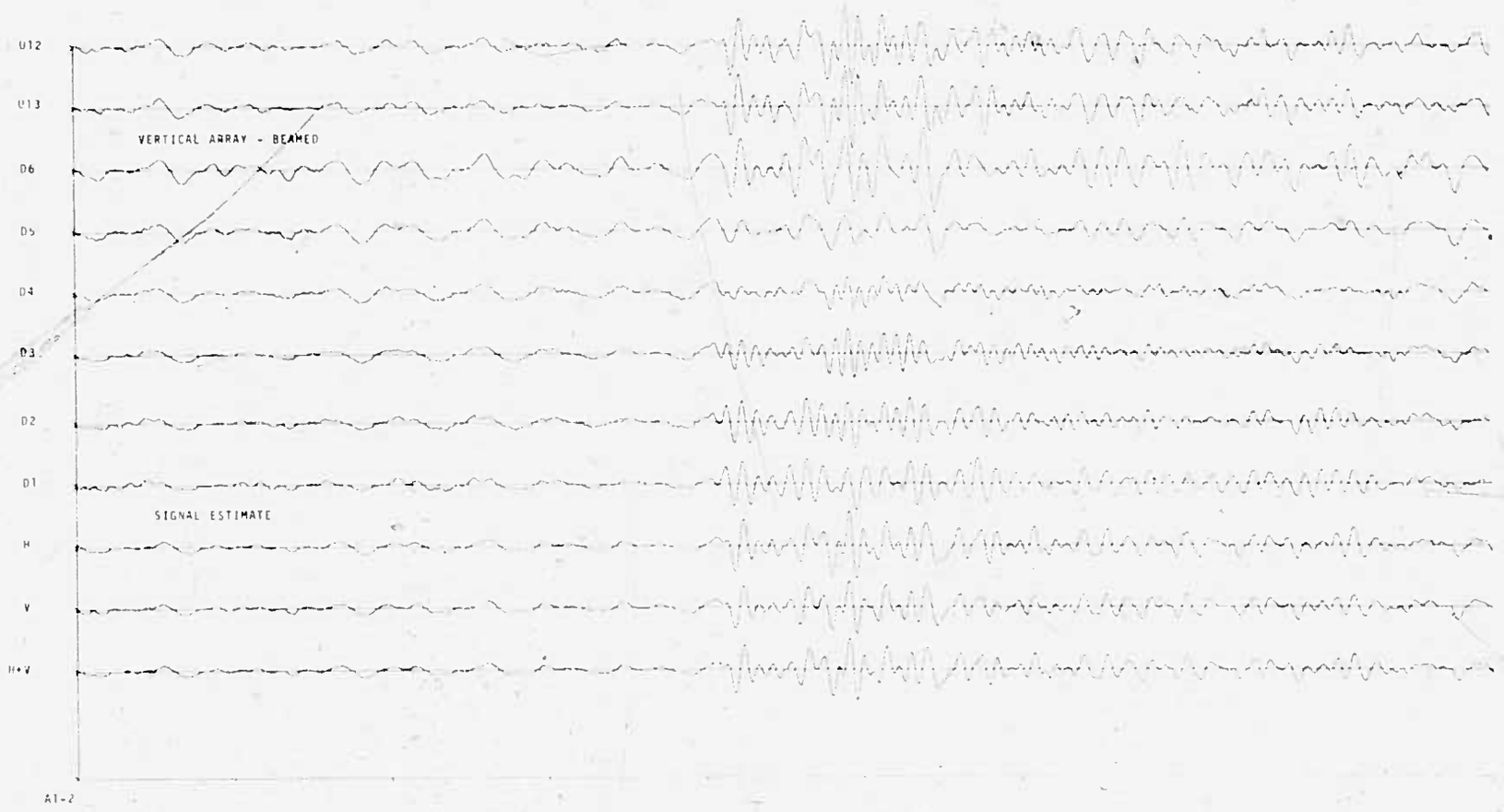
U12
U13
VERTICAL ARRAY - BEAMED
D6
D5
D4
D3
D2
D1
SIGNAL ESTIMATE
H
V
H+V
AT-2

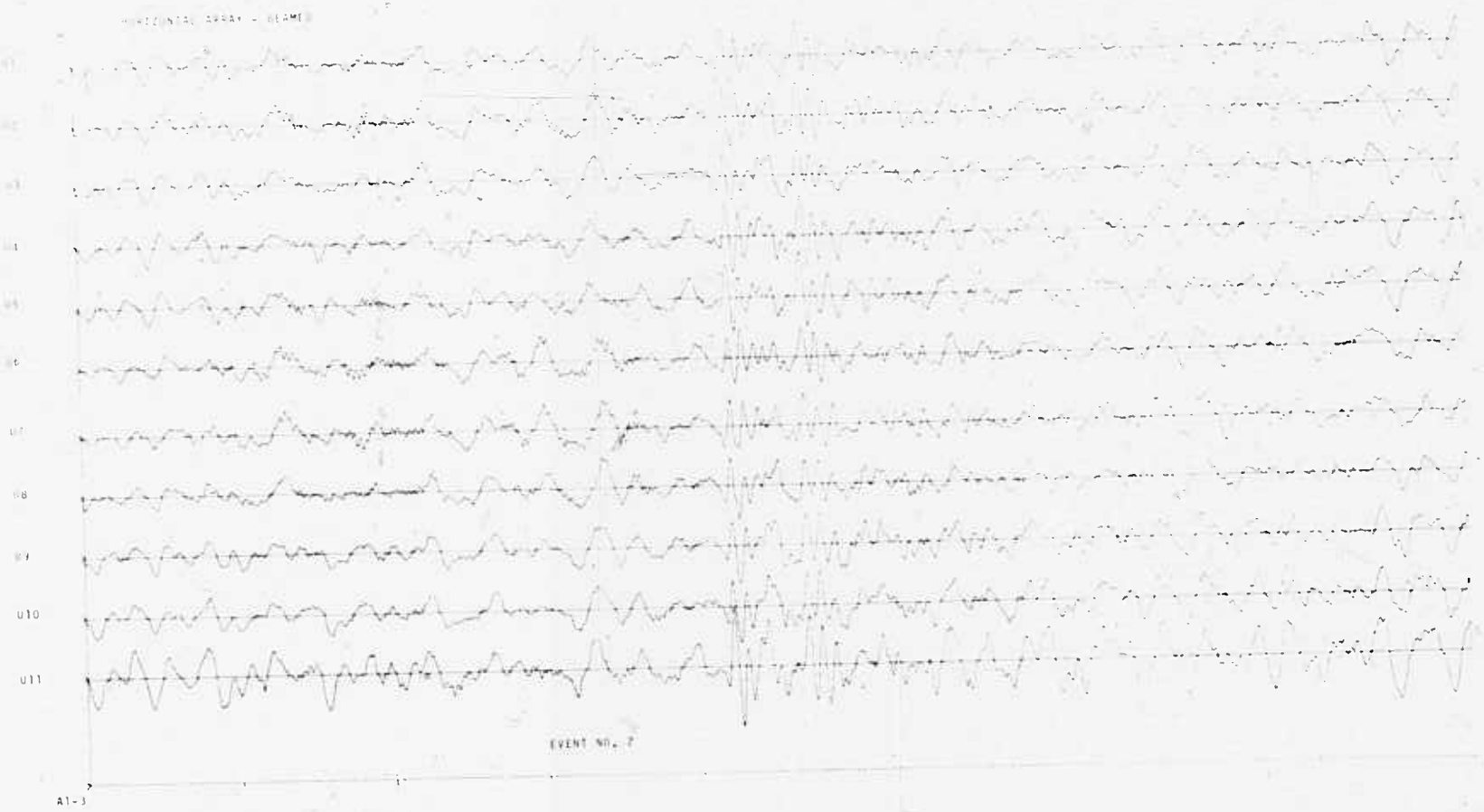
U10
U11
EVENT NR. 7
A1-3

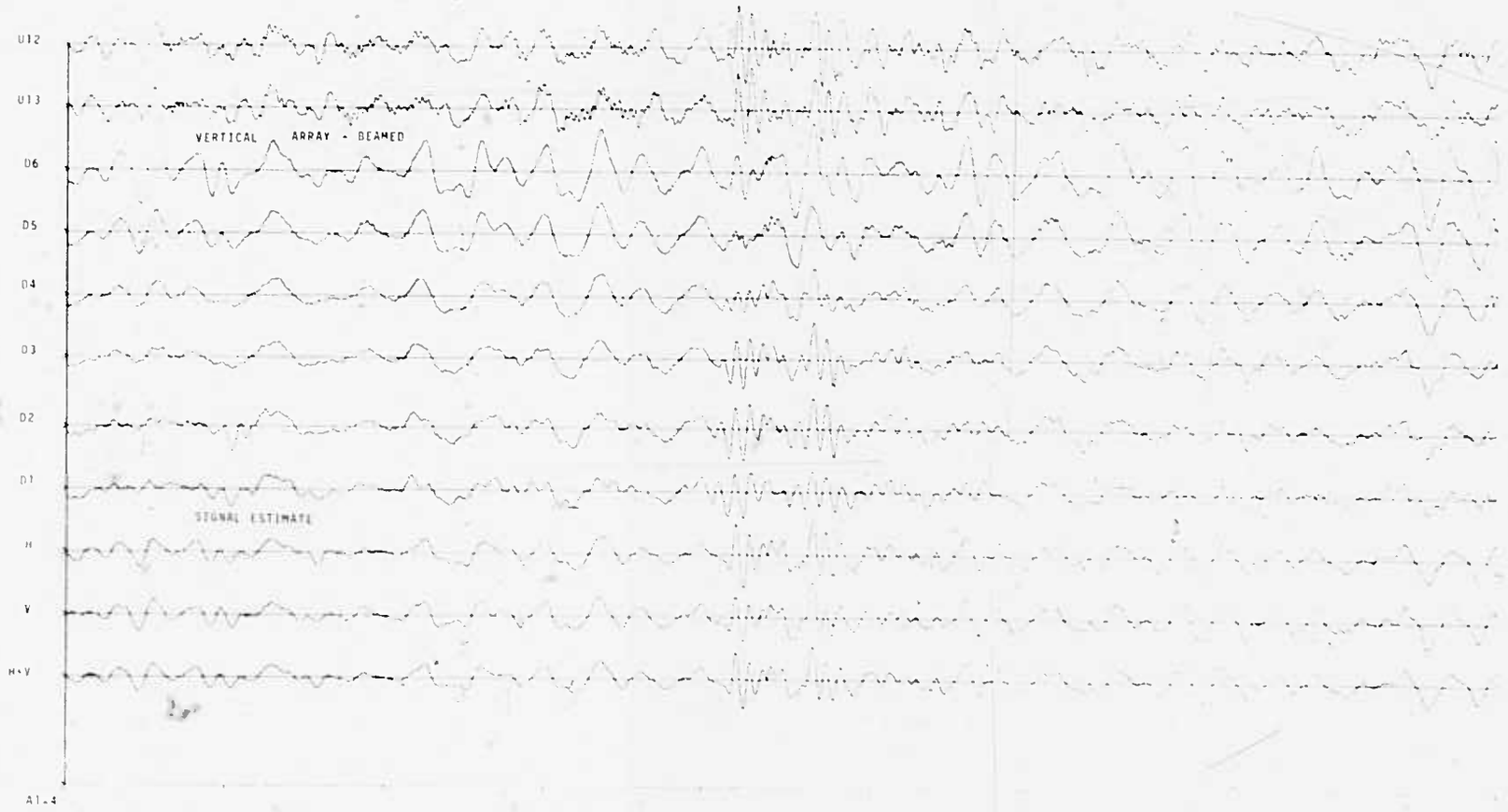
U12
U13
VERTICAL ARRAY - BEAMED
D6
D5
D4
D3
D2
D1
SIGNAL ESTIMATE
H
V
H+V
A1-4

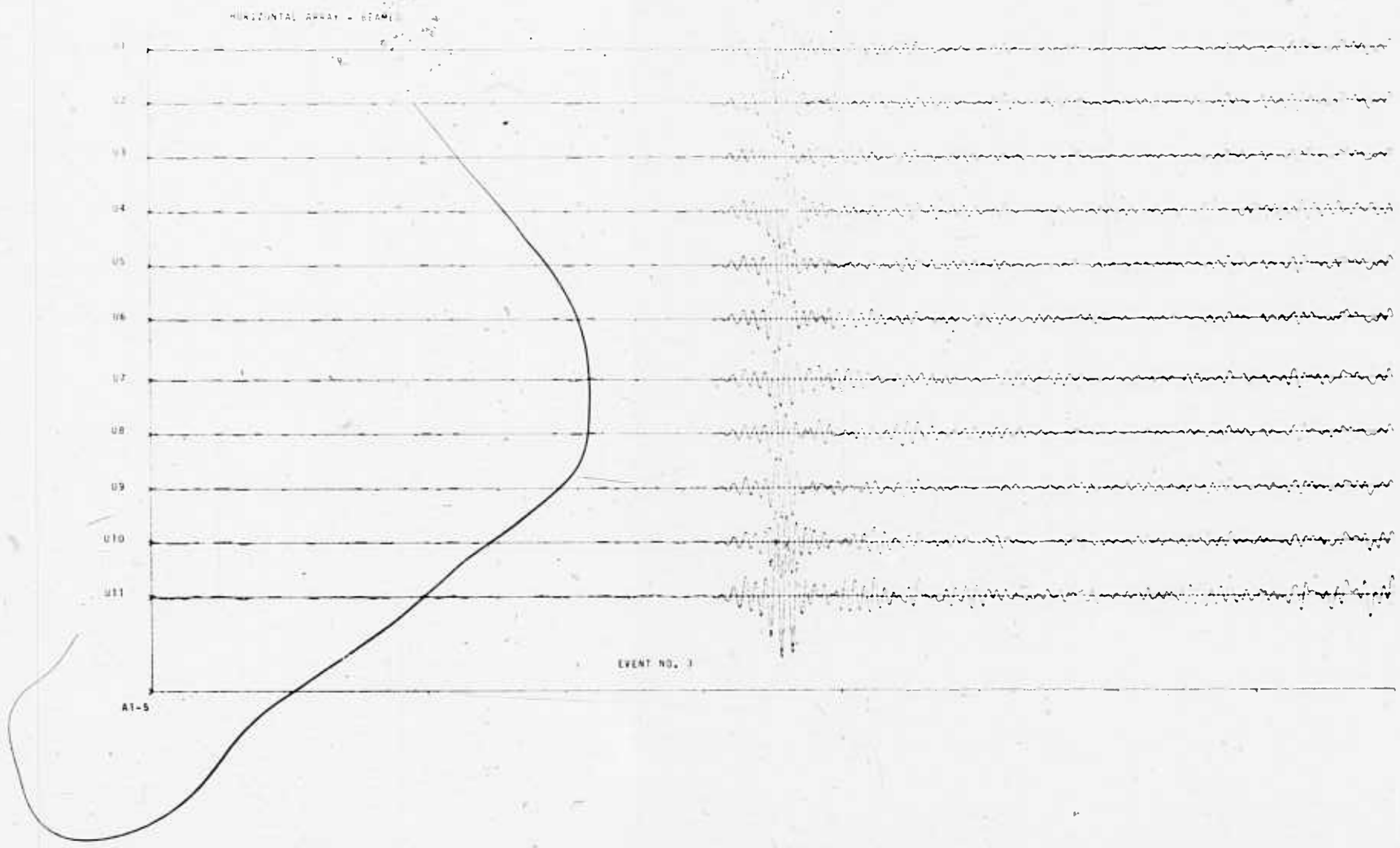
HORIZONTAL ARRAY - BEAM
U1
U2
U3
U4
U5
U6
U7
U8
U9
U10
U11
EVENT NO. 1
A1-S

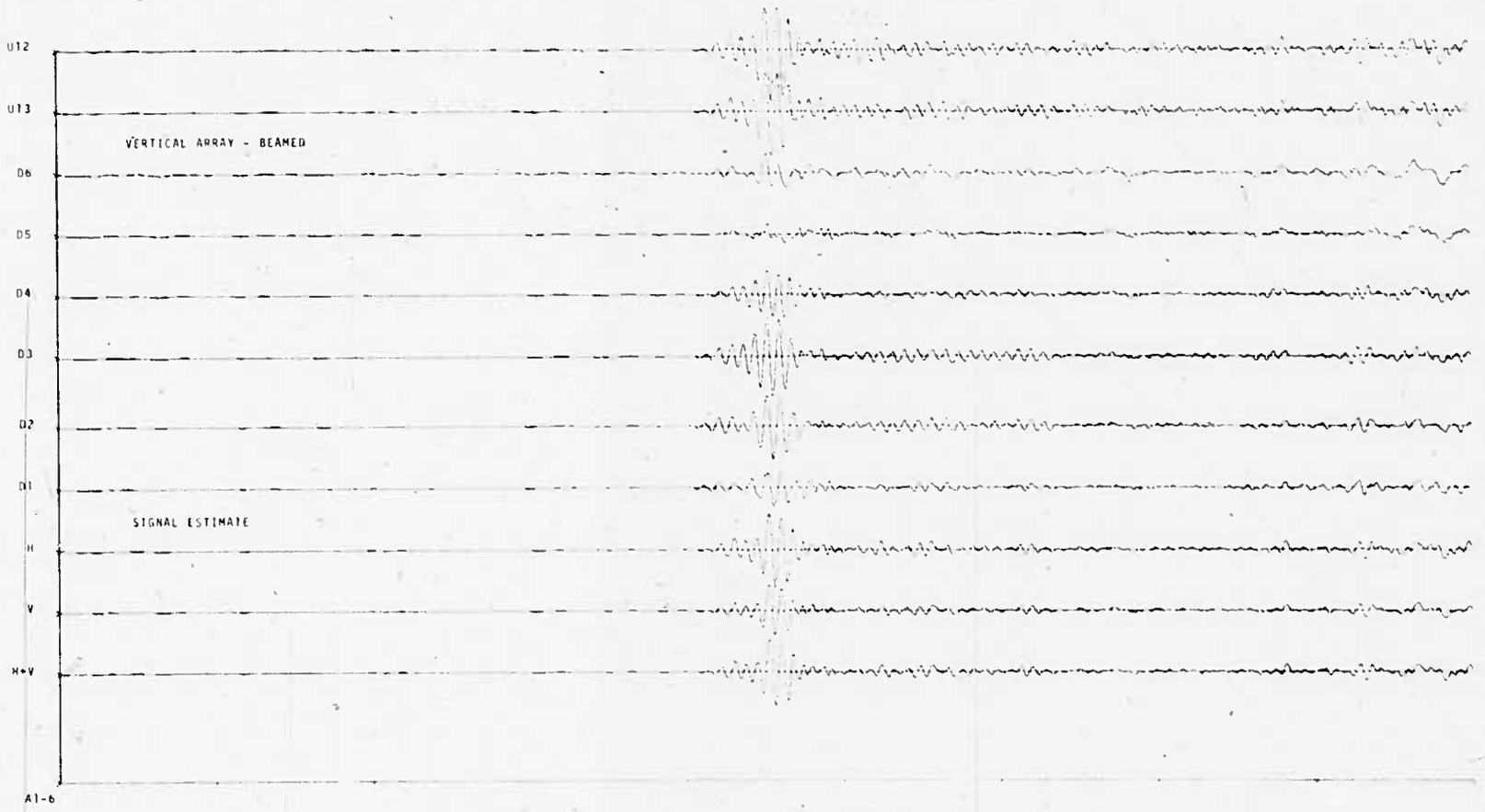
U12
U13
VERTICAL ARRAY - BEAMED
D6
D5
D4
D3
D2
D1
SIGNAL ESTIMATE
H
V
H+V
A1-6

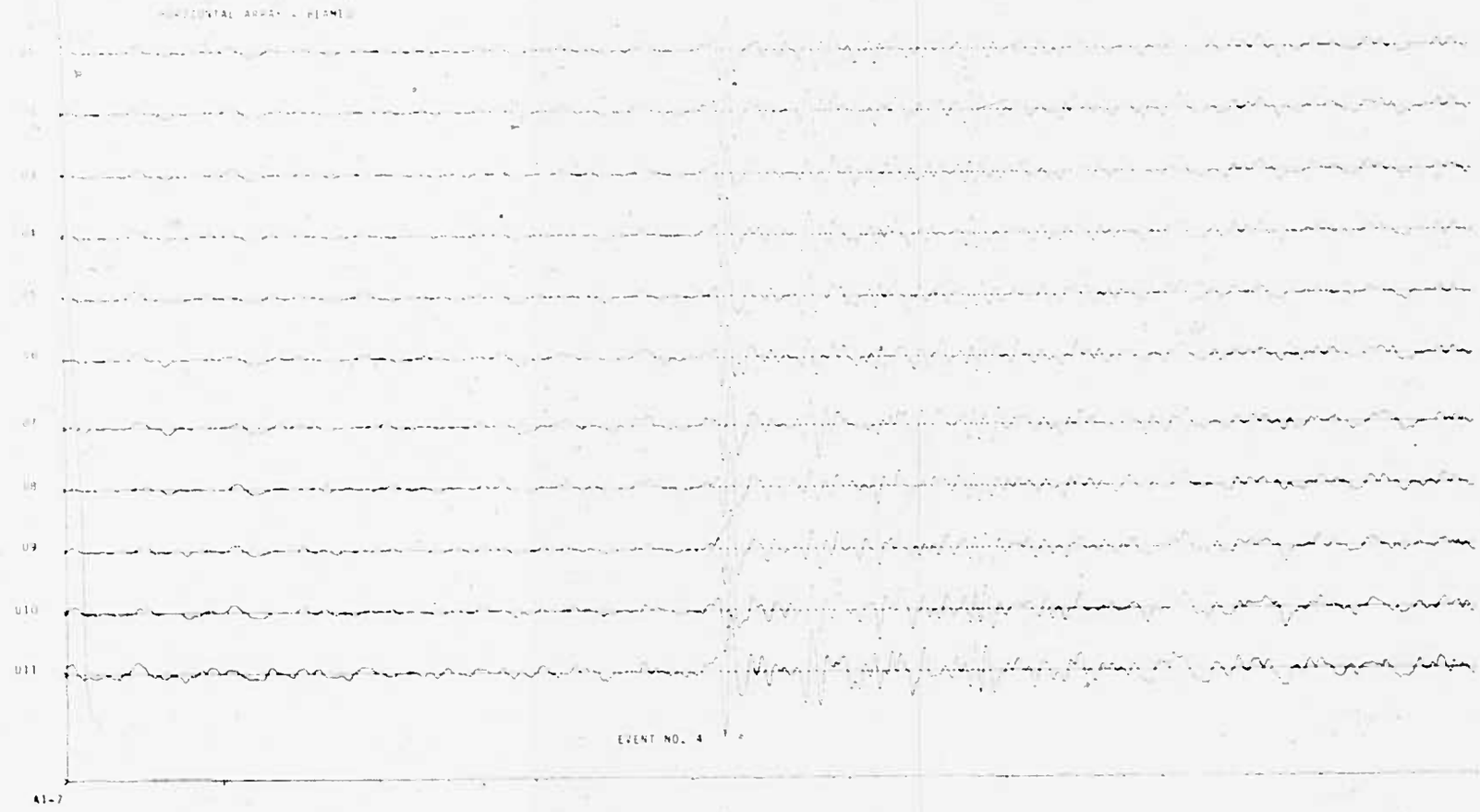

A1-7

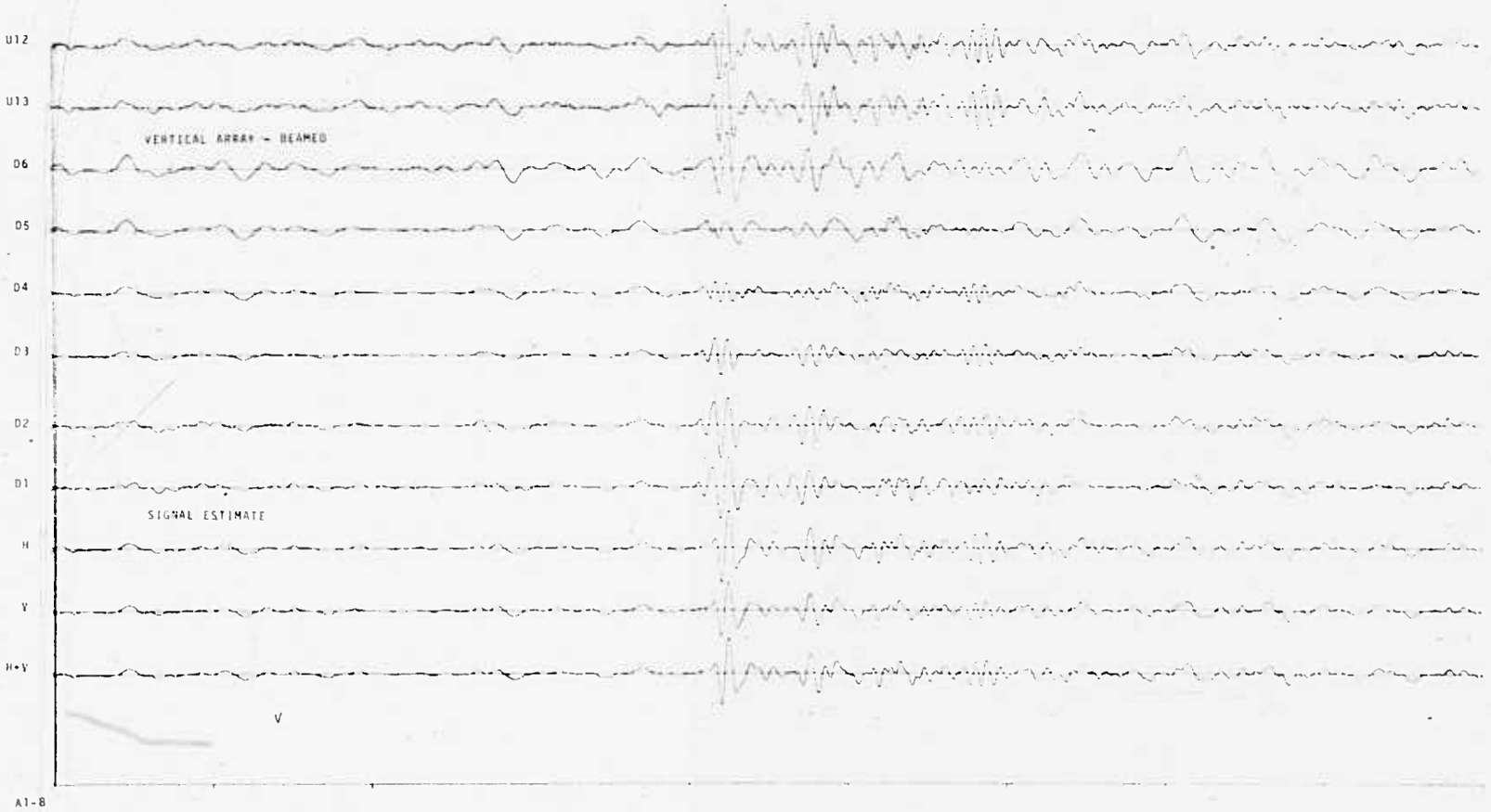
U12
U13
VERTICAL ARRAY - BEAMED
D6
D5
D4
D3
D2
D1
SIGNAL ESTIMATE
H
V
H+V
V
A1-8

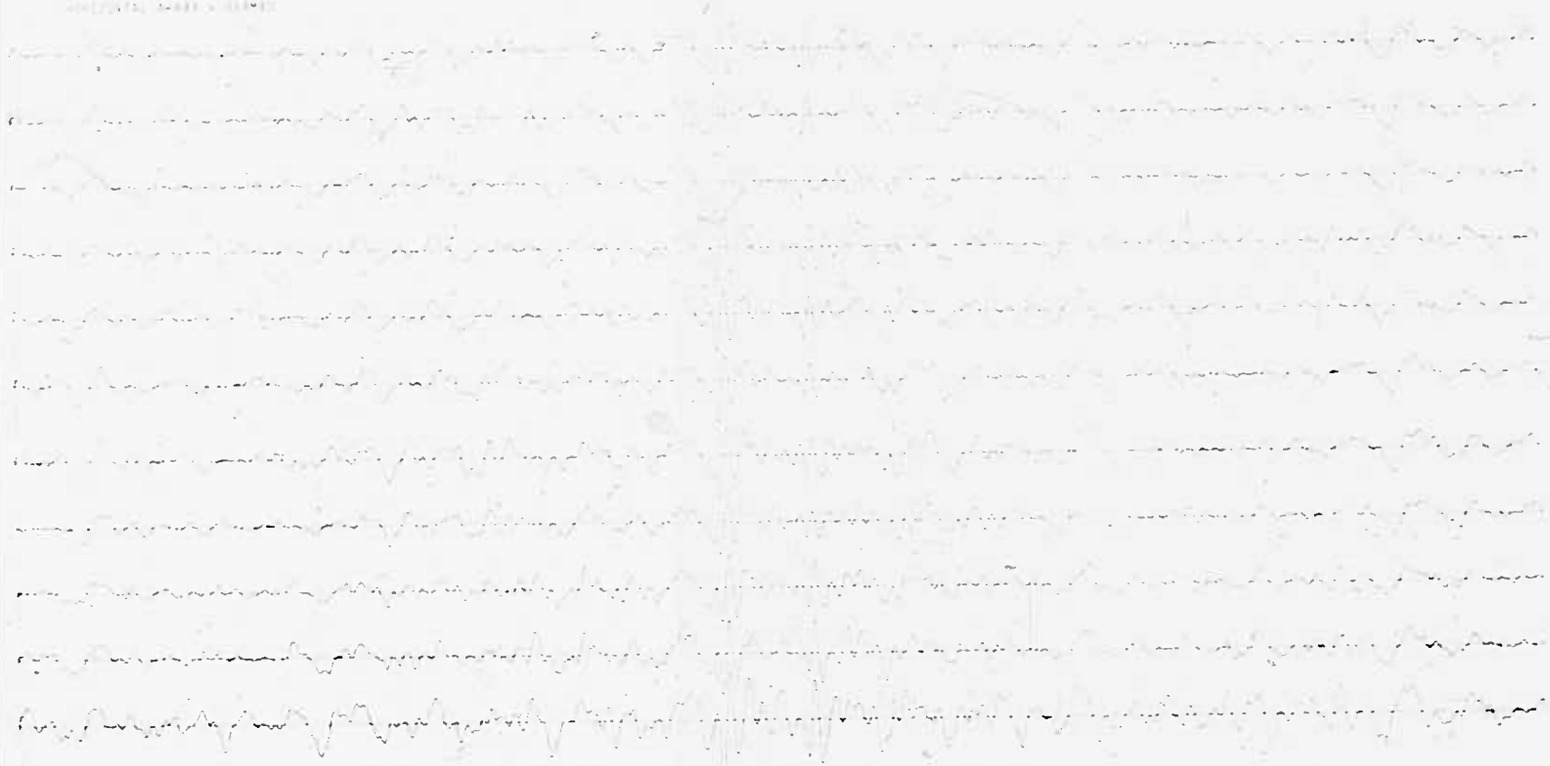

EVENT NO. 5

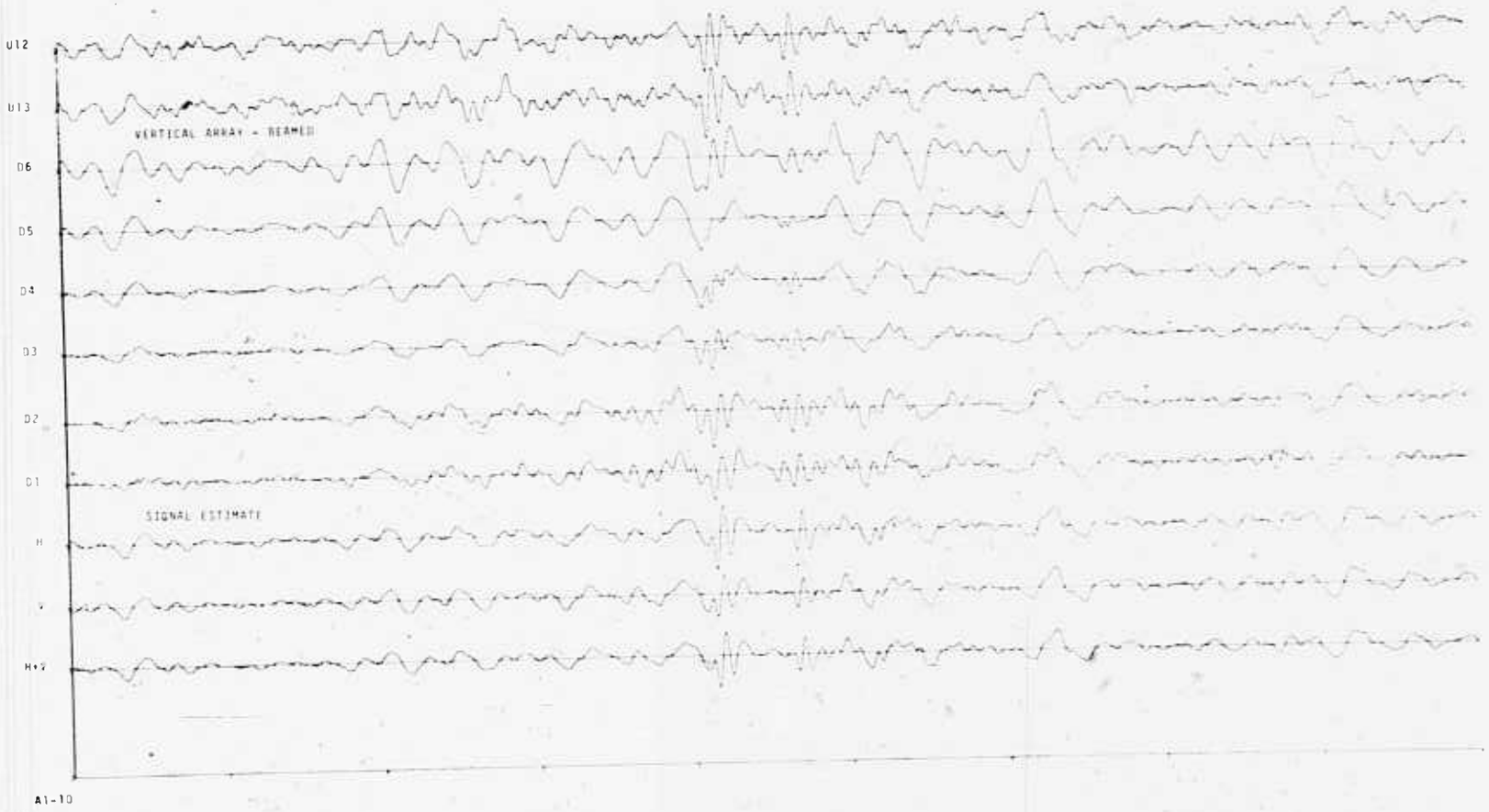
U12
U13
VERTICAL ARRAY - BEAMED
D6
D5
D4
D3
D2
D1
SIGNAL ESTIMATE
H
V
H+V
A1-10

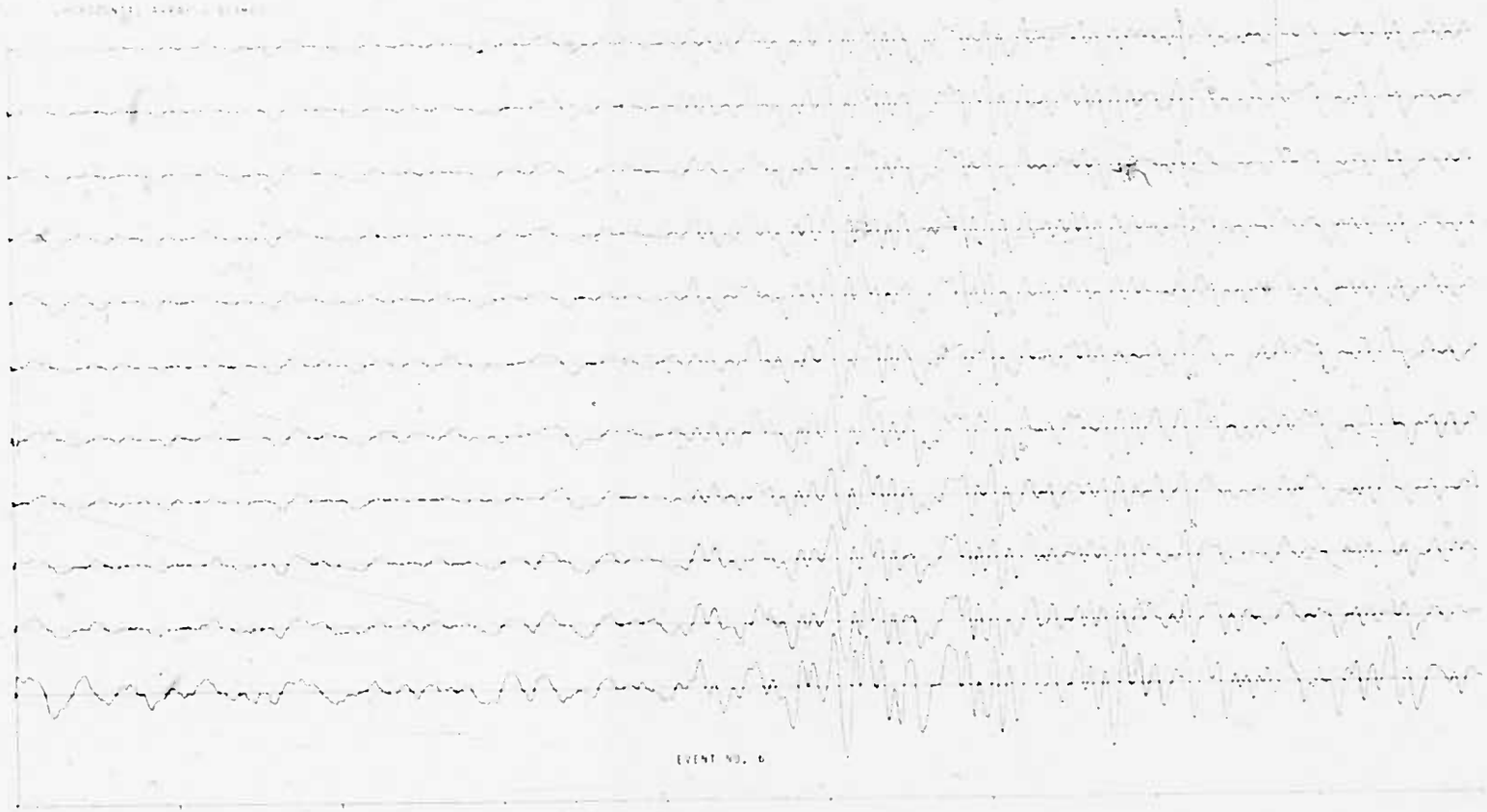
EVENT NO. 6

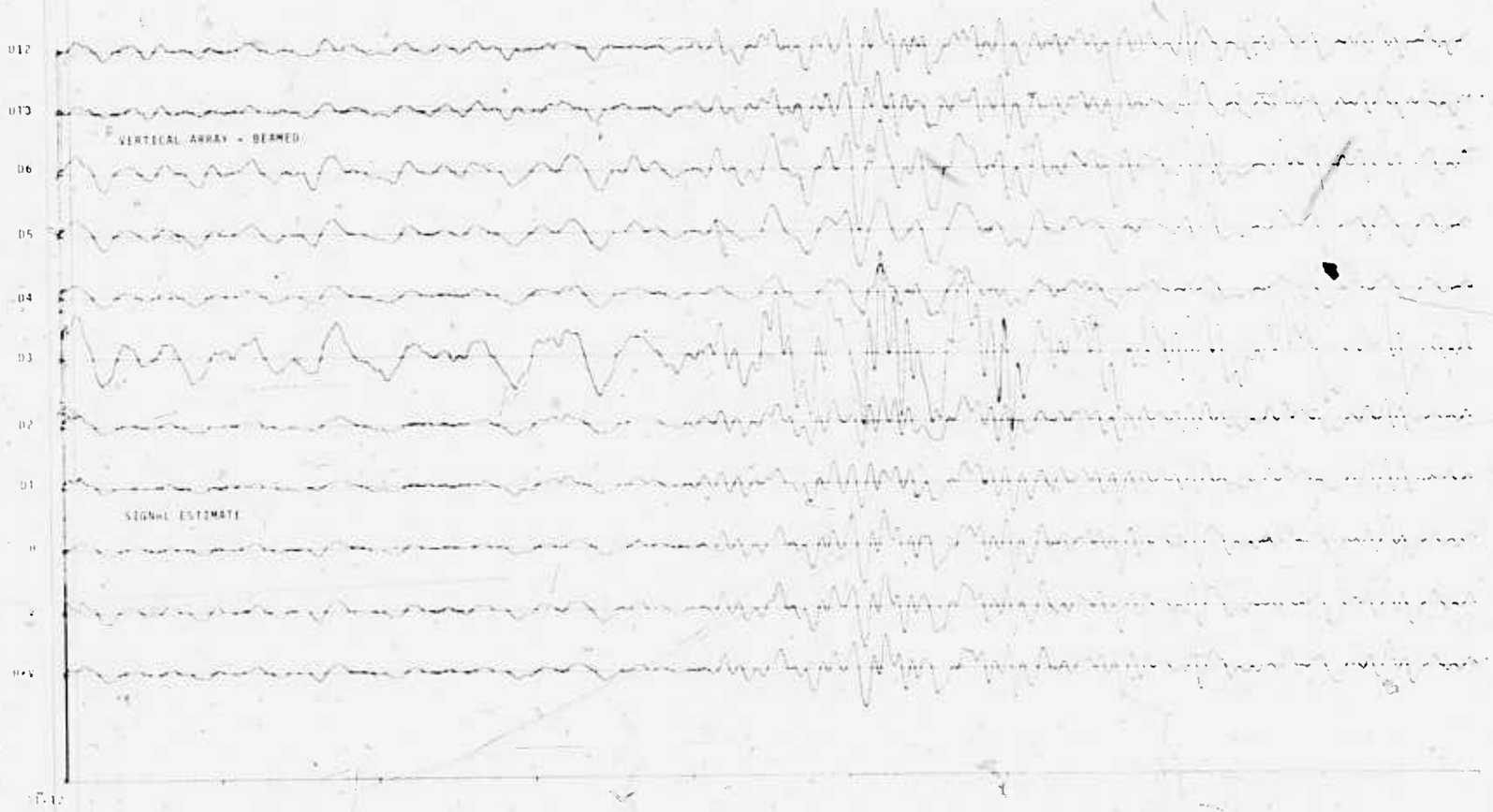
VERTICAL ARRAY - BEAMED
SIGNAL ESTIMATE

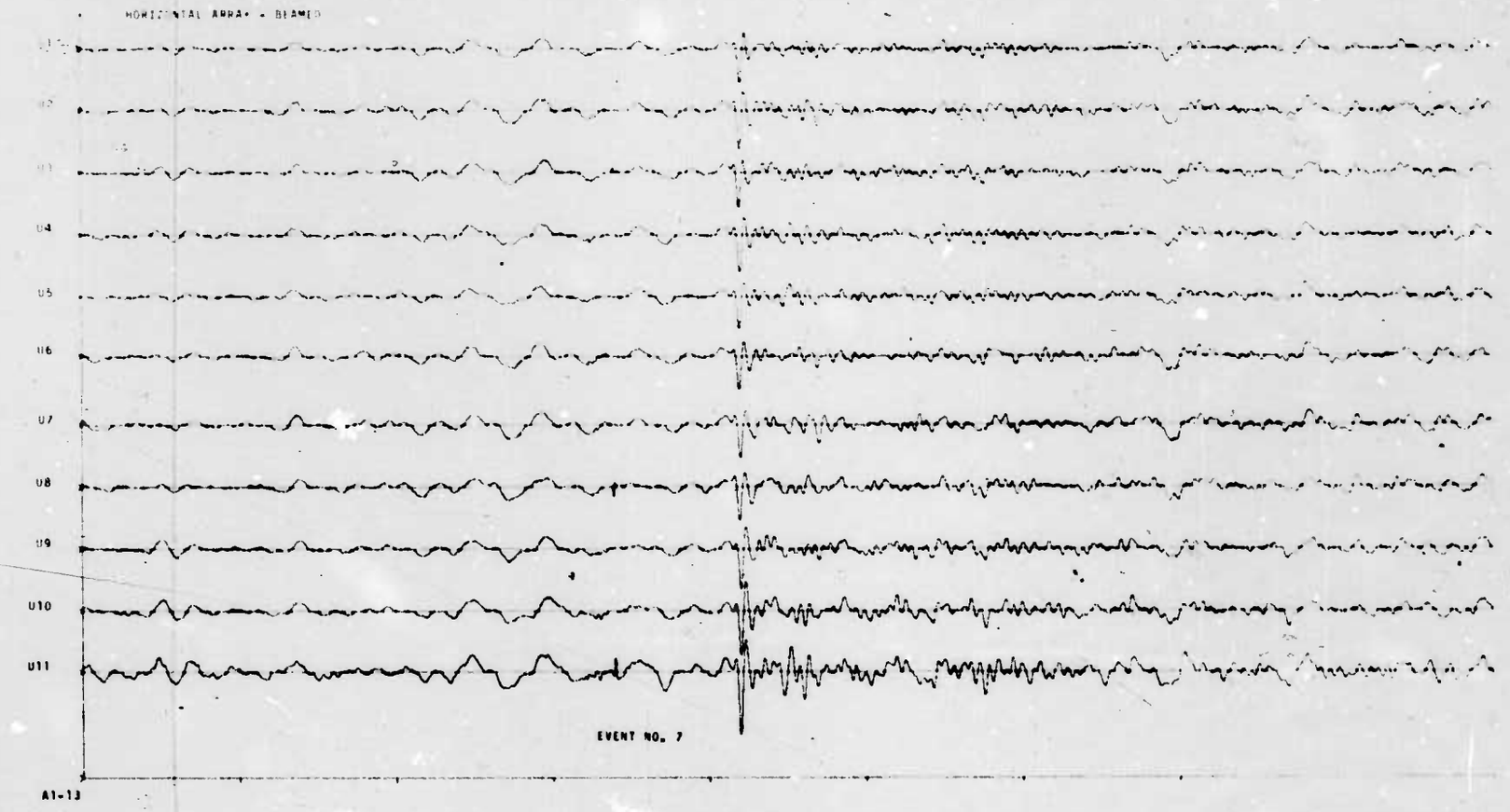
HORIZONTAL ARRAY - BEAMED
U1
U2
U3
U4
U5
U6
U7
U8
U9
U10
U11
EVENT NO. 7
A1-13

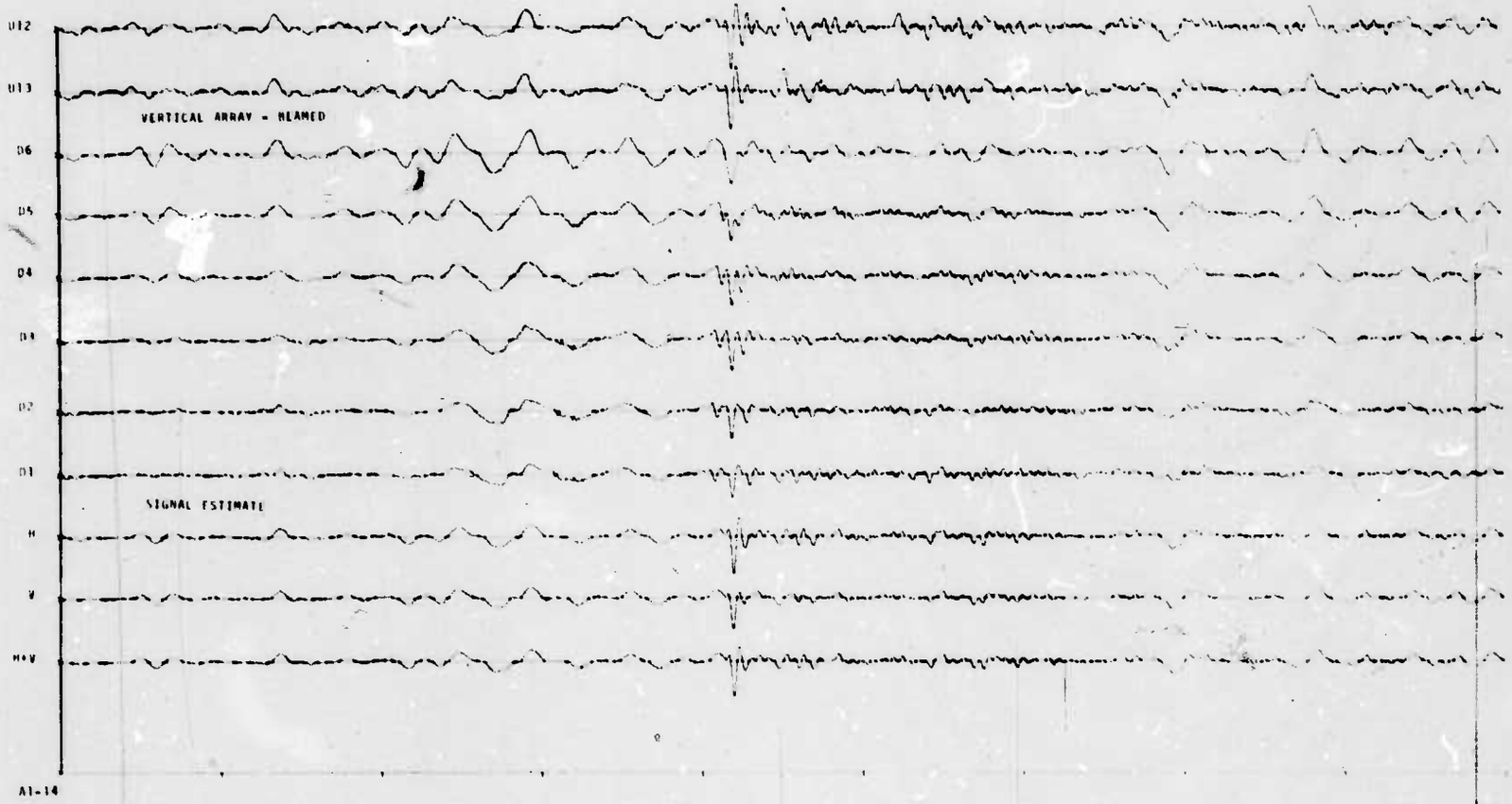
U12
U13
VERTICAL ARRAY - BEAMED
D6
D5
D4
D3
D2
D1
SIGNAL ESTIMATE
H
V
H+V
A1-14

APPENDIX 2

GAIN EQUALIZED CHANNELS

U1-U13	Horizontal Array
D6-D1	Vertical Array
H	Signal Estimate on Horizontal Array After Gain Equalization
V	Signal Estimate on Vertical Array After Gain Equalization
H+V	Signal Estimate on Combined Array After Gain Equalization

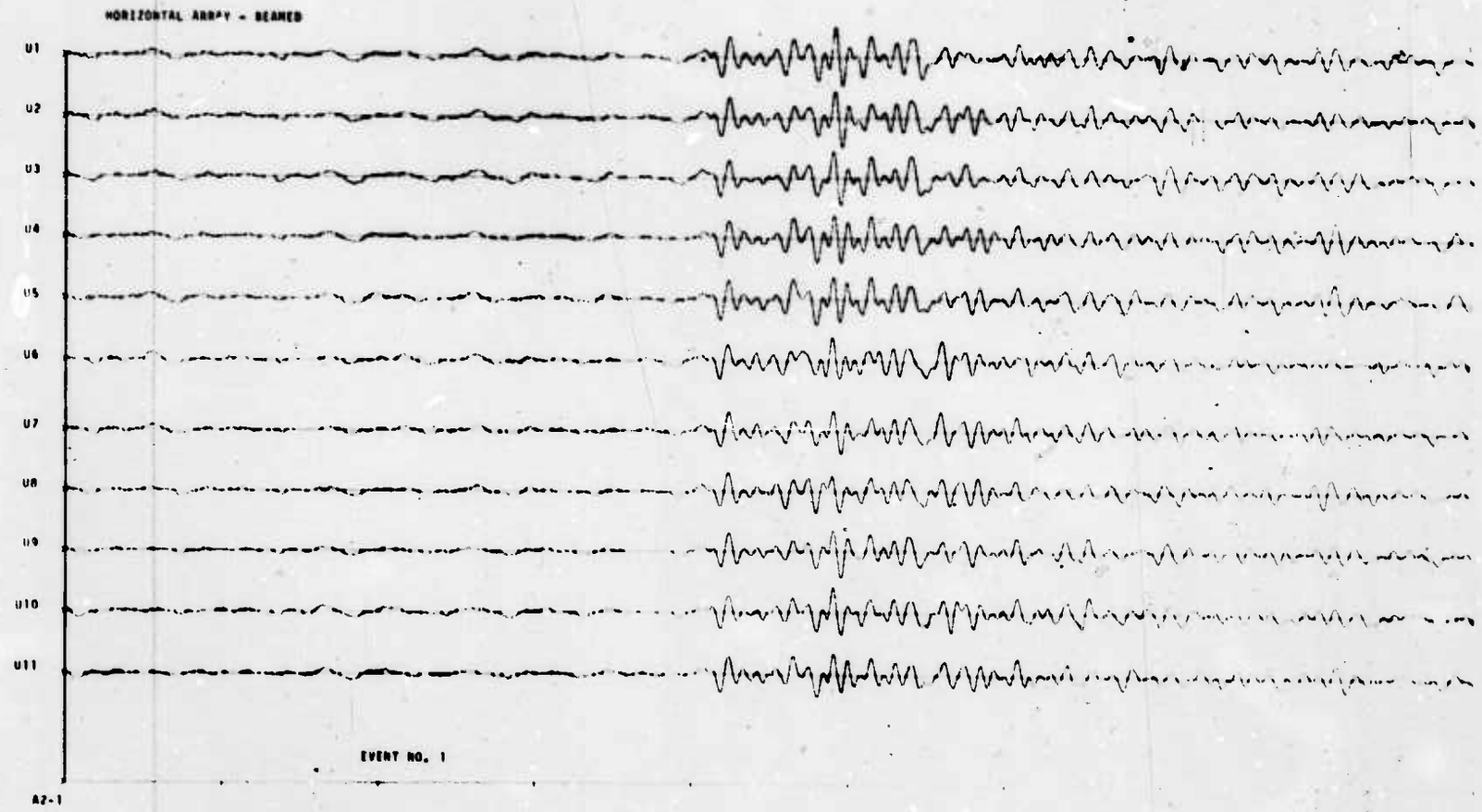
HORIZONTAL ARRAY - BEAMED
U1
U2
U3
U4
U5
U6
U7
U8
U9
U10
U11
EVENT NO. 1
A2-1

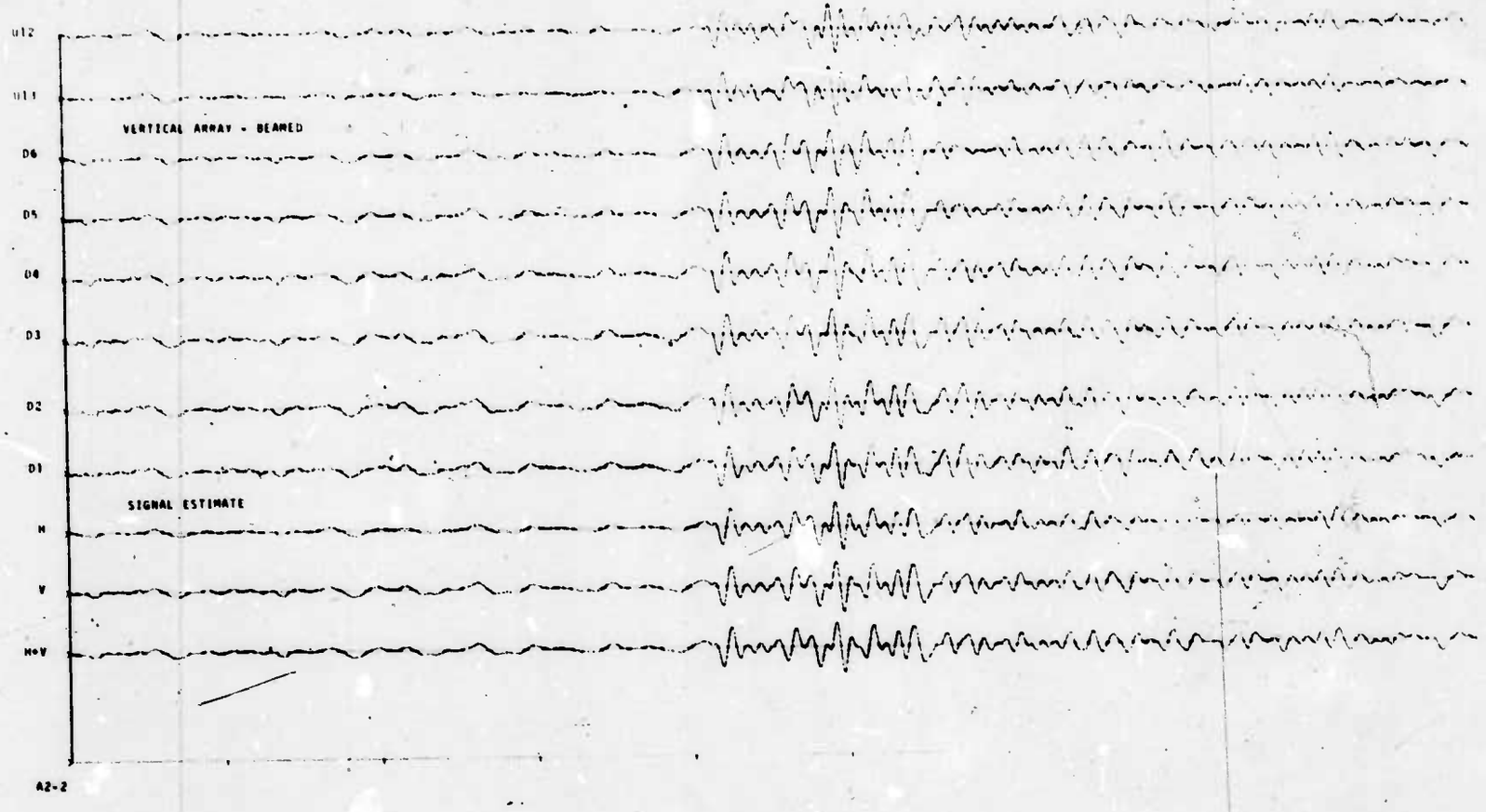
U12
U11
VERTICAL ARRAY - BEAMED
D6
D5
D4
D3
D2
D1
SIGNAL ESTIMATE
H
V
H+V
A2-2

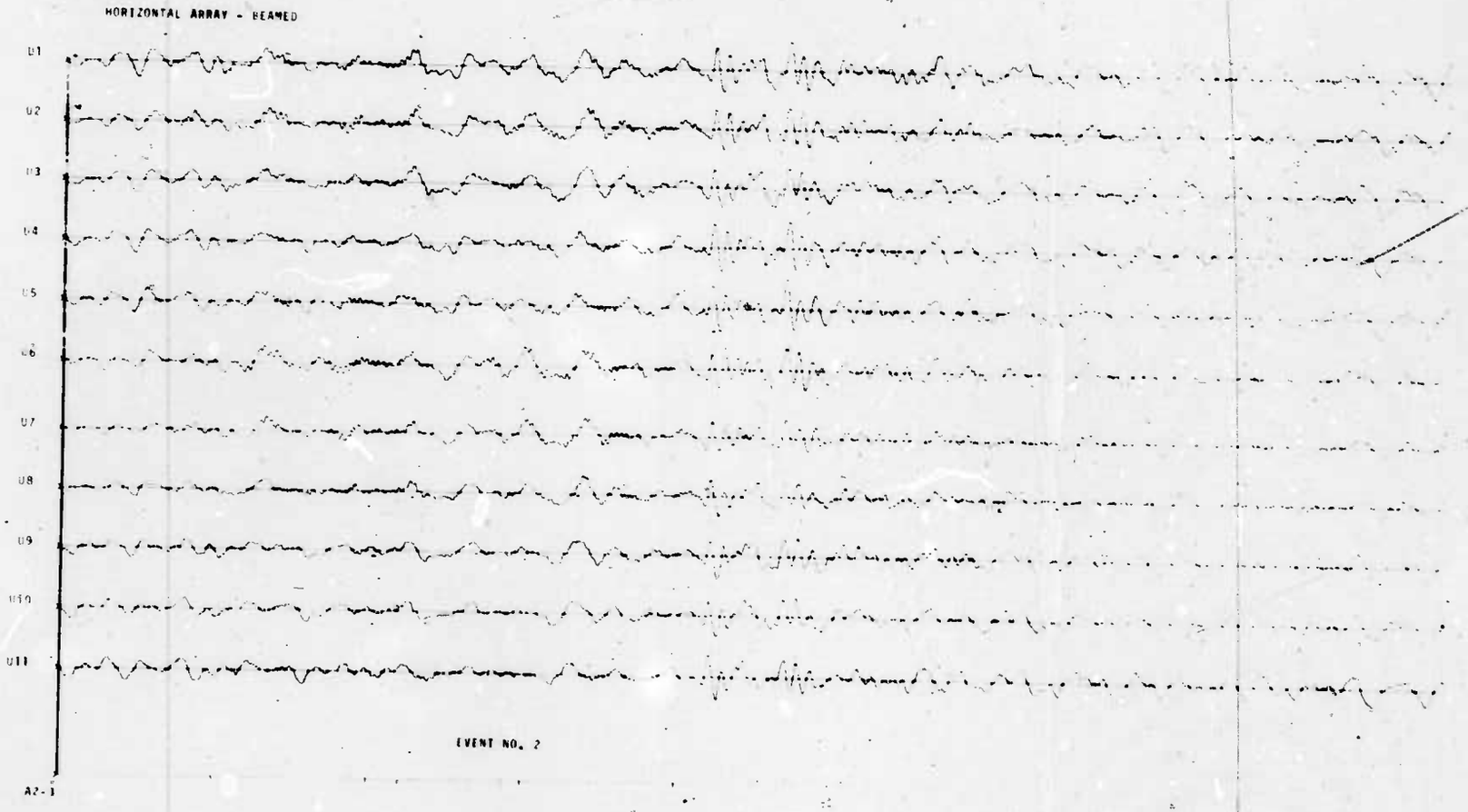
HORIZONTAL ARRAY - BEAMED
U1
U2
U3
U4
U5
U6
U7
U8
U9
U10
U11
A2-1
EVENT NO. 2

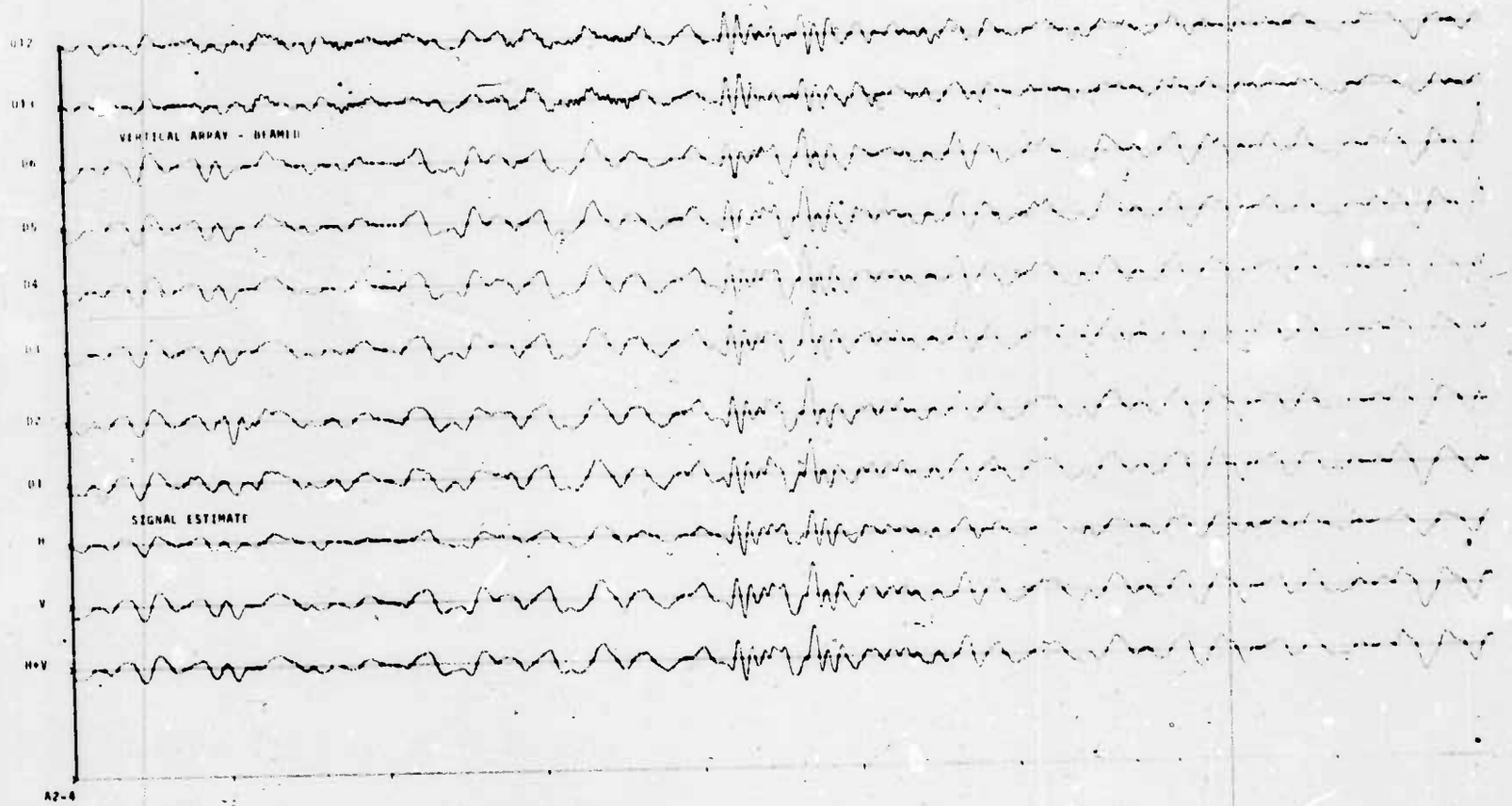
VERTICAL ARRAY - BEAM 11
SIGNAL ESTIMATE
H
V
H+V
A2-6

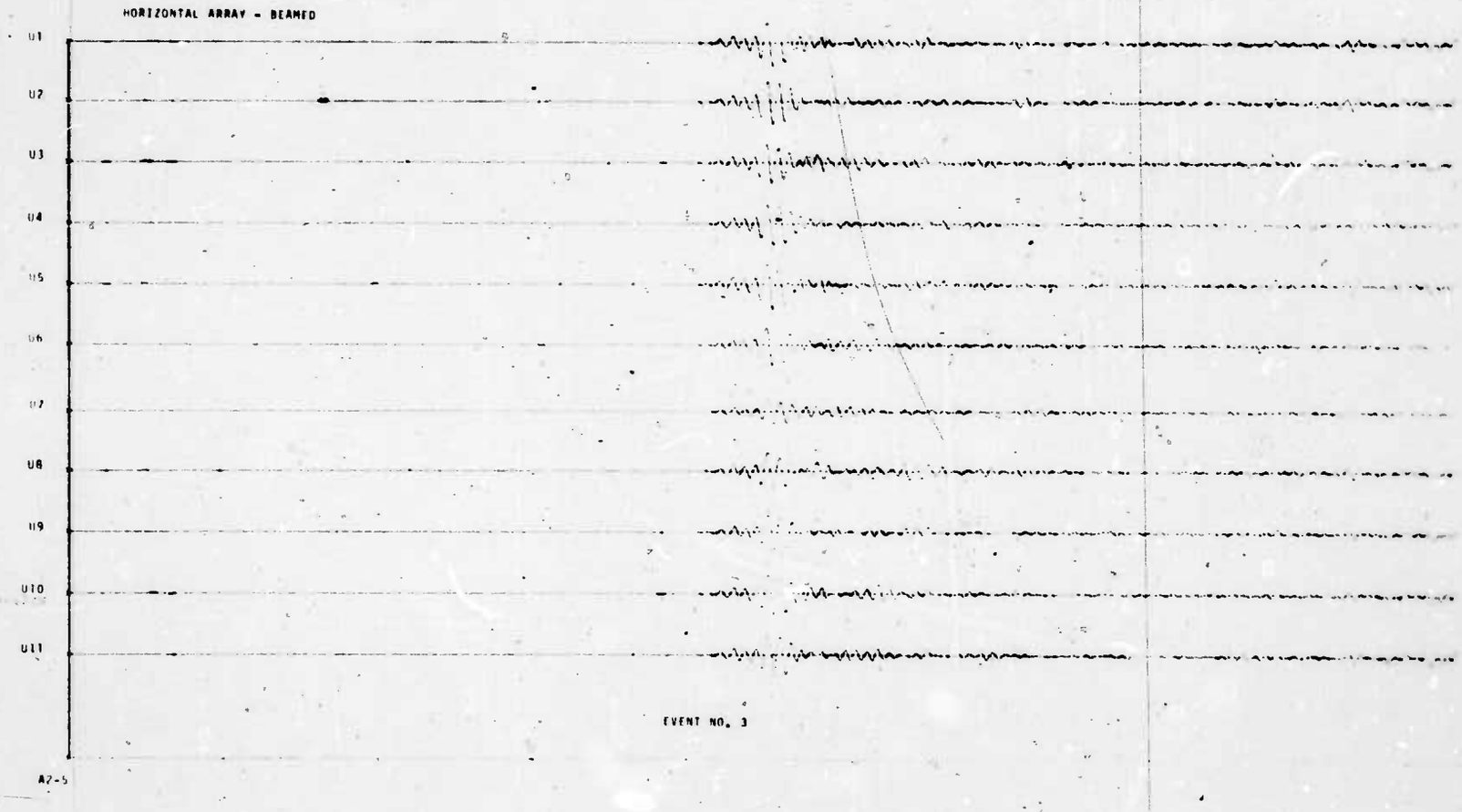
HORIZONTAL ARRAY - BEAMED
U1
U2
U3
U4
U5
U6
U7
U8
U9
U10
U11
EVENT NO. 3
A2-5

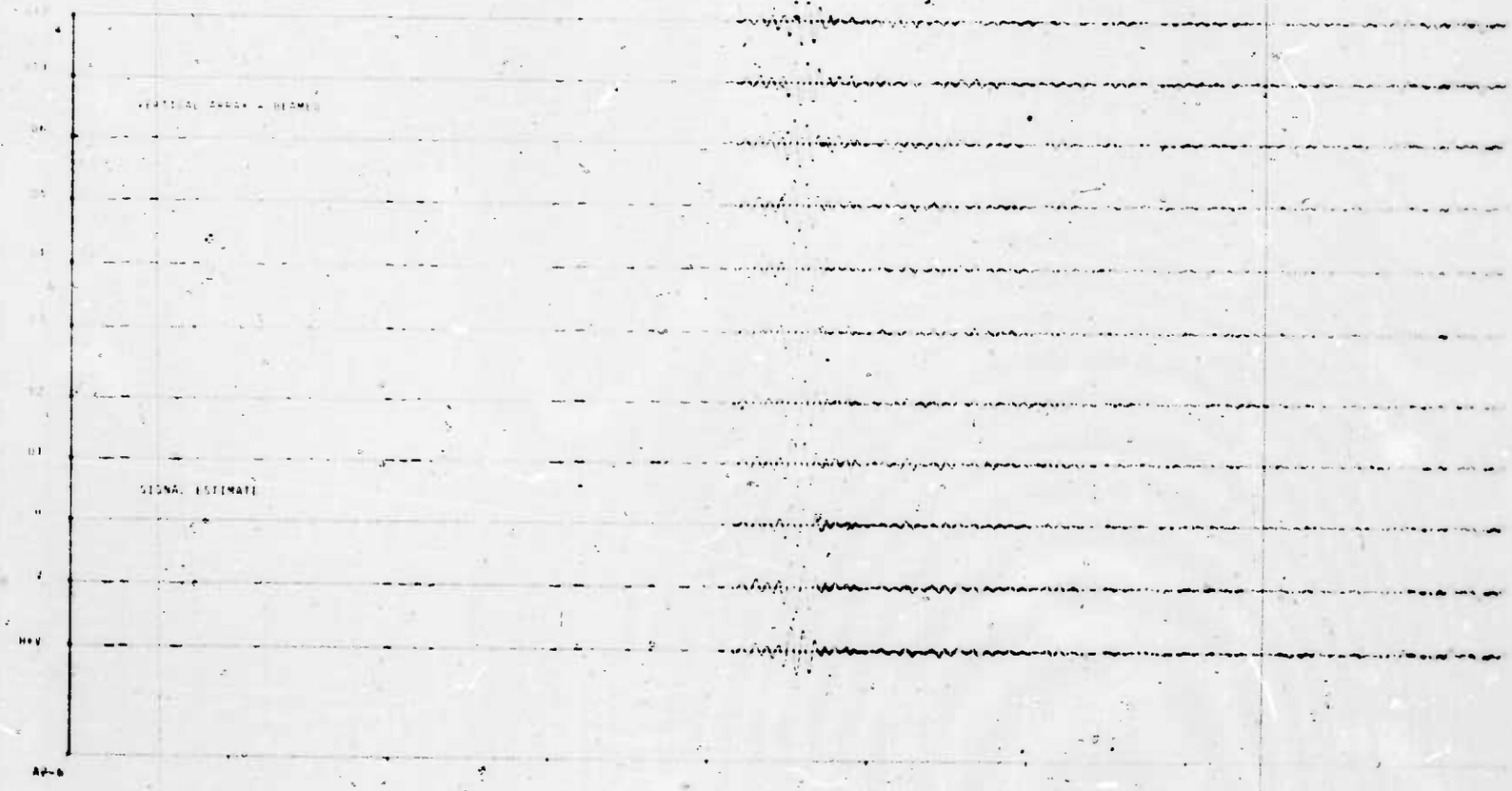
SIGNAL ESTIMATE

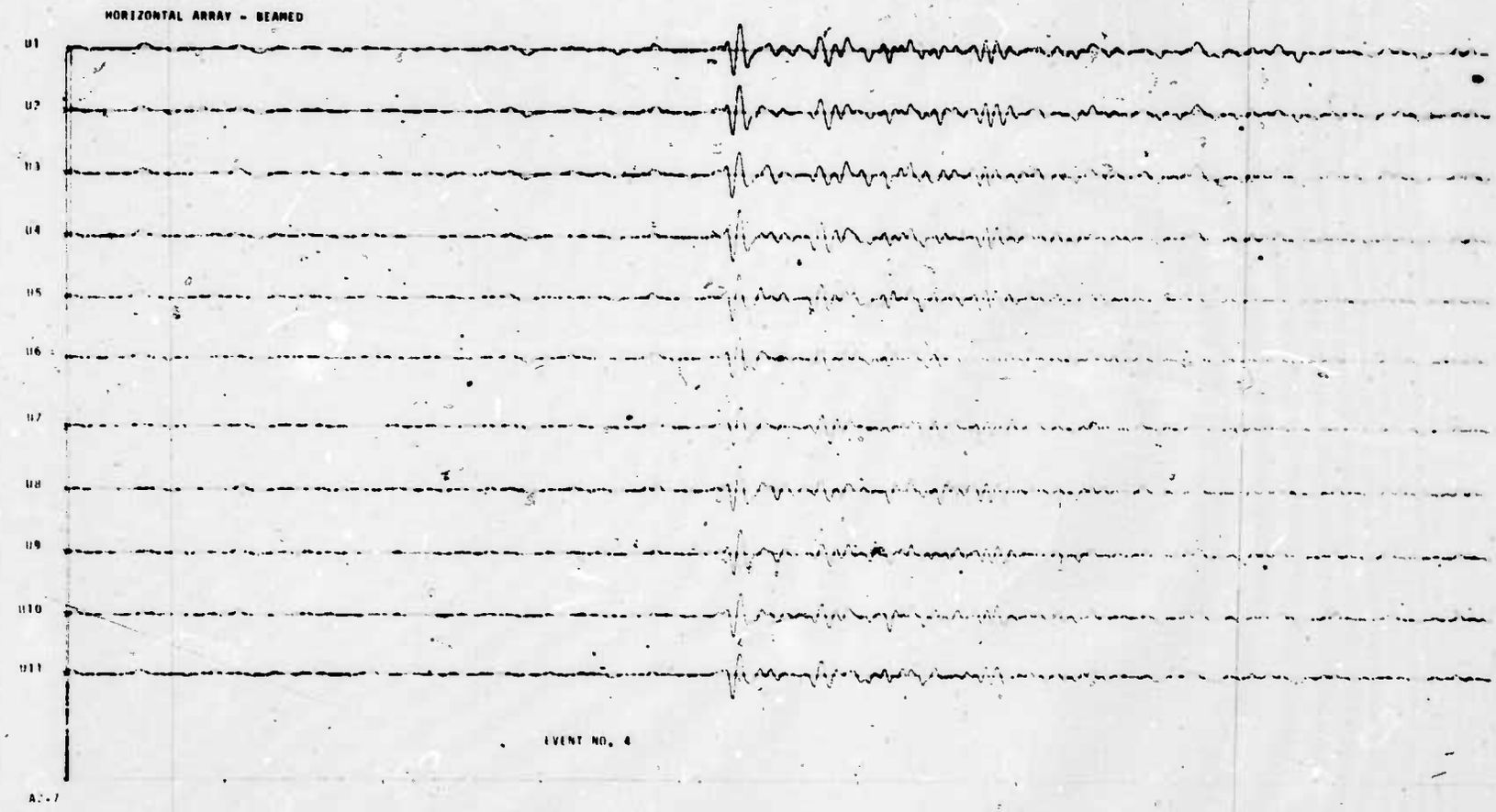
HORIZONTAL ARRAY - BEAMED
U1
U2
U3
U4
U5
U6
U7
U8
U9
U10
U11
EVENT NO. 4

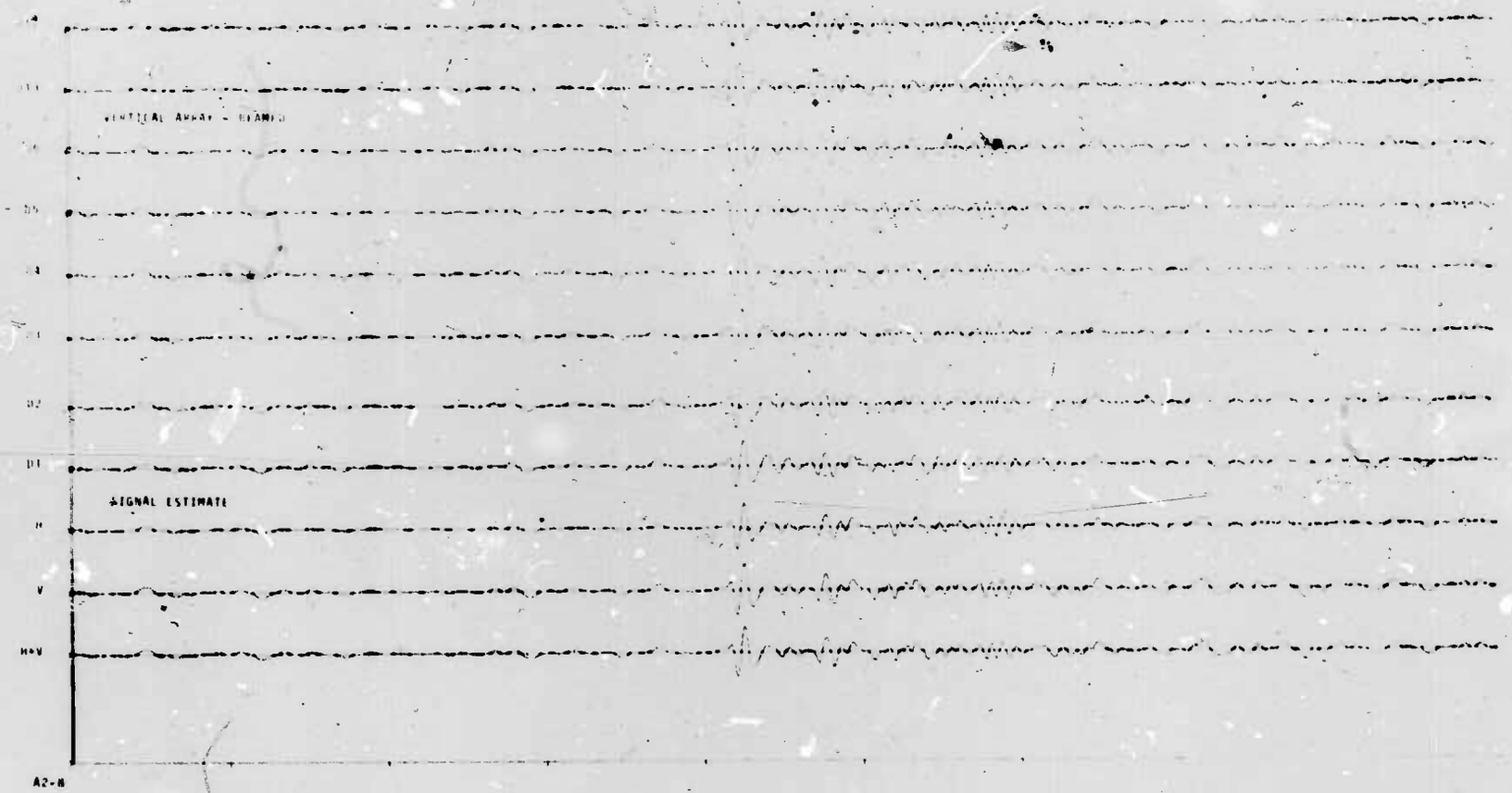
VERTICAL ARRAY - BEAM 0
SIGNAL ESTIMATE
A2-8

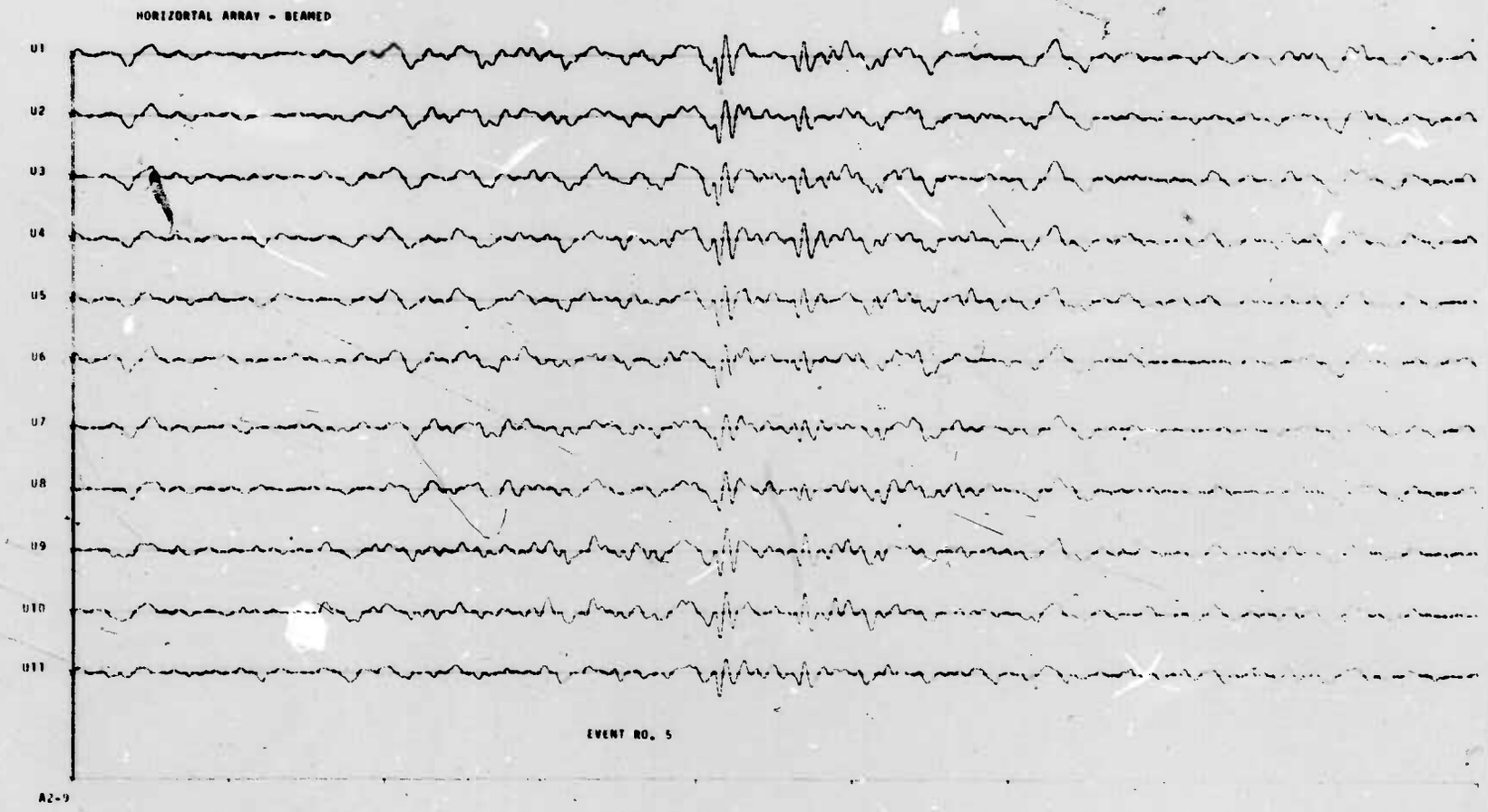
HORIZONTAL ARRAY - BEAMED
U1
U2
U3
U4
U5
U6
U7
U8
U9
U10
U11
EVENT NO. 5
A2-9

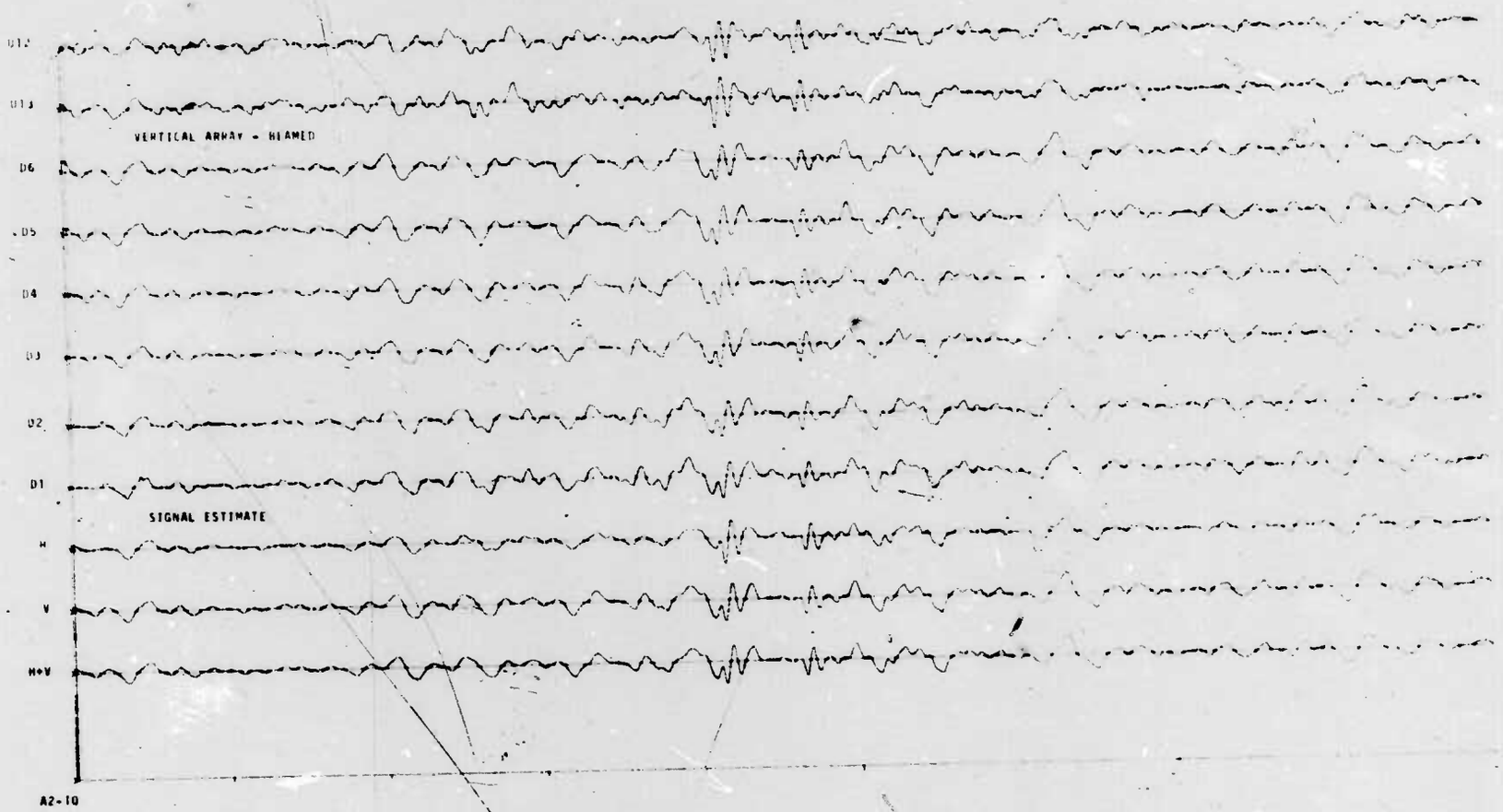
D12
D11
VERTICAL ARRAY - BEAMED
D6
D5
D4
D3
D2
D1
SIGNAL ESTIMATE
H
V
H+V
A2-10

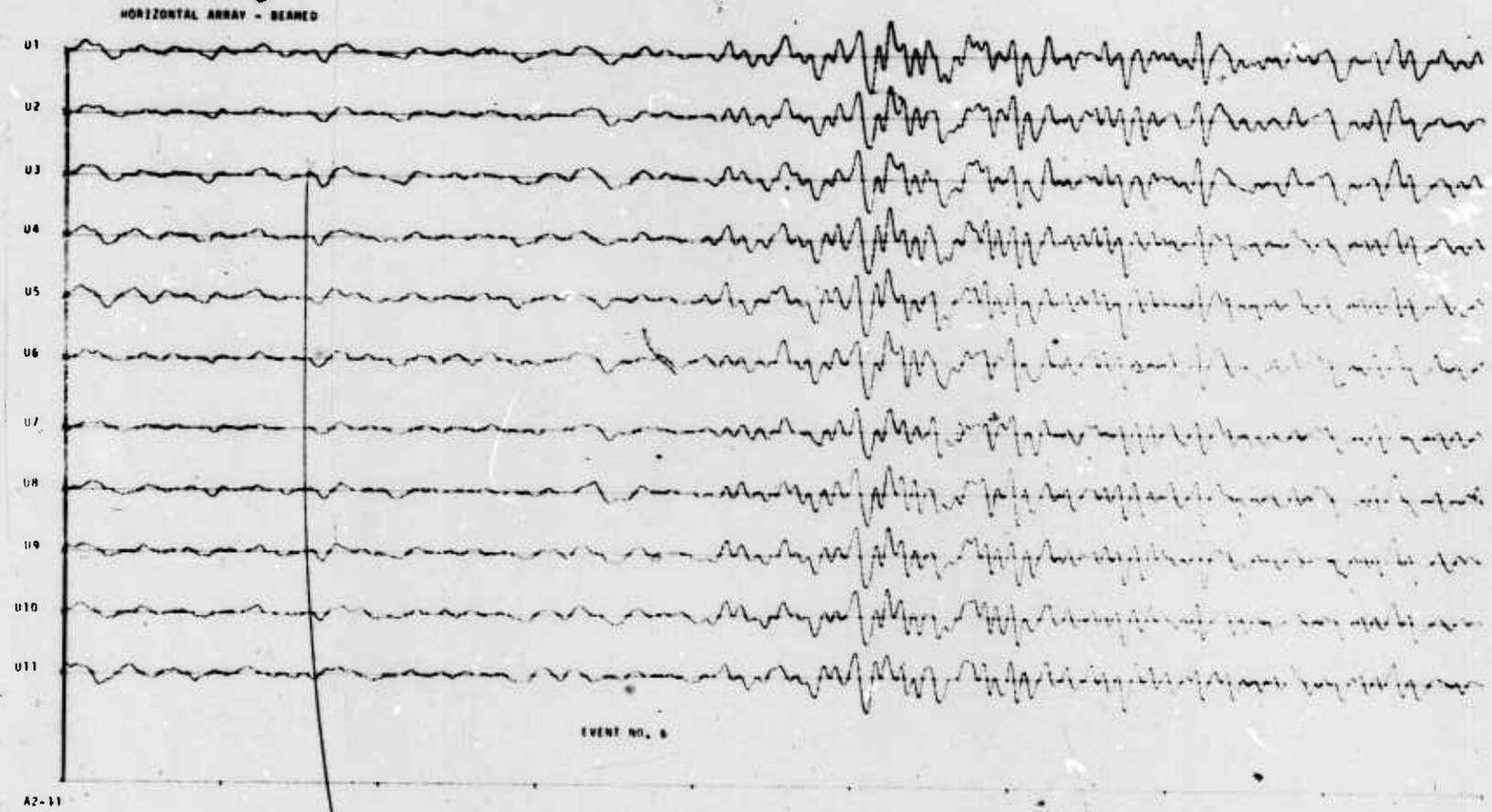
HORIZONTAL ARRAY - BEAMED
U1
U2
U3
U4
U5
U6
U7
U8
U9
U10
U11
EVENT NO. 6
A2-11

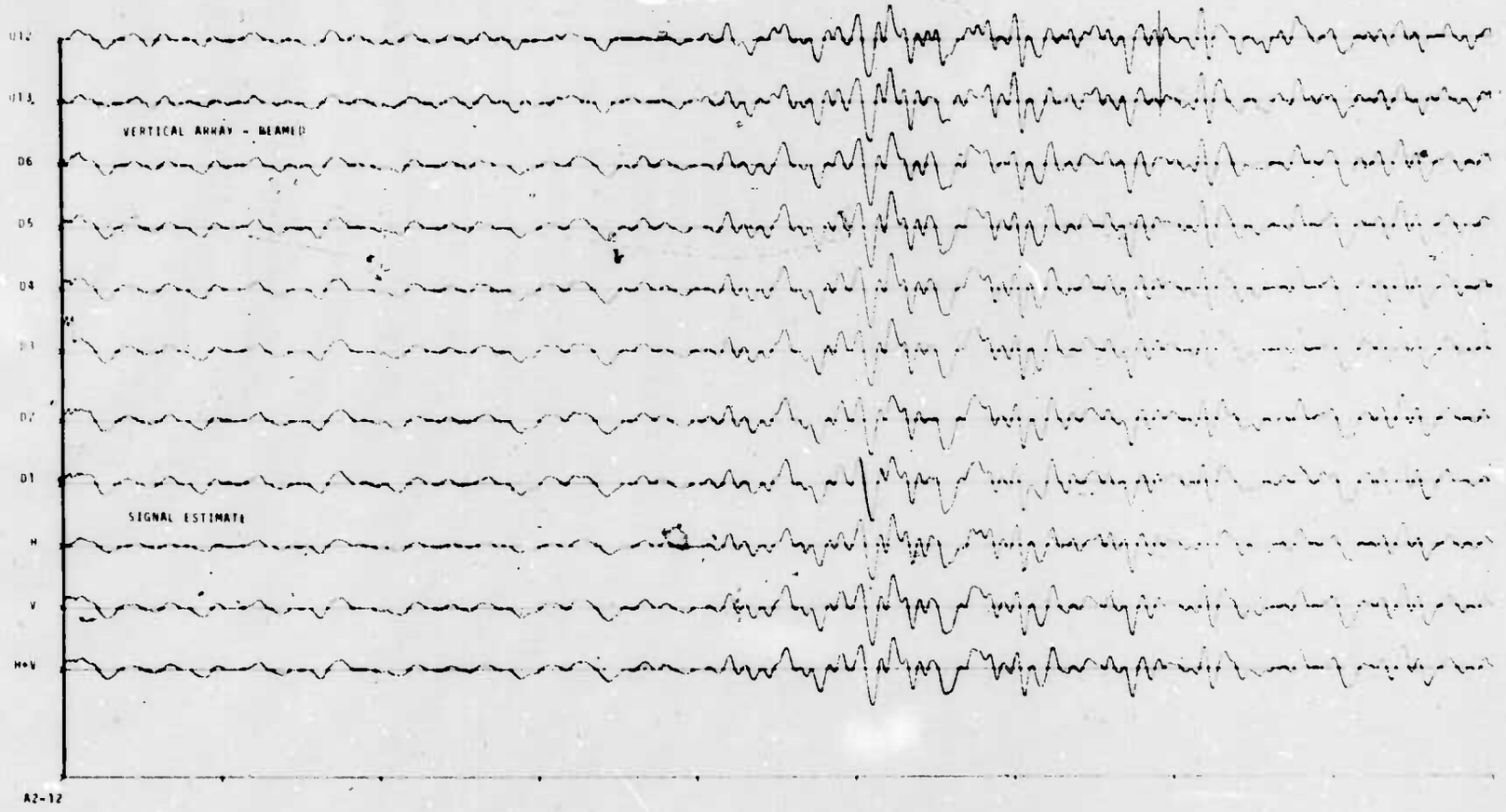
VERTICAL ARRAY - BEAMED
SIGNAL ESTIMATE
H
V
H+V
A2-12

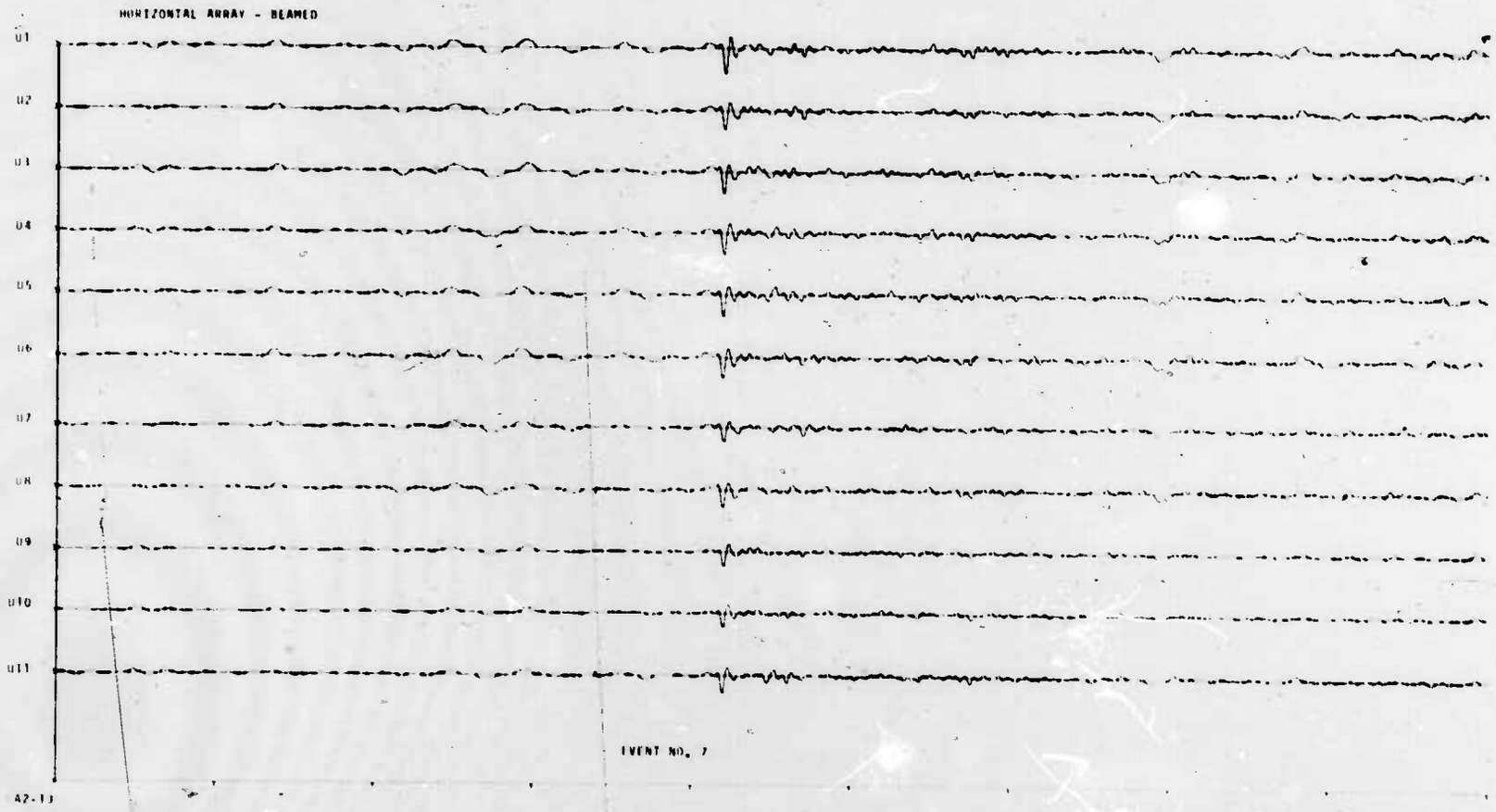
HORIZONTAL ARRAY - BEAMED
U1
U2
U3
U4
U5
U6
U7
U8
U9
U10
U11
EVENT NO. 7
A2-13

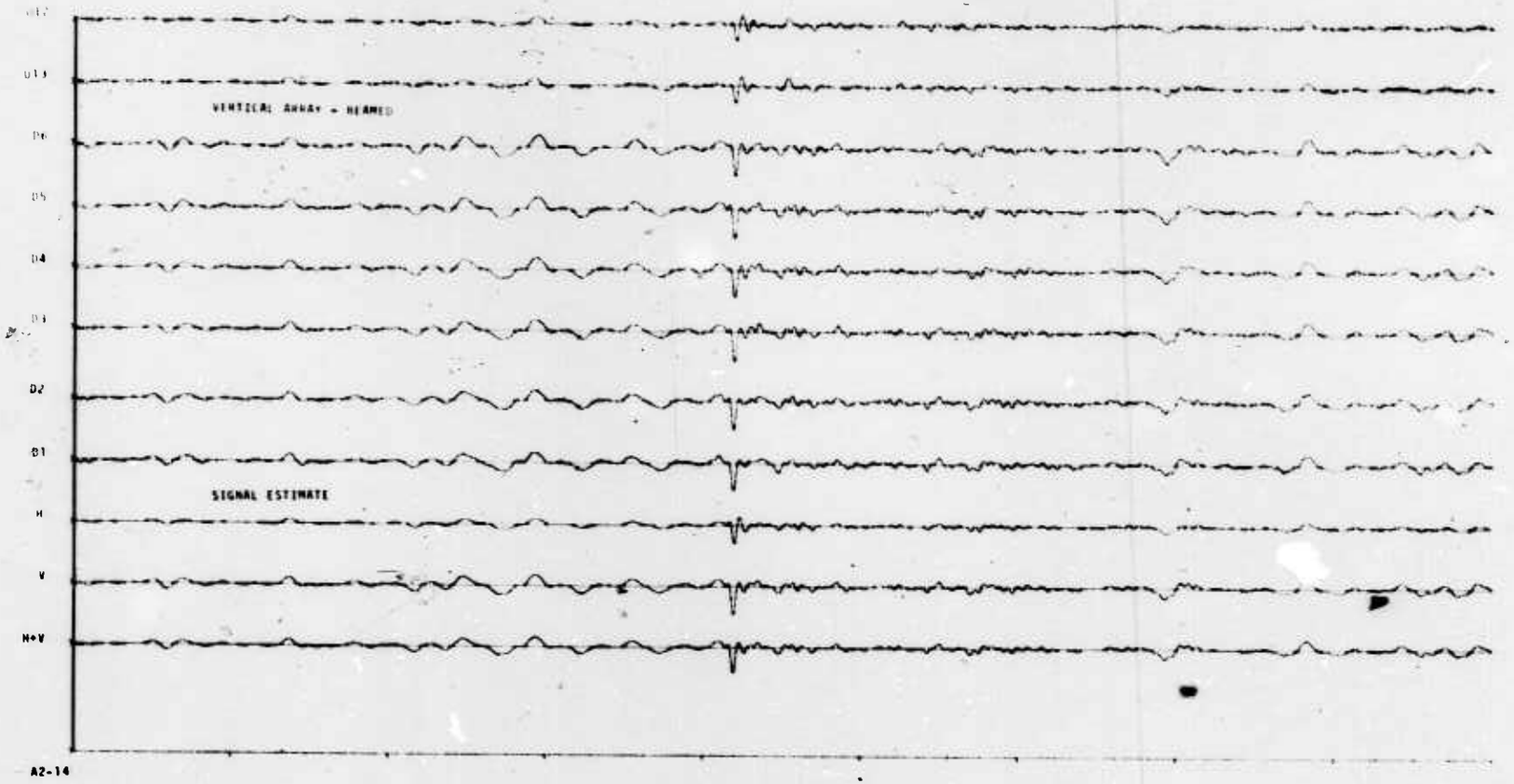
VERTICAL AWAY = REARED
D4
D3
D2
B1
SIGNAL ESTIMATE
H
V
H+V
A2-14

APPENDIX 3

RESIDUAL NOISE MEASUREMENTS

Vertical Array Estimate of Signal Subtracted from each Channel

Signal estimates on H, V, and H+V use unequal weights proportional to inverse variance from above residual noise measurements taken under the signal.

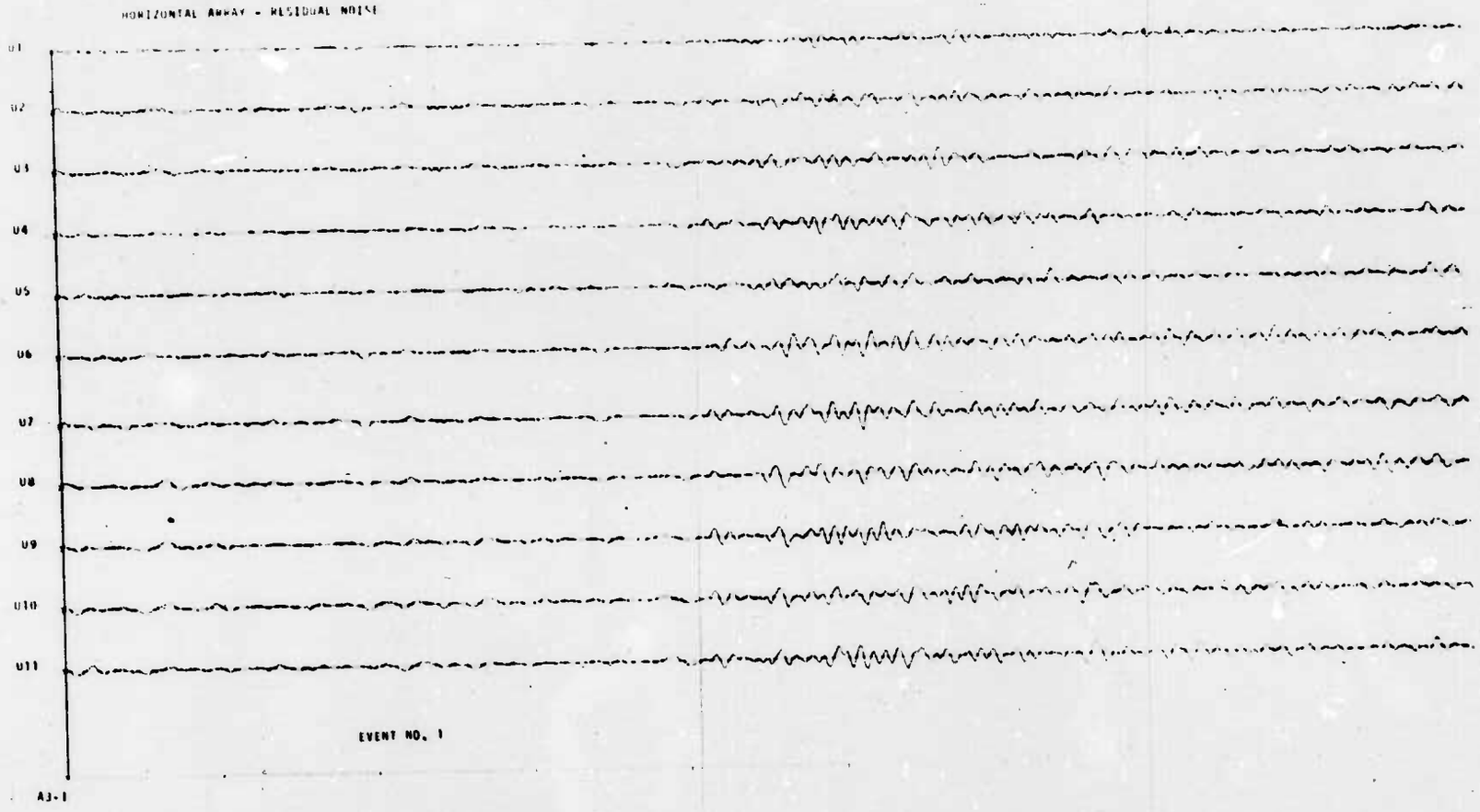
HORIZONTAL ARRAY - RESIDUAL NOISE
U1
U2
U3
U4
U5
U6
U7
U8
U9
U10
U11
EVENT NO. 1
AJ-1

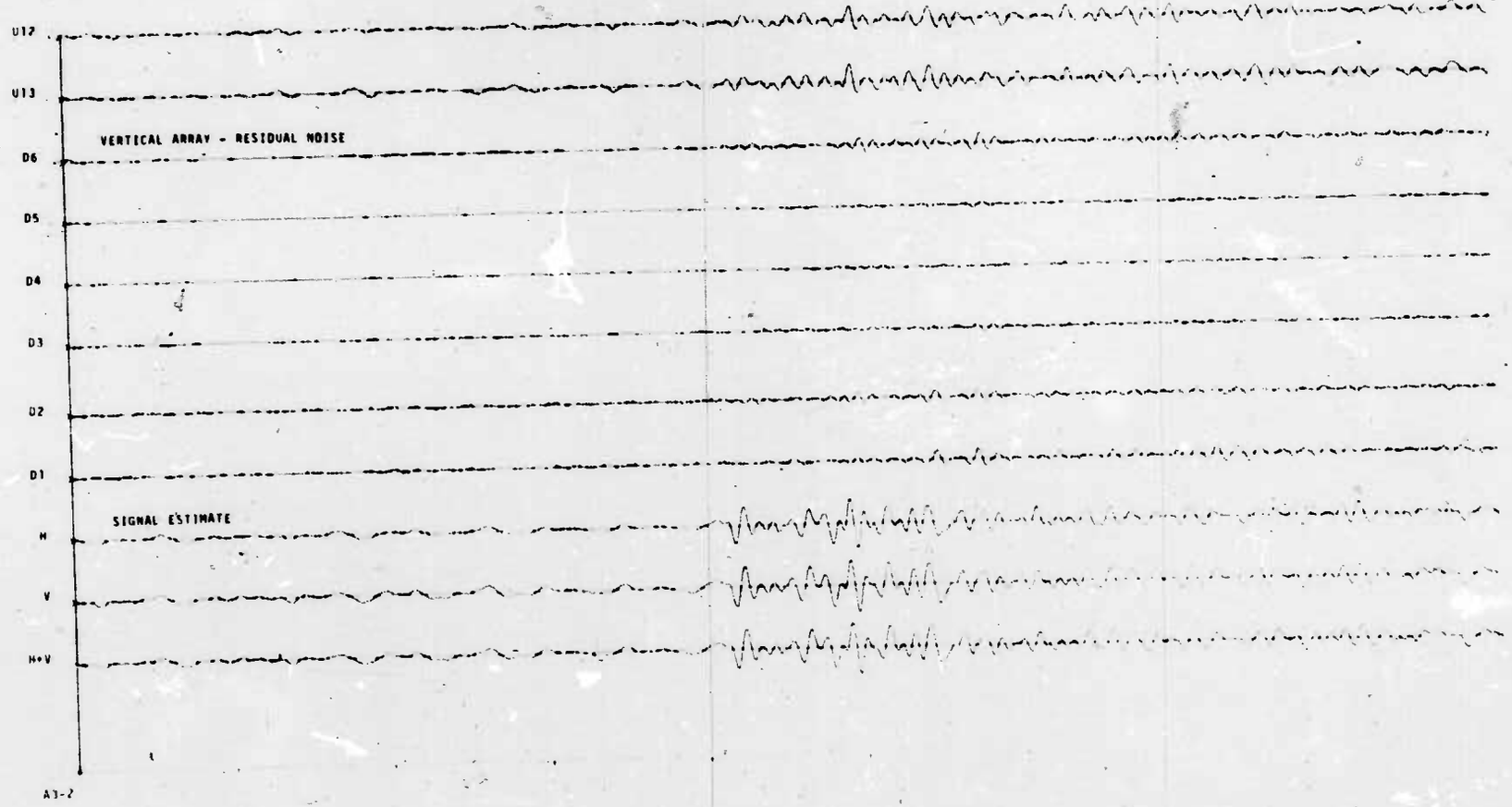
U12
U13
VERTICAL ARRAY - RESIDUAL NOISE
D6
D5
D4
D3
D2
D1
SIGNAL ESTIMATE
H
V
H+V
A3-2

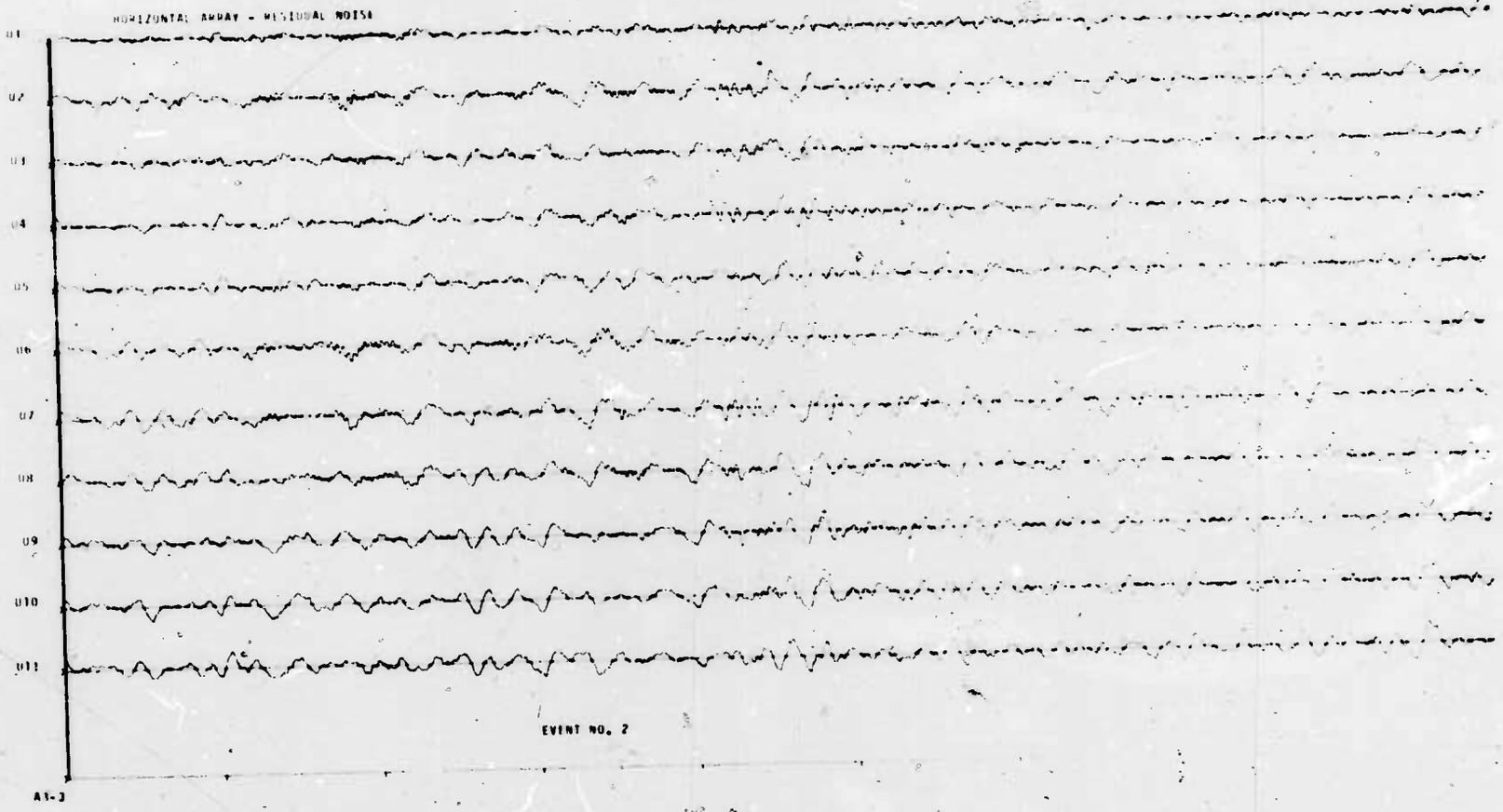
HORIZONTAL ARRAY - RESIDUAL NOISE
U1
U2
U3
U4
U5
U6
U7
U8
U9
U10
U11
EVENT NO. 2
AS-3

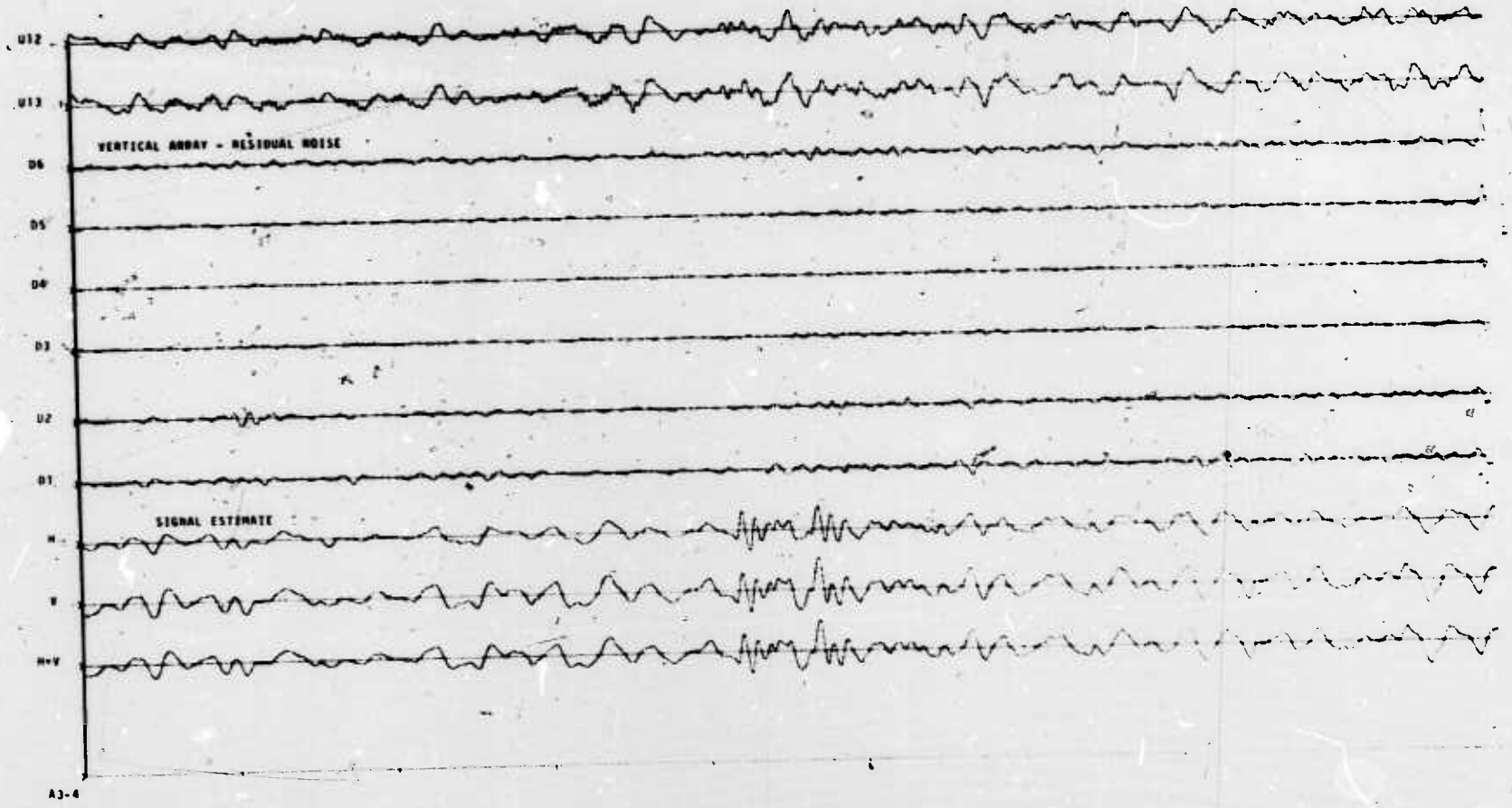
U12
U13
VERTICAL ARRAY - RESIDUAL NOISE
D6
D5
D4
D3
U2
D1
SIGNAL ESTIMATE
H
V
H+V
A3-4

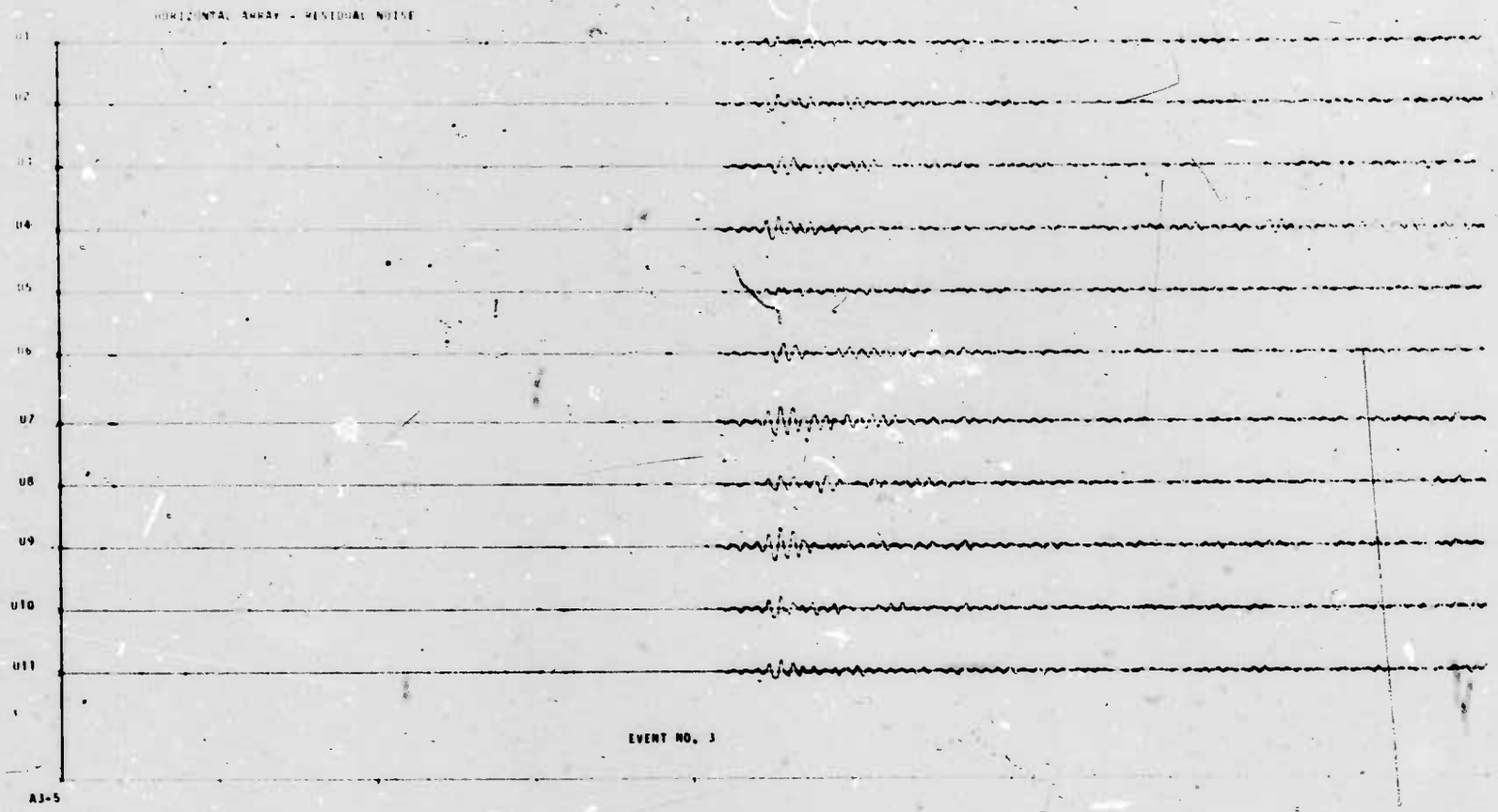
HORIZONTAL ARRAY - RESIDUAL NOISE
U1
U2
U3
U4
U5
U6
U7
U8
U9
U10
U11
EVENT NO. 3
A3-5

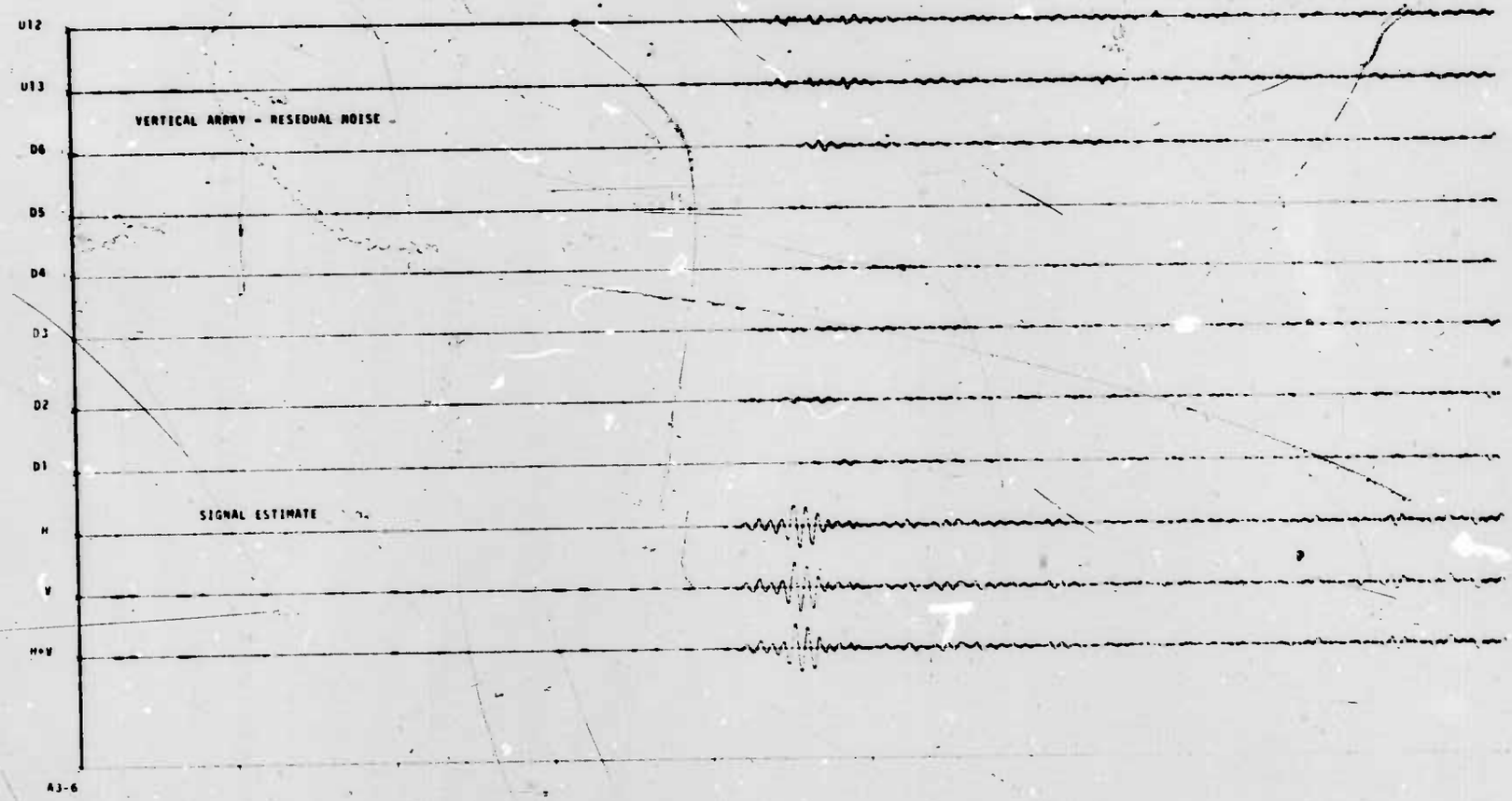
U12
U13
VERTICAL ARRAY - RESEDUAL NOISE
D6
D5
D4
D3
D2
D1
SIGNAL ESTIMATE
H
V
H+V
A3-6

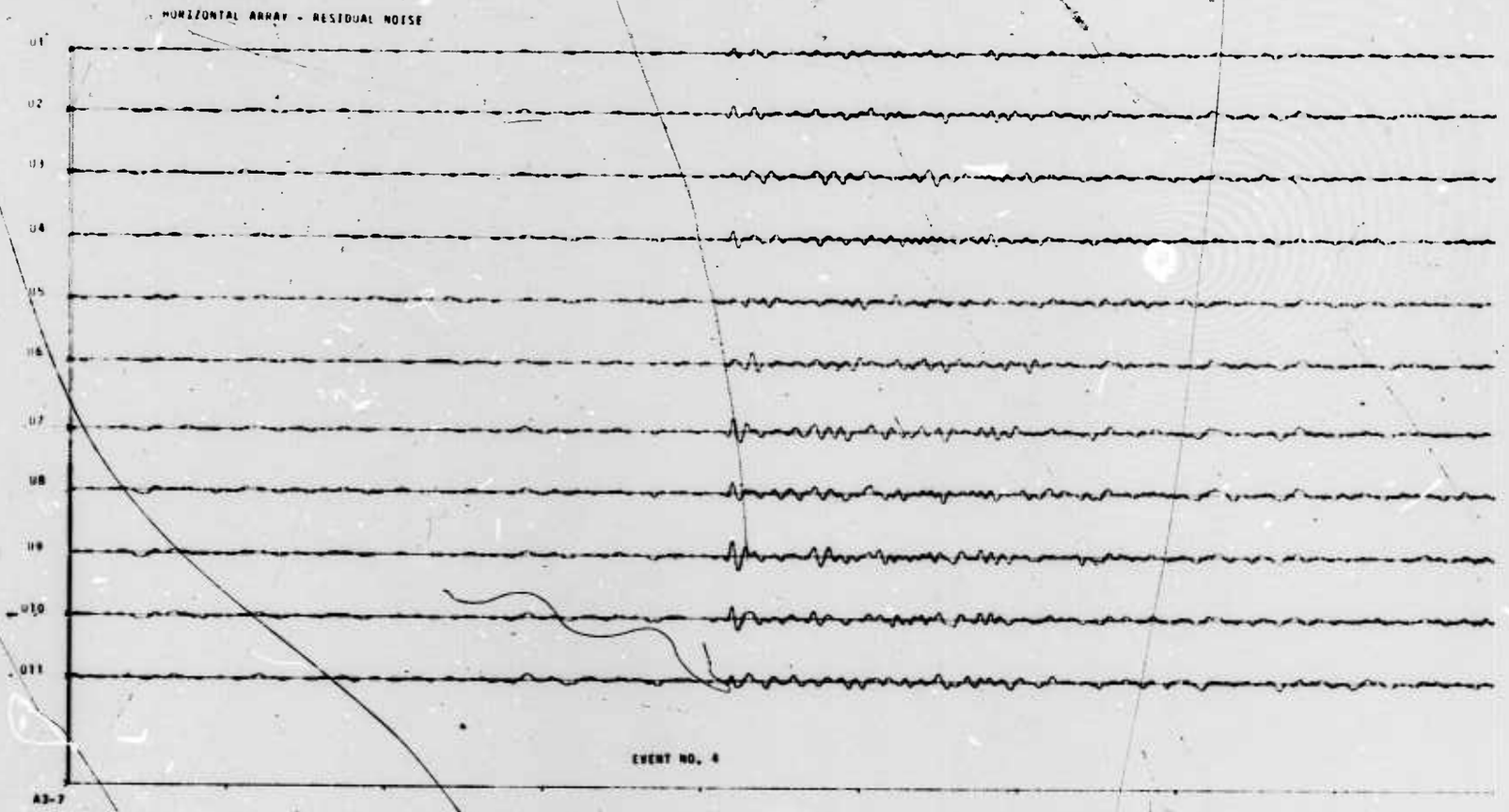
HORIZONTAL ARRAY - RESIDUAL NOISE
U1
U2
U3
U4
U5
U6
U7
U8
U9
U10
U11
EVENT NO. 4
A3-7

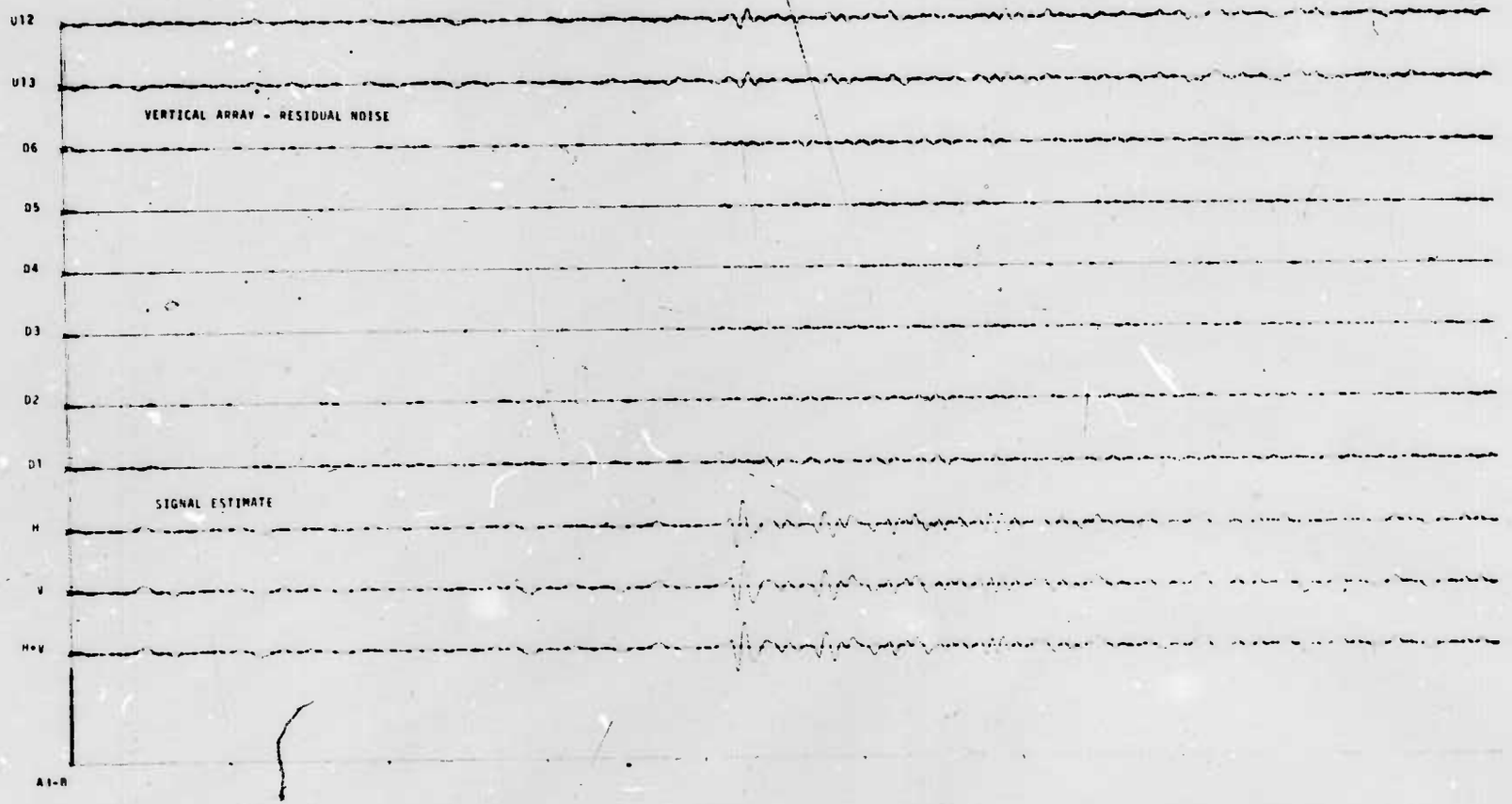
U12
U13
VERTICAL ARRAY - RESIDUAL NOISE
D6
D5
D4
D3
D2
D1
SIGNAL ESTIMATE
H
V
H+V
A1-A

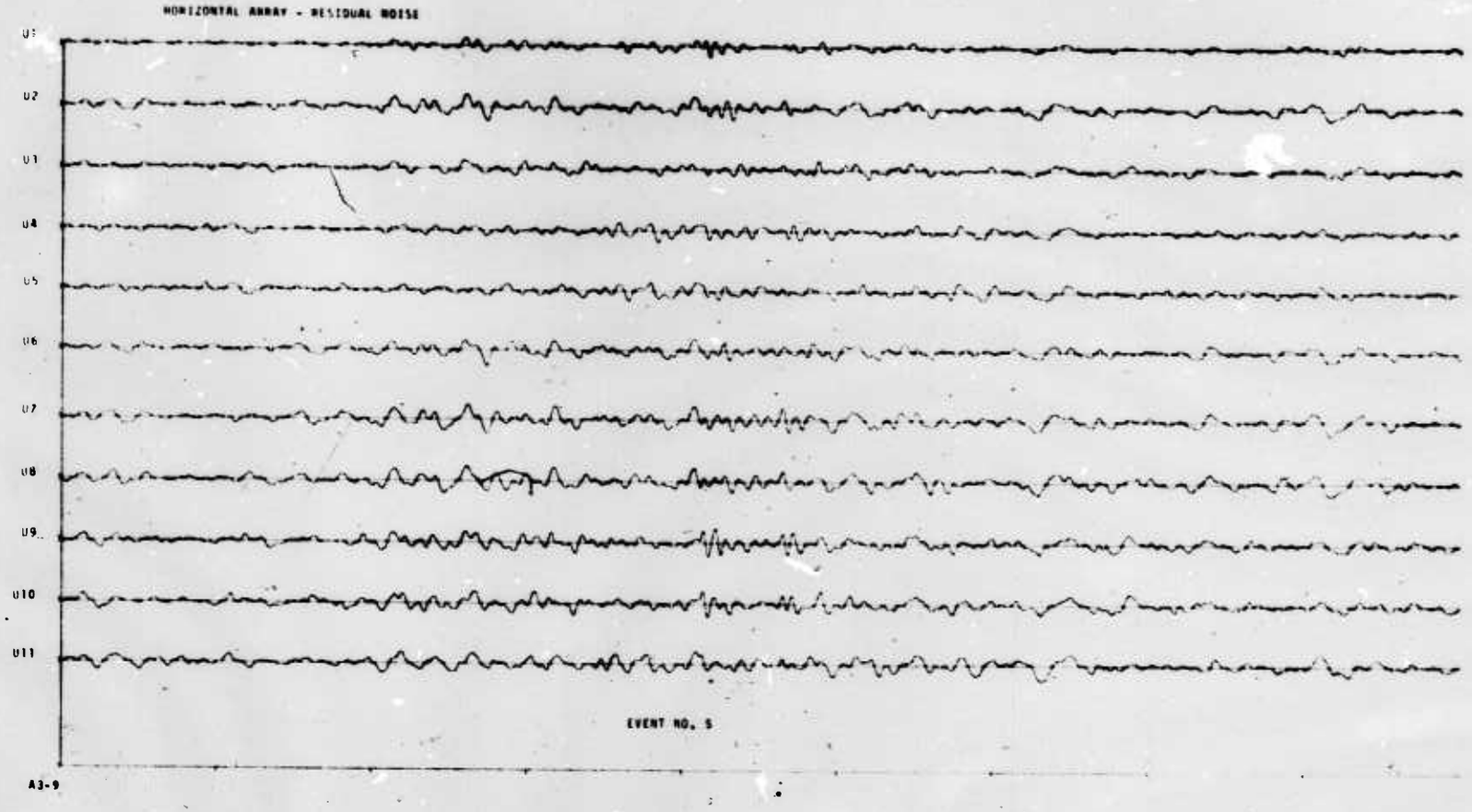
HORIZONTAL ARRAY - RESIDUAL NOISE
U1
U2
U3
U4
U5
U6
U7
U8
U9
U10
U11
EVENT NO. 5
A3-9

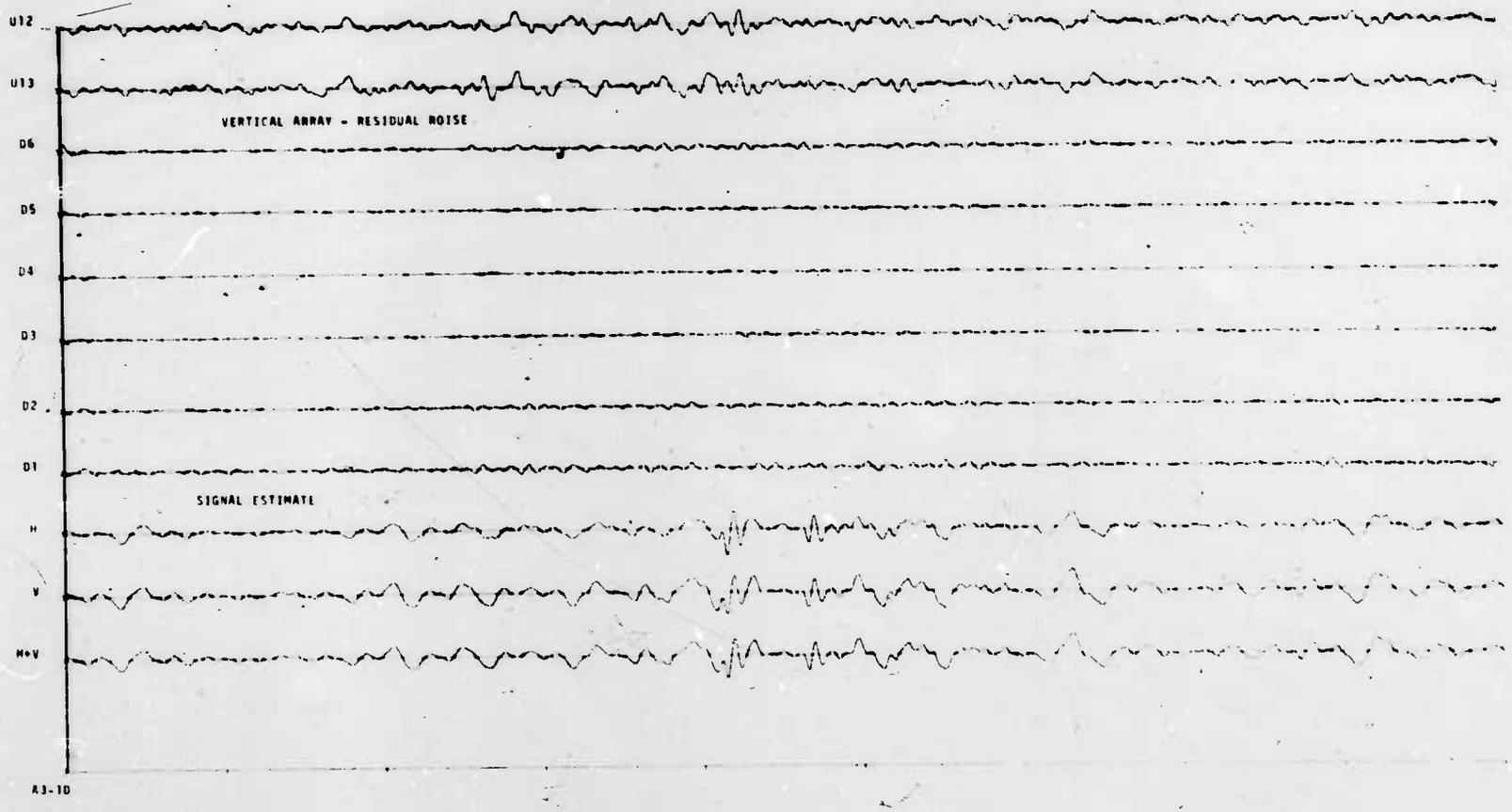
U12
U13
VERTICAL ARRAY - RESIDUAL NOISE
D6
D5
D4
D3
D2
D1
SIGNAL ESTIMATE
H
V
H+V
A3-10

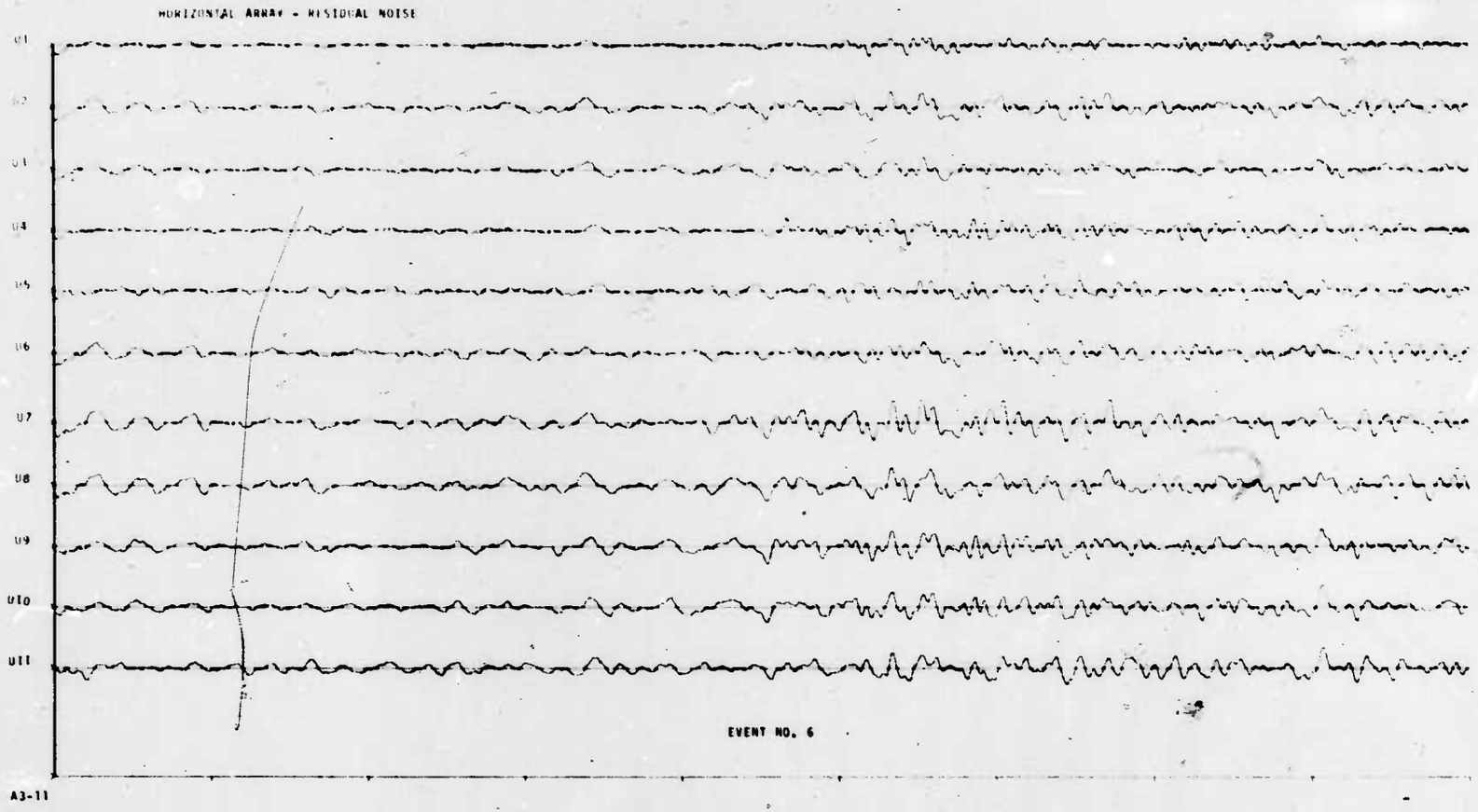
HORIZONTAL ARRAY - RESIDUAL NOISE
U1
U2
U3
U4
U5
U6
U7
U8
U9
U10
U11
EVENT NO. 6
A3-11

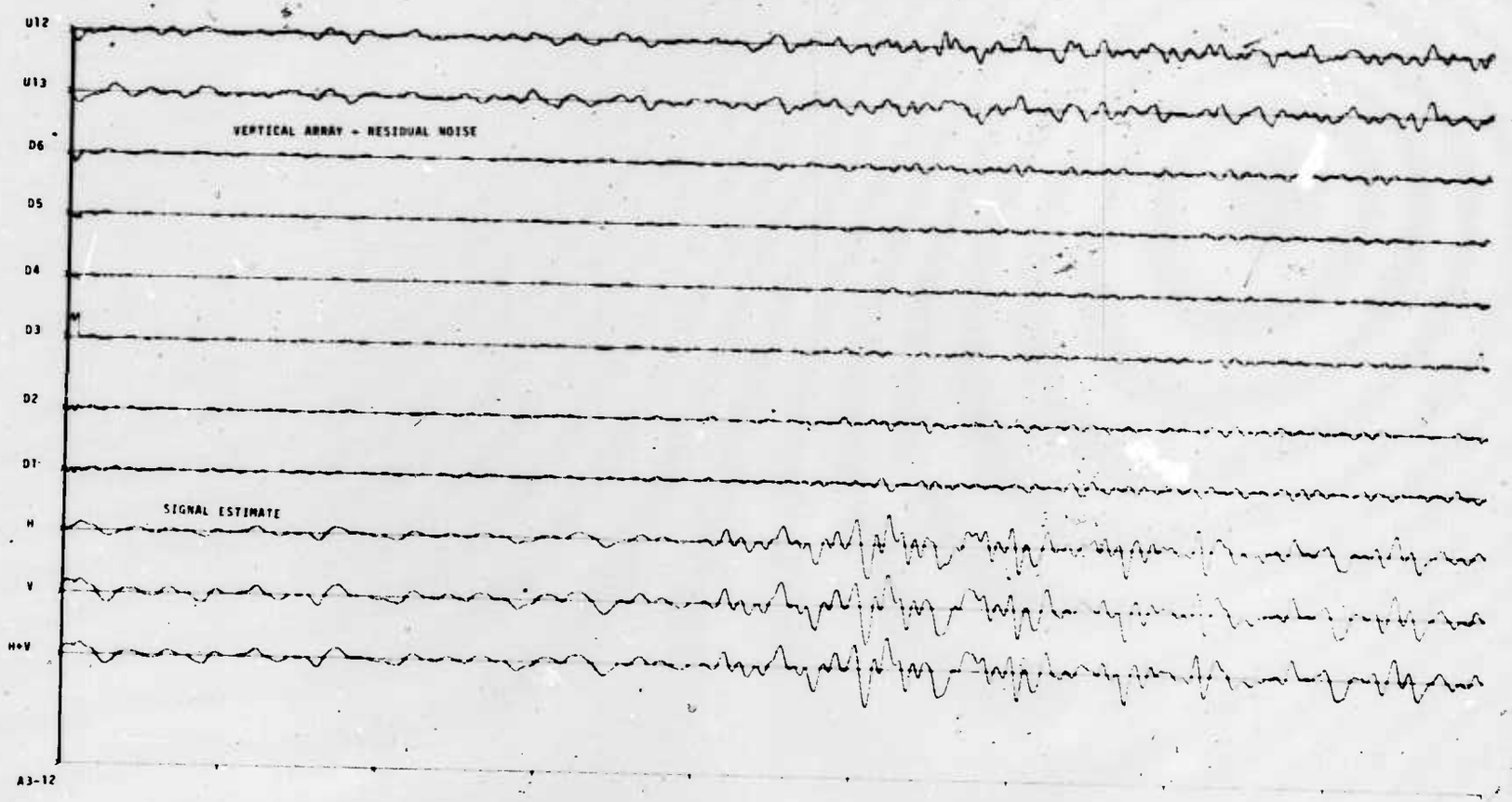
U12
U13
VERTICAL ARRAY - RESIDUAL NOISE
D6
D5
D4
D3
D2
D1
SIGNAL ESTIMATE
H
V
H+V
A3-12

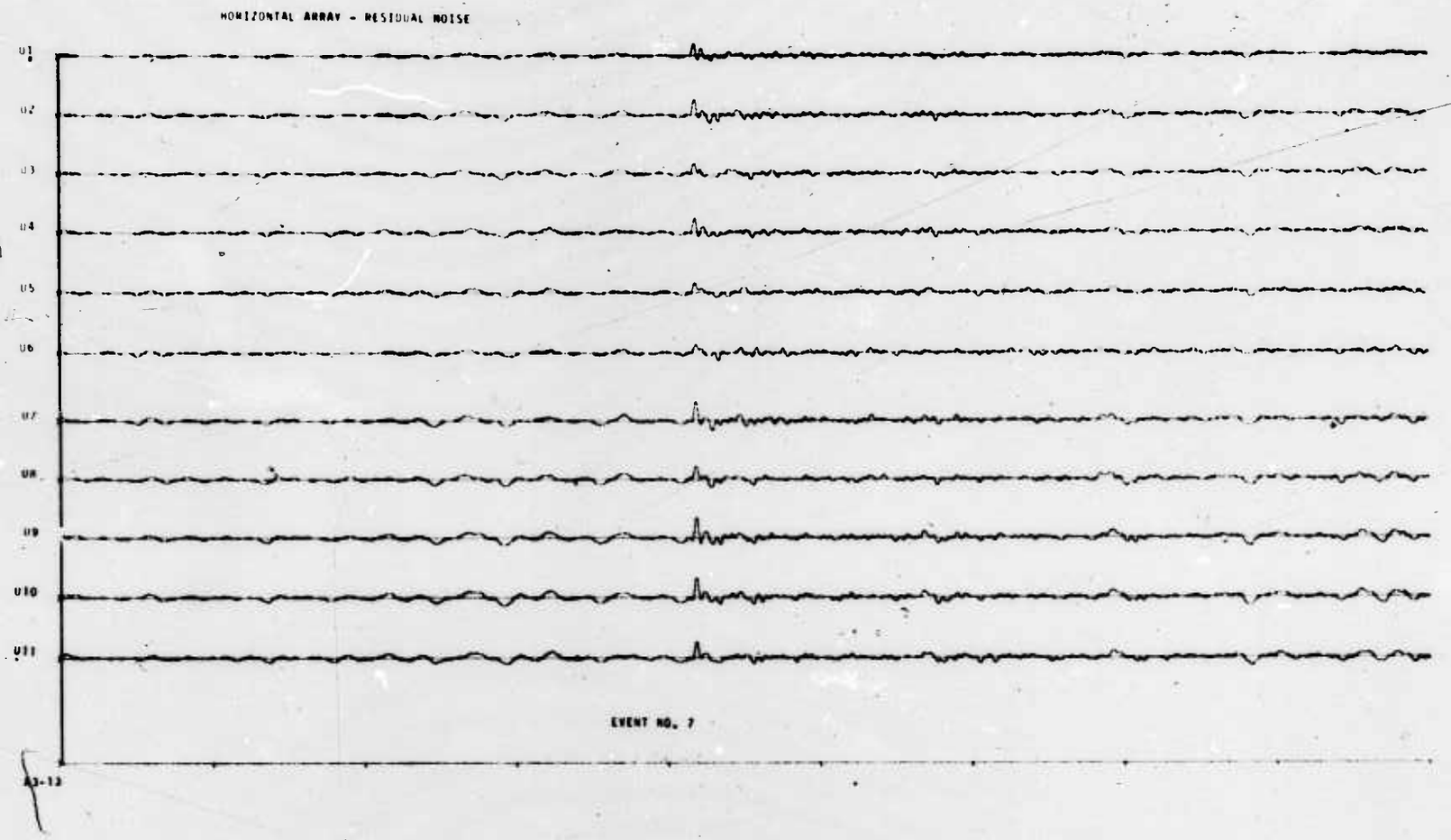
HORIZONTAL ARRAY - RESIDUAL NOISE
U1
U2
U3
U4
U5
U6
U7
U8
U9
U10
U11
EVENT NO. 7
A3-13

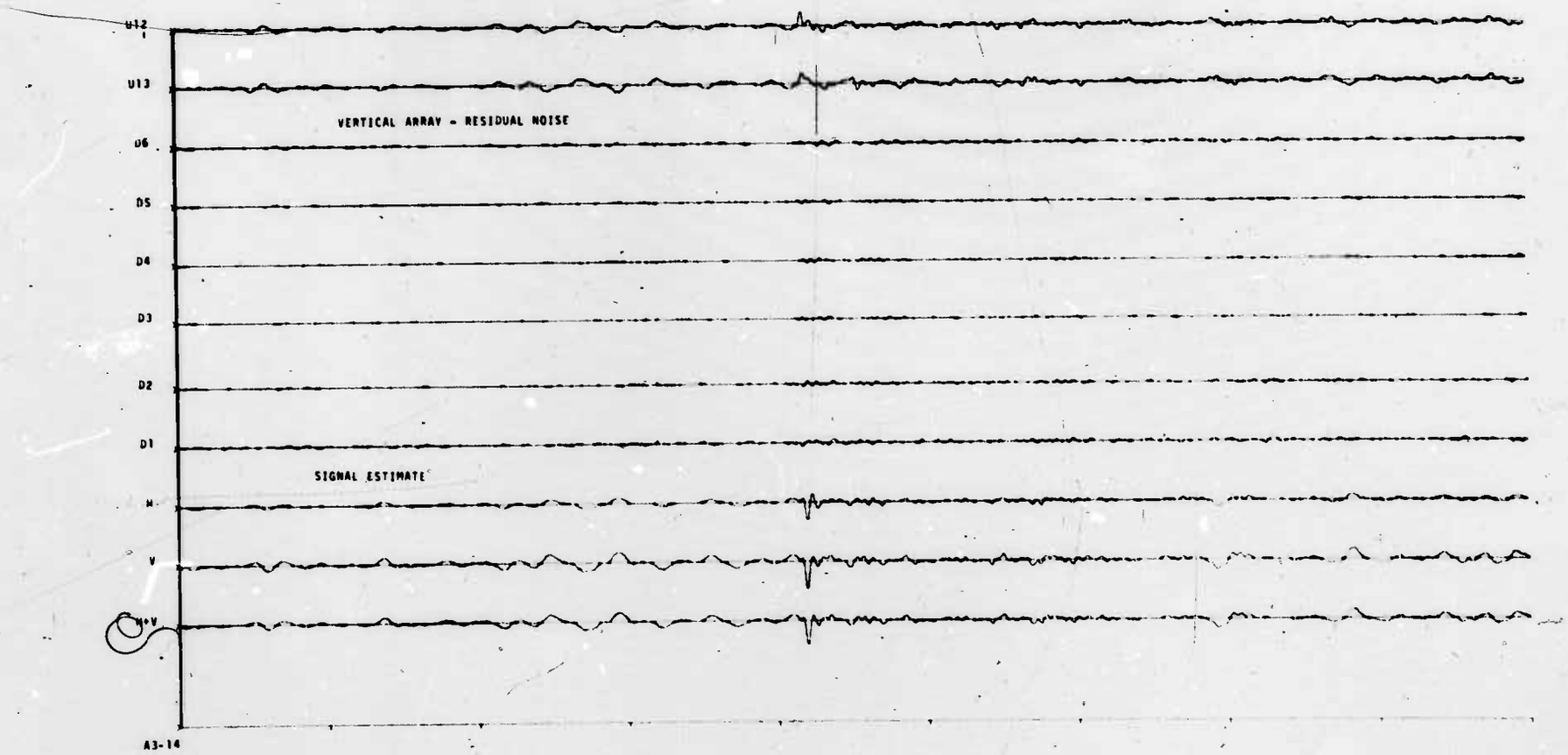
U12
U13
VERTICAL ARRAY - RESIDUAL NOISE
D6
D5
D4
D3
D2
D1
SIGNAL ESTIMATE
H
V
H+V
A3-14

APPENDIX 4

1. Spectral analysis of the residual noise on each channel.

2. Two time windows before the expected arrival time of the teleseismic event.

3. Two time windows after the expected arrival time of the teleseismic event.

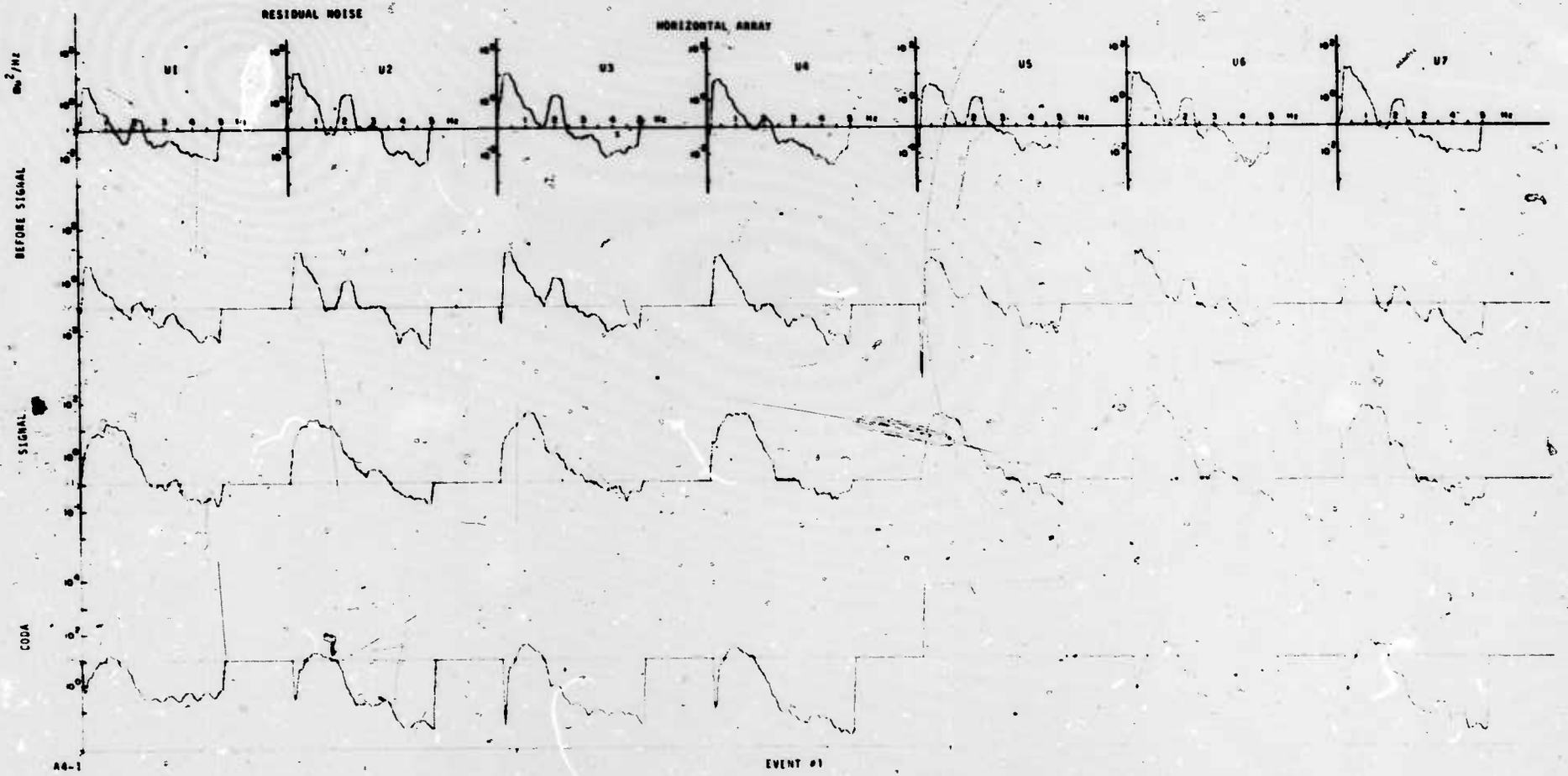
RESIDUAL NOISE
HORIZONTAL ARRAY
U1
U2
U3
U4
U5
U6
U7
BEFORE SIGNAL
SIGNAL
CODA
A4-1
EVENT #1

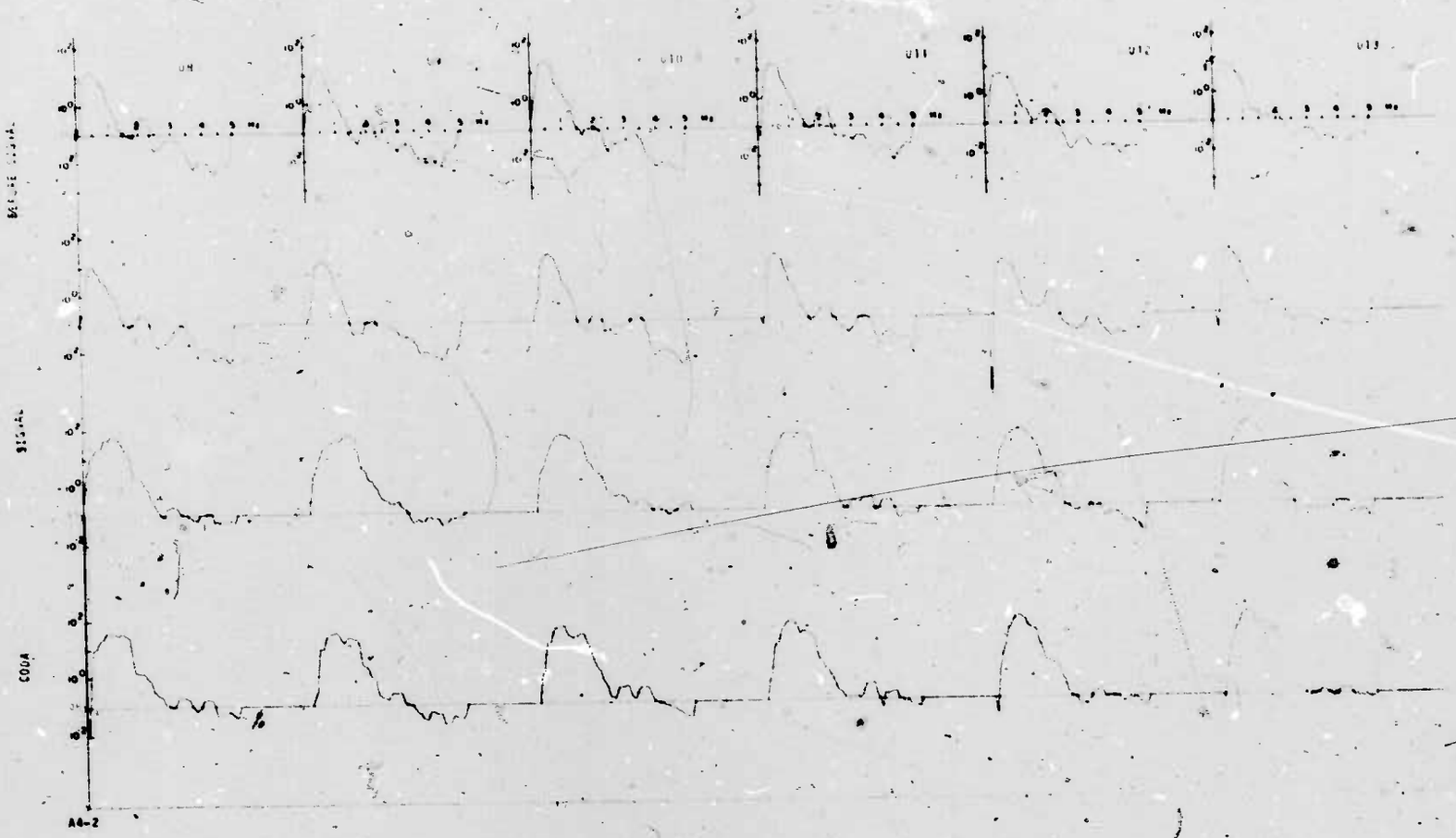
A4-2

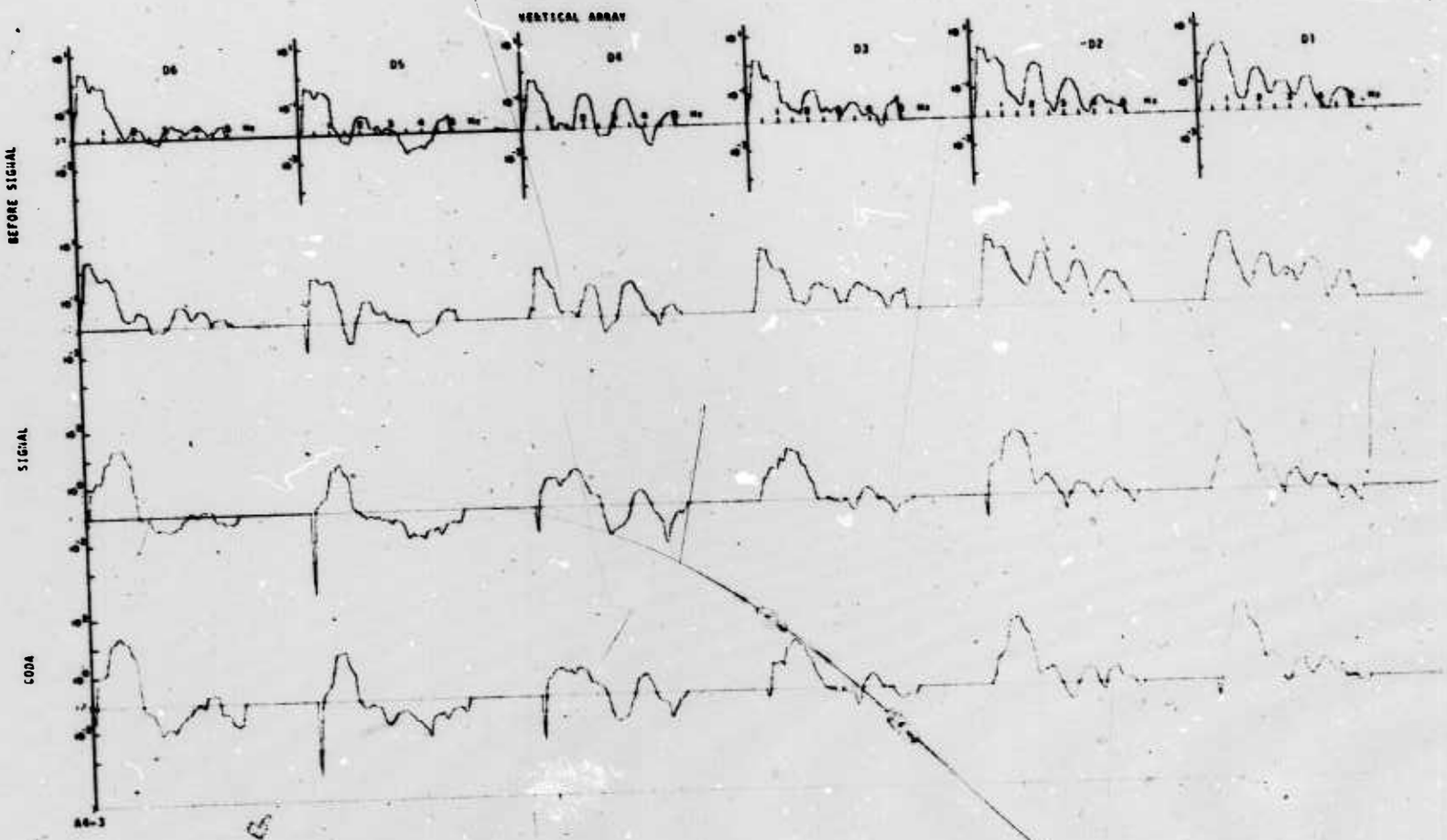
VERTICAL ARRAY
D6
D5
D4
D3
D2
D1
BEFORE SIGNAL
SIGNAL
CODA

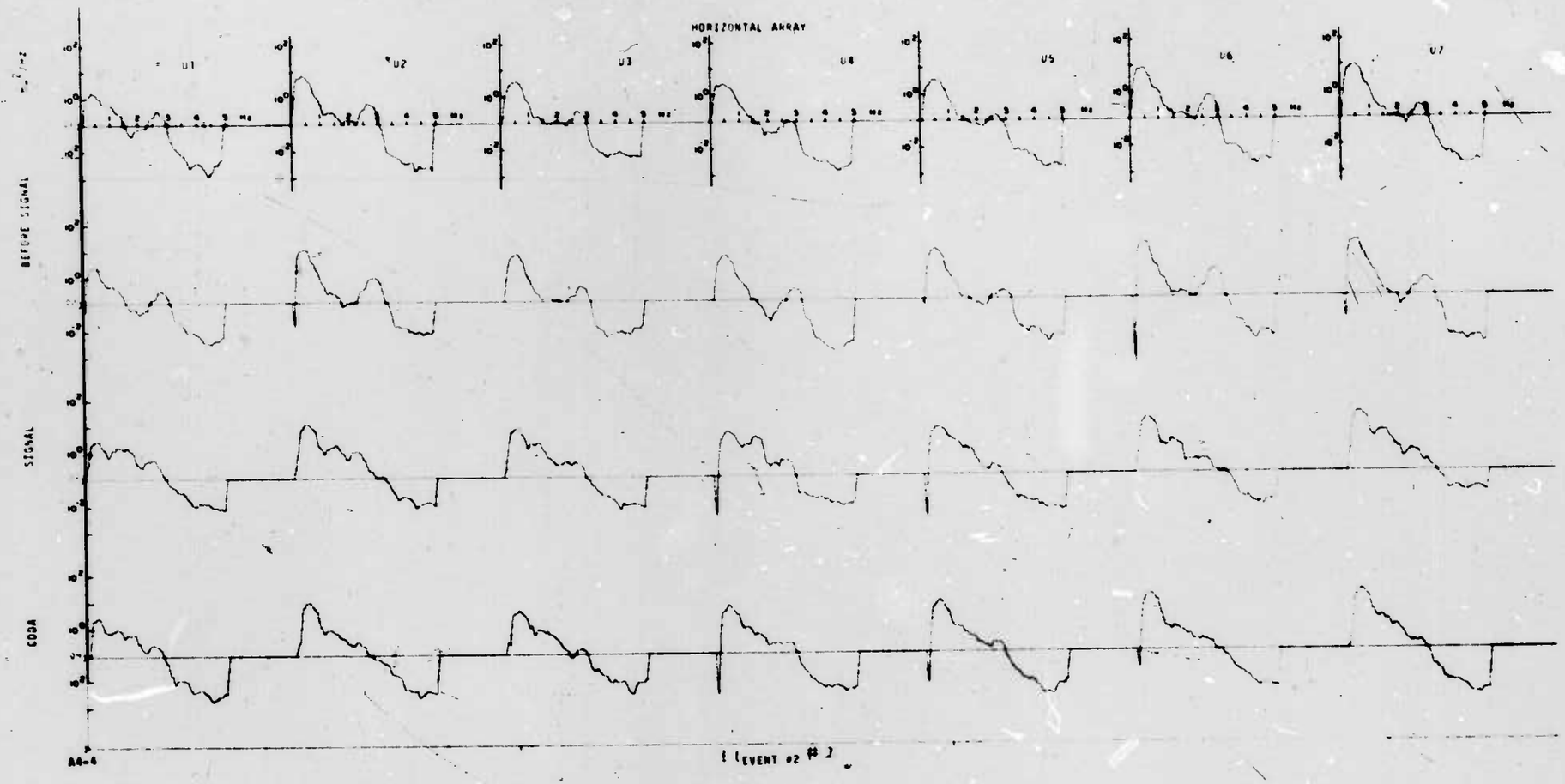
HORIZONTAL ARRAY
U1
U2
U3
U4
U5
U6
U7
BEFORE SIGNAL
SIGNAL
CODA
EVENT #2 #3

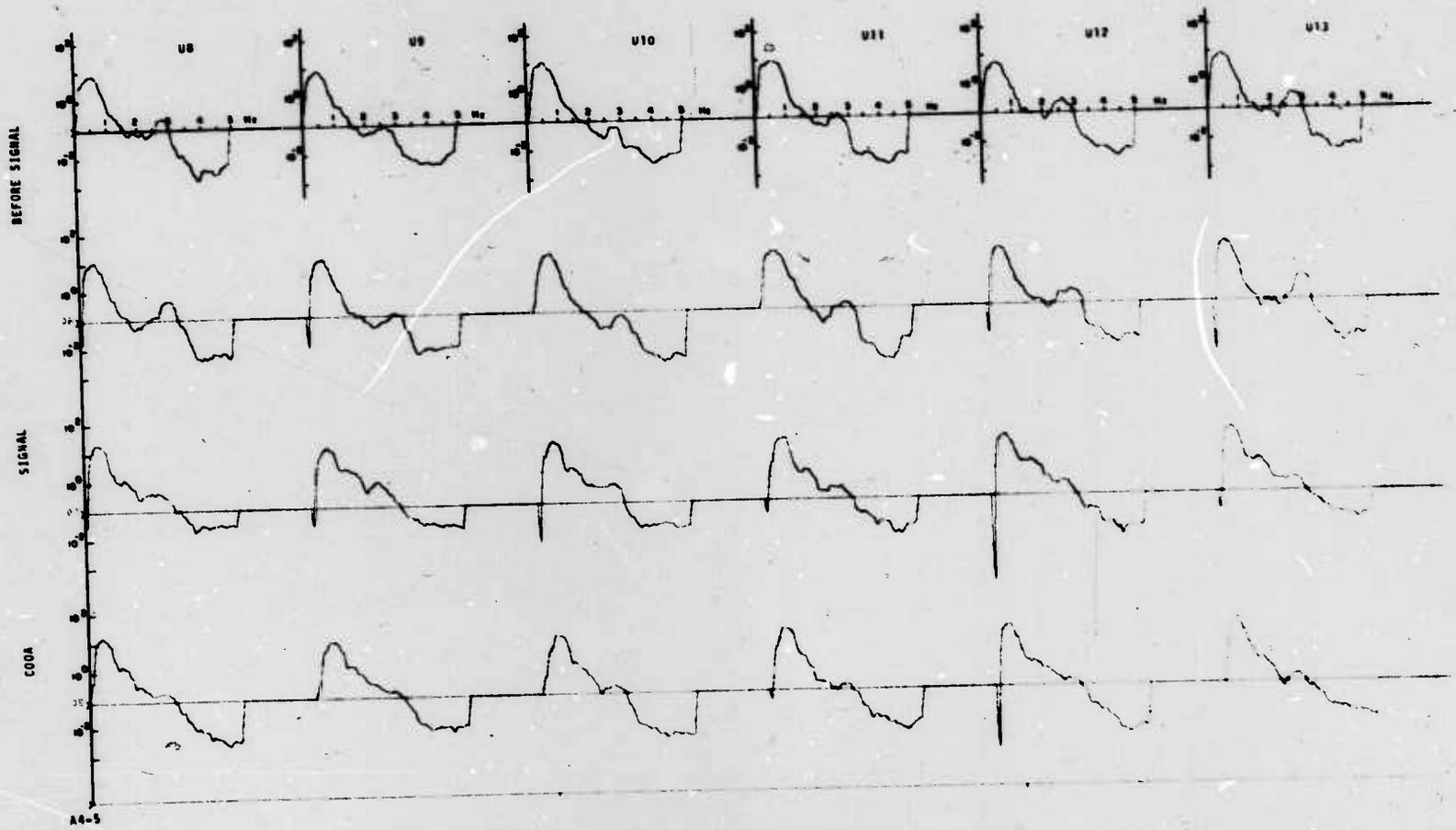
U8
U9
U10
U11
U12
U13
BEFORE SIGNAL
SIGNAL
CODA
A4-5

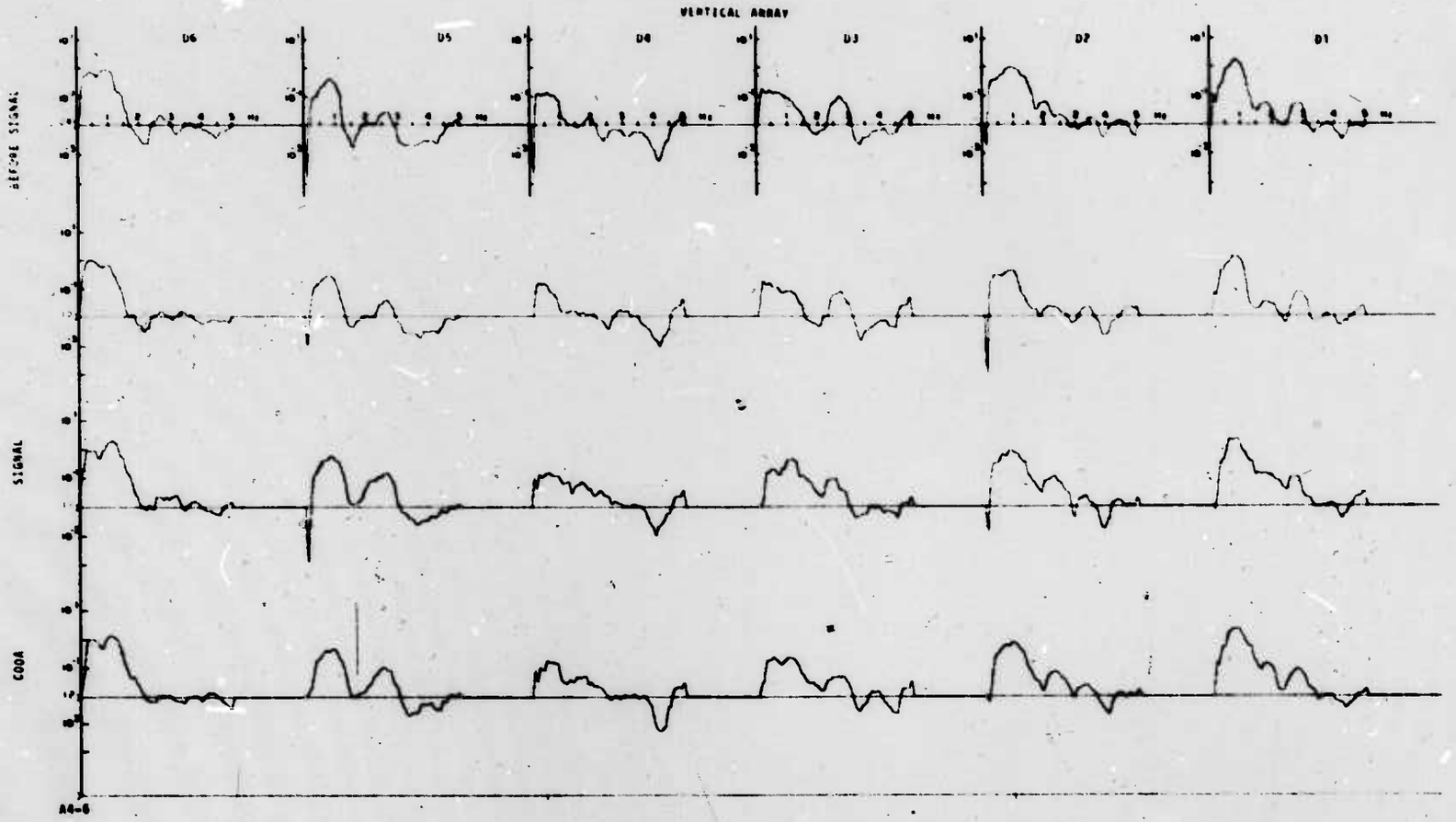
VERTICAL ARRAY
D6
D5
D4
D3
D2
D1
SIGNAL
CODA

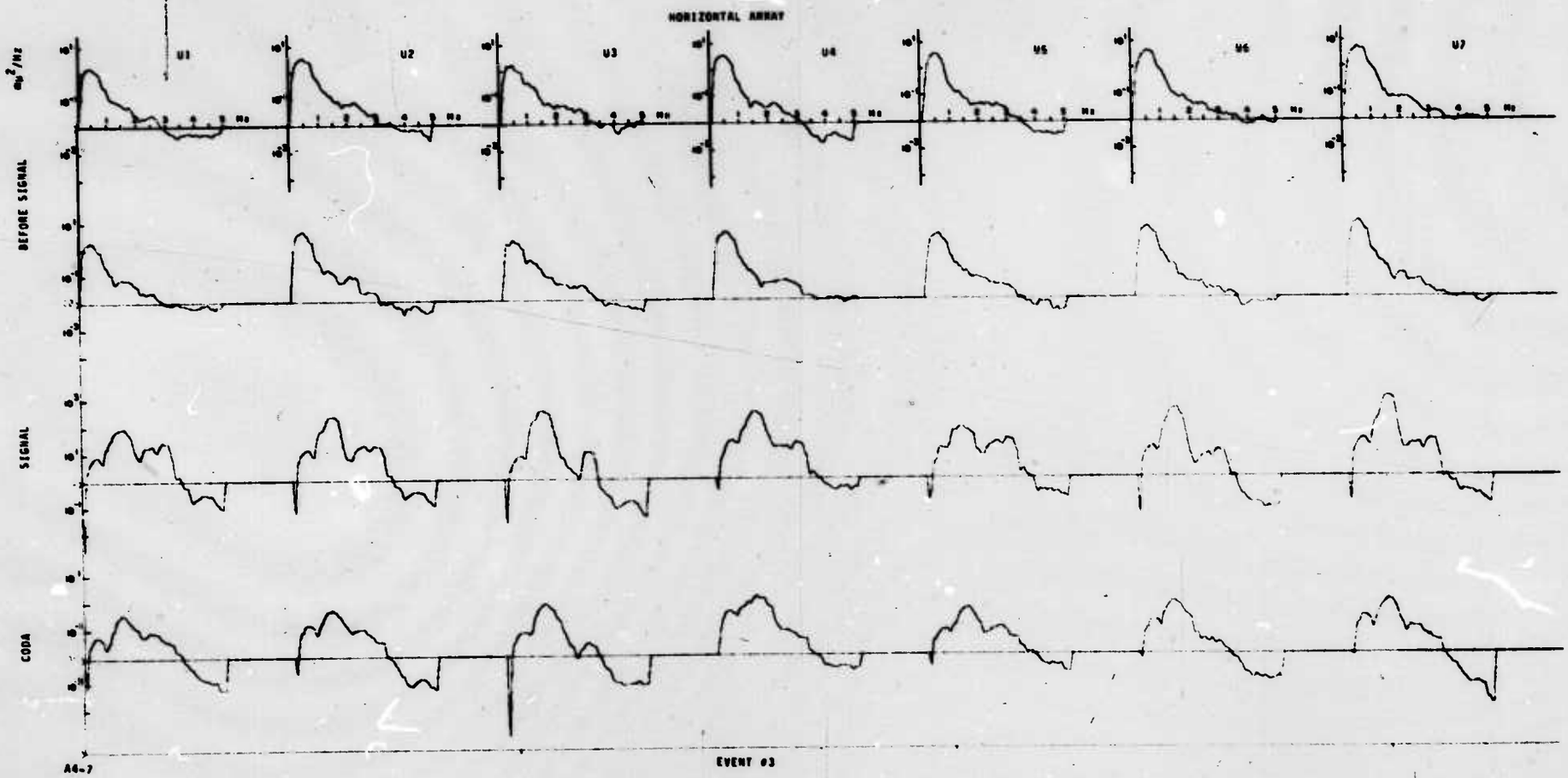
HORIZONTAL ARRAY
U1
U2
U3
U4
U5
U6
U7
BEFORE SIGNAL
SIGNAL
CODA
EVENT #3

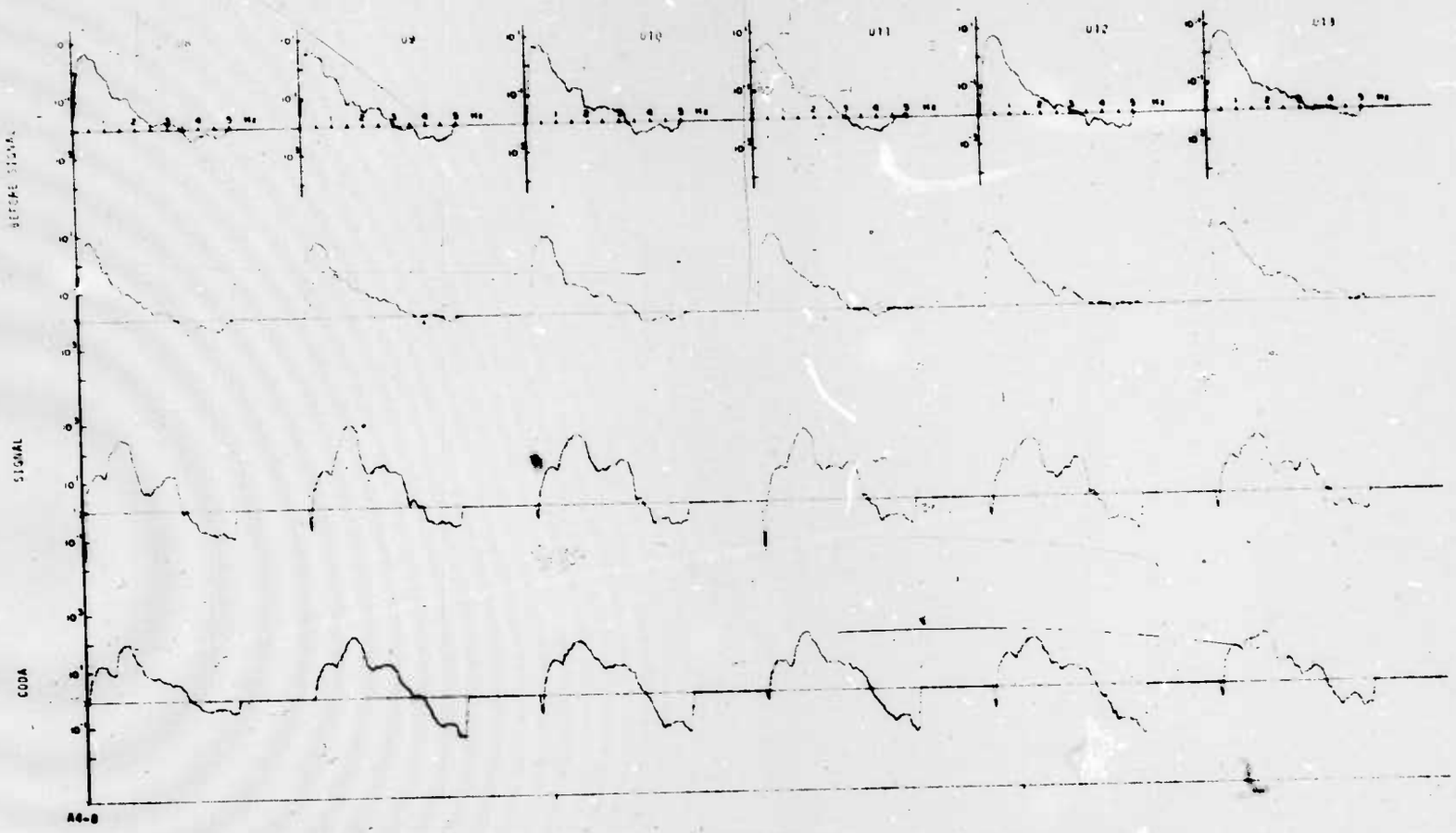
U9
U10
U11
U12
U13
SIGNAL
CODA

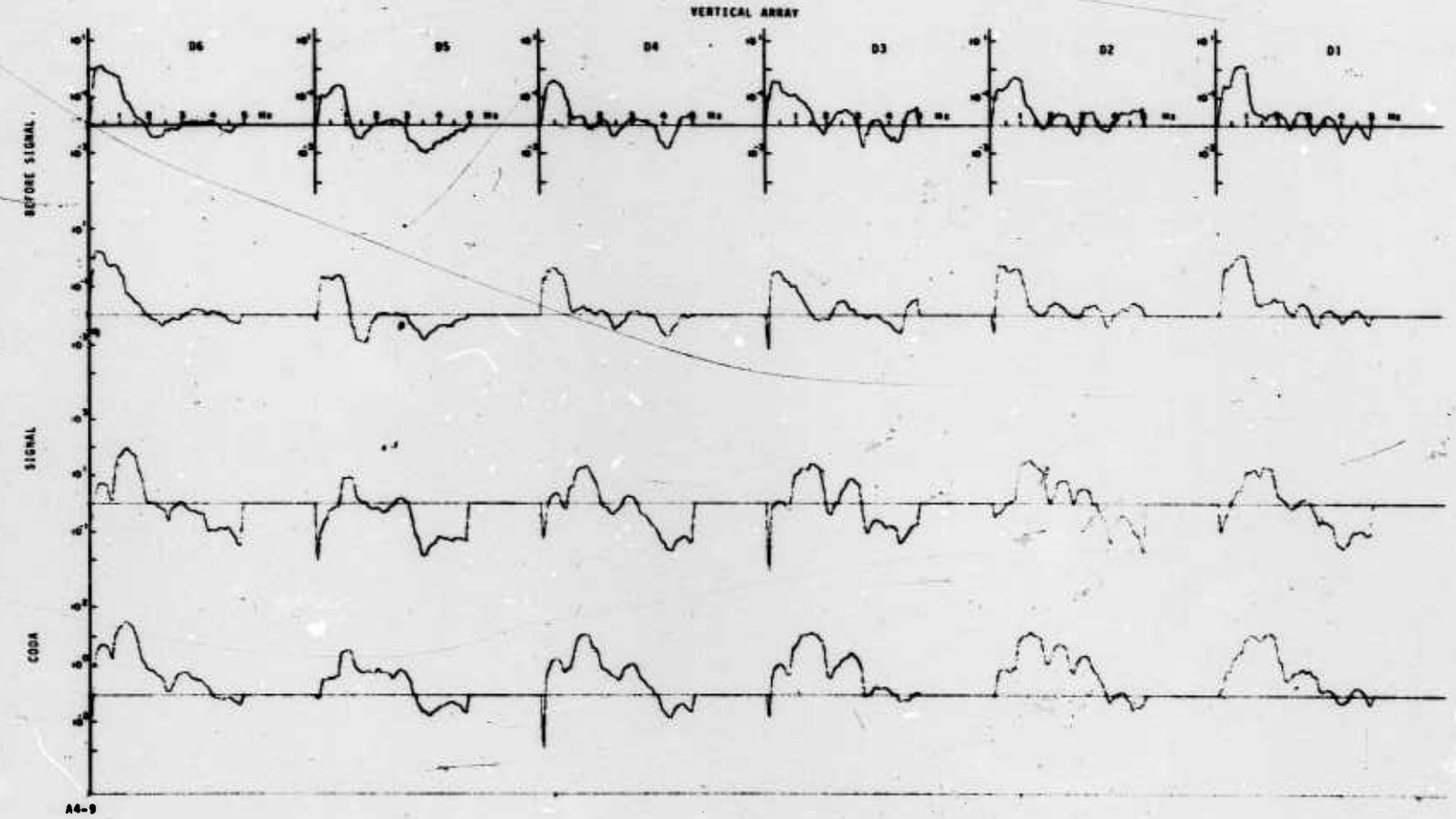
VERTICAL ARRAY
D6
D5
D4
D3
D2
D1
BEFORE SIGNAL
SIGNAL
CODA
A6-9

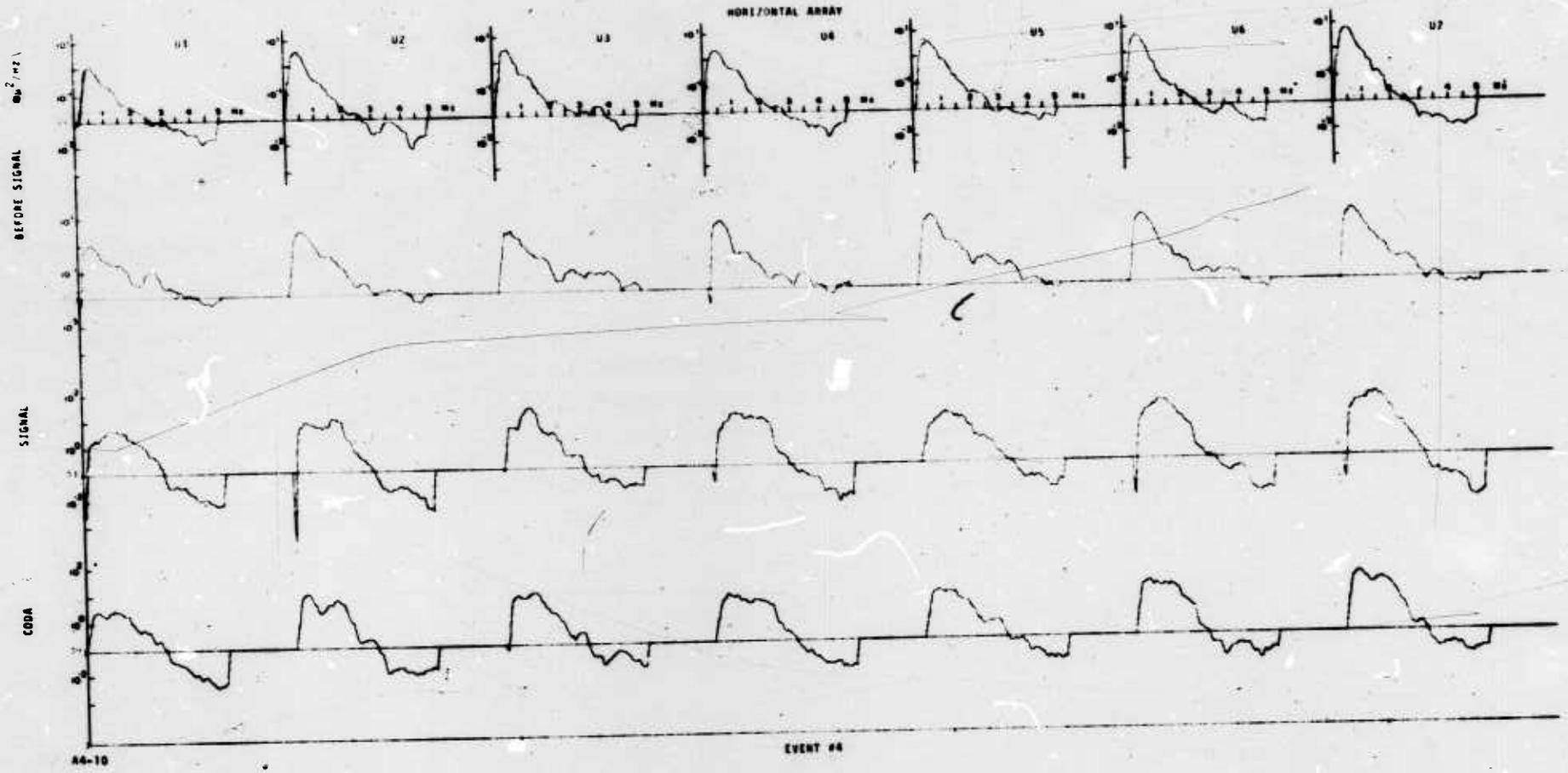
HORIZONTAL ARRAY
U1
U2
U3
U4
U5
U6
U7
BEFORE SIGNAL
SIGNAL
CODA
A4-10
EVENT #4

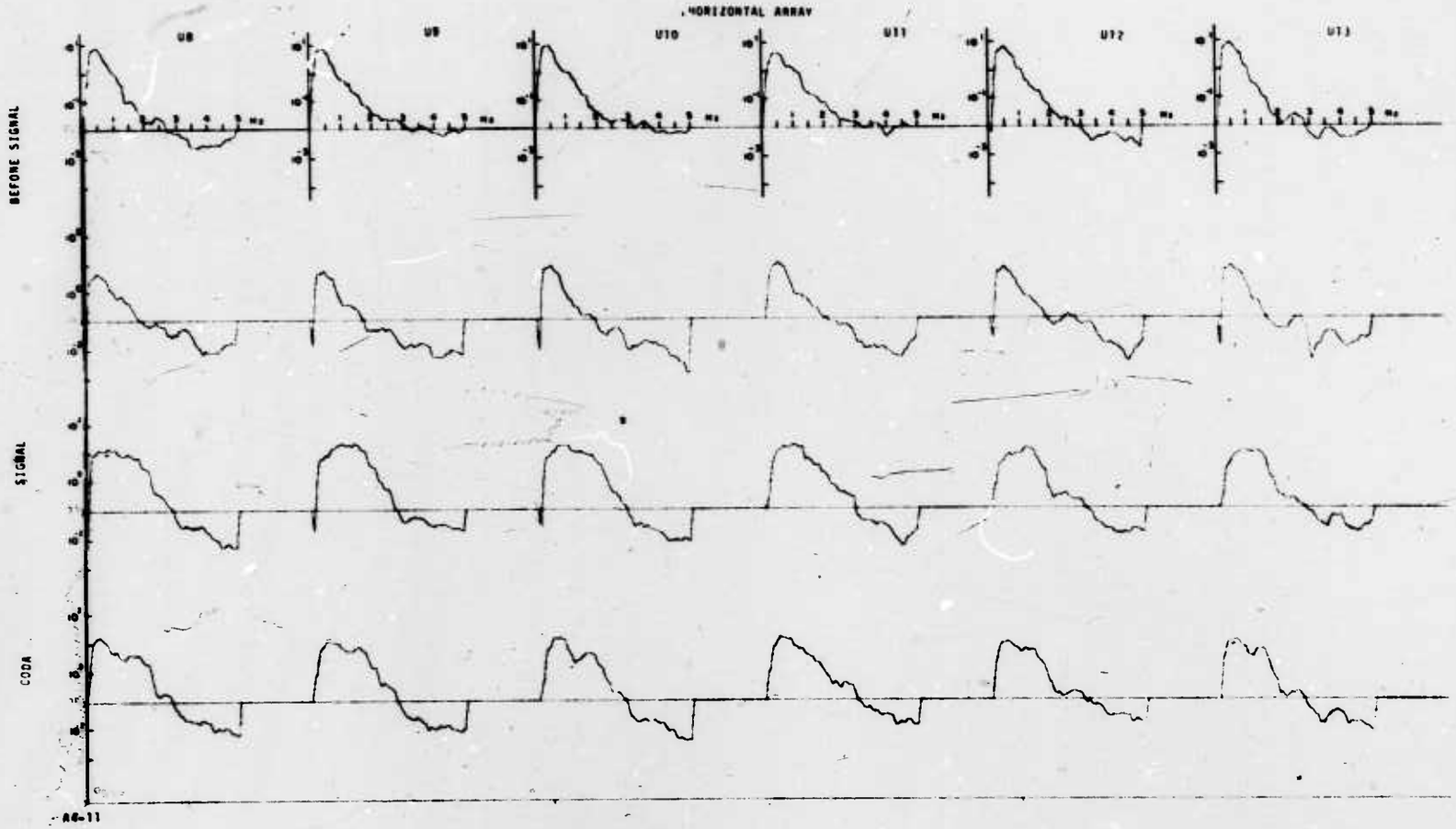
HORIZONTAL ARRAY
U8
U9
U10
U11
U12
U13
BEFORE SIGNAL
SIGNAL
CODA
A6-11

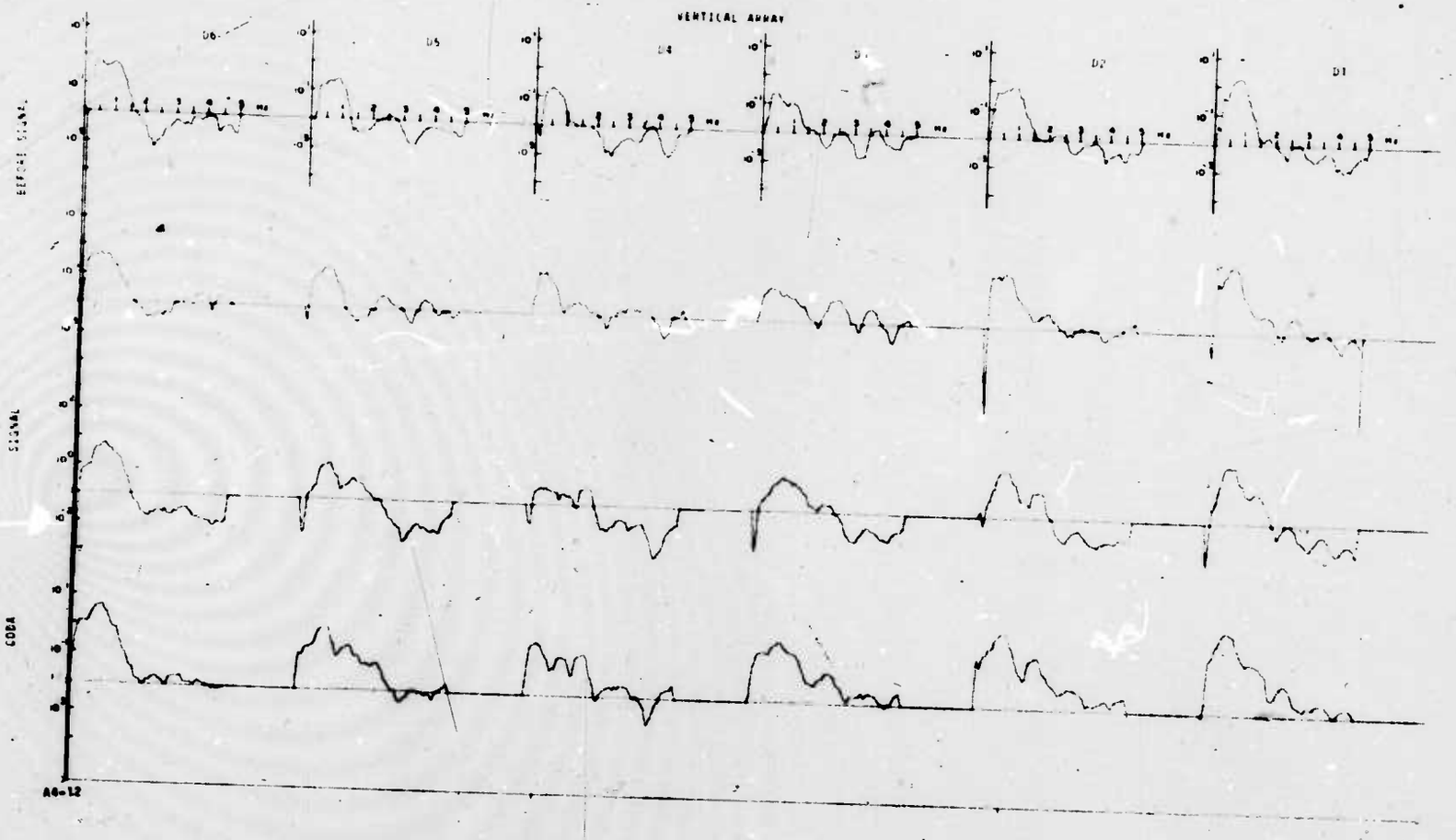
VERTICAL ARRAY
D6
D5
D4
D3
D2
D1
EFFORT SIGNAL
SIGNAL
CODA
A6-L2

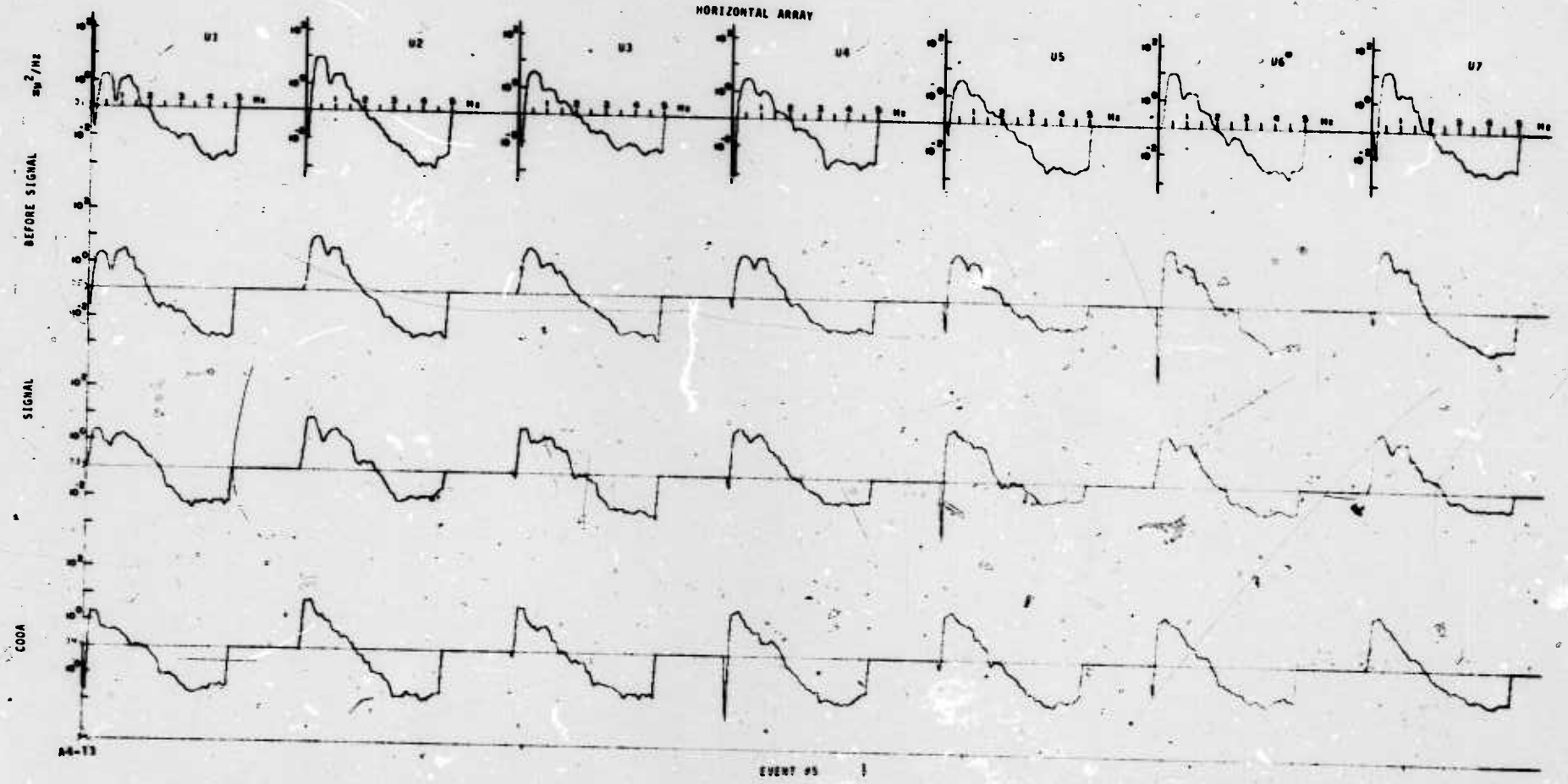
HORIZONTAL ARRAY
U1
U2
U3
U4
U5
U6
U7
BEFORE SIGNAL
SIGNAL
CODA
A4-13
EVENT #5

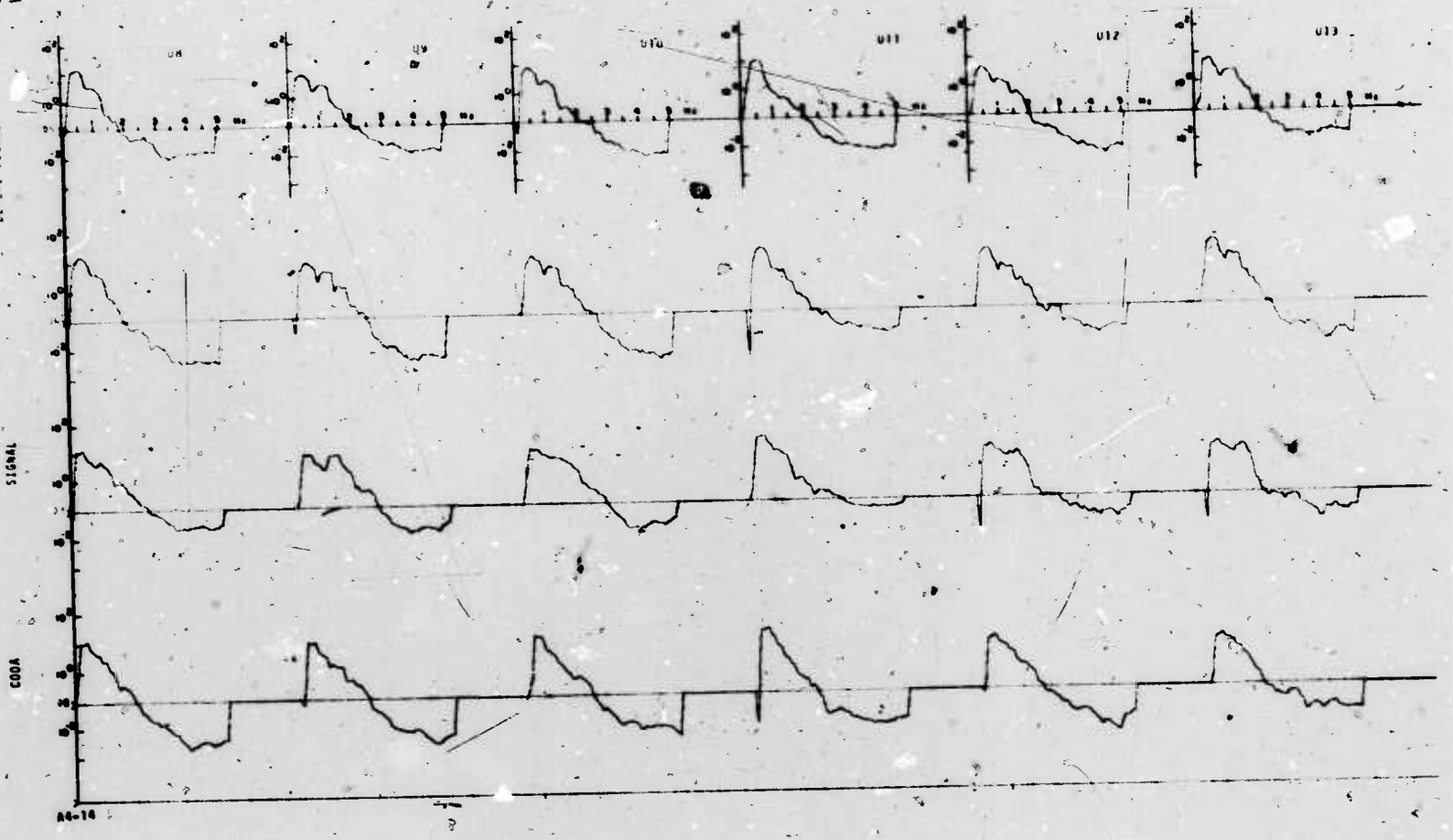
U10
U11
U12
U13
BEFORE SIGNAL
SIGNAL
CODA
A6-14

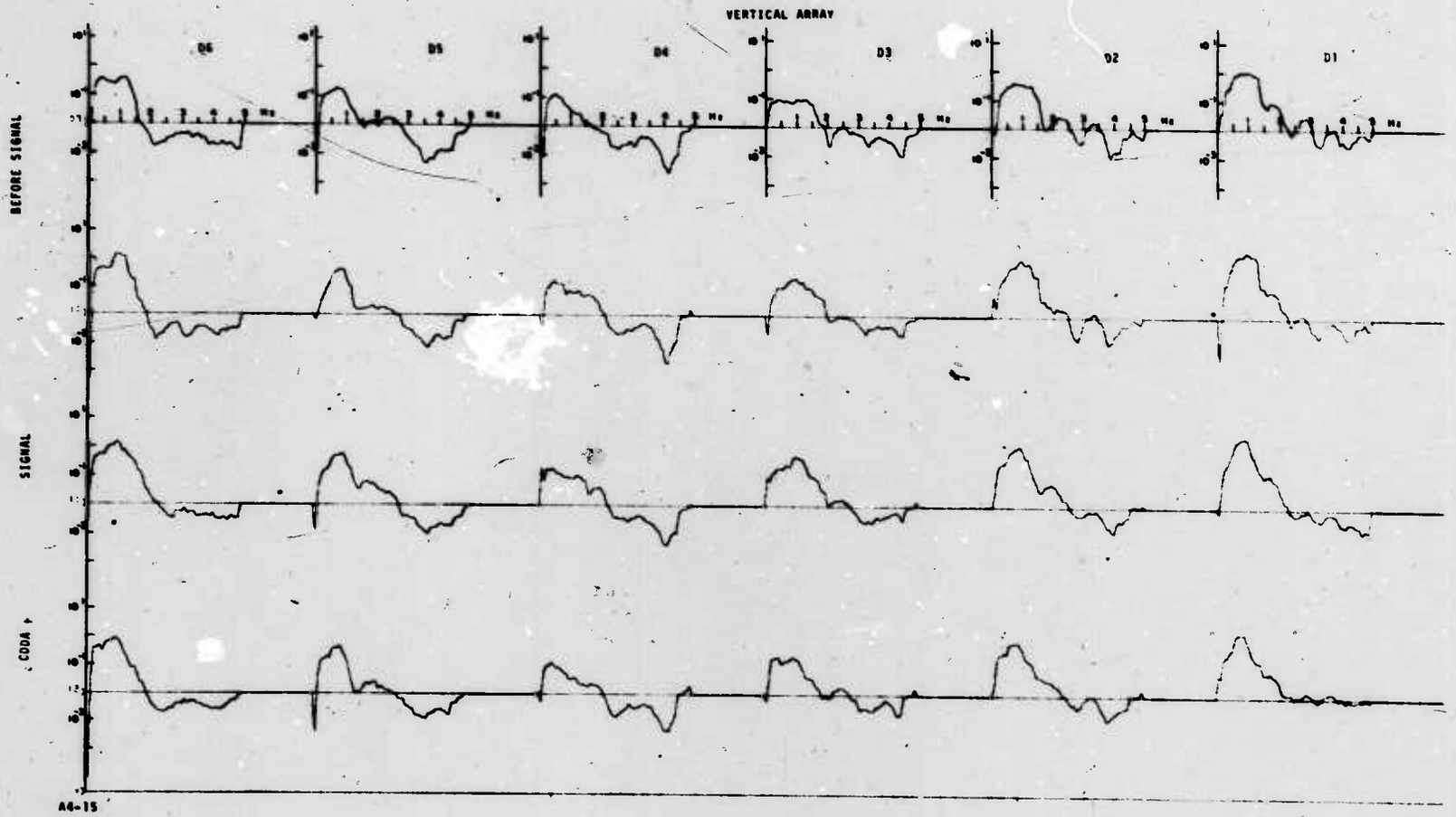
VERTICAL ARRAY
D6
D5
D4
D3
D2
D1
BEFORE SIGNAL
SIGNAL
CODA
A4-15

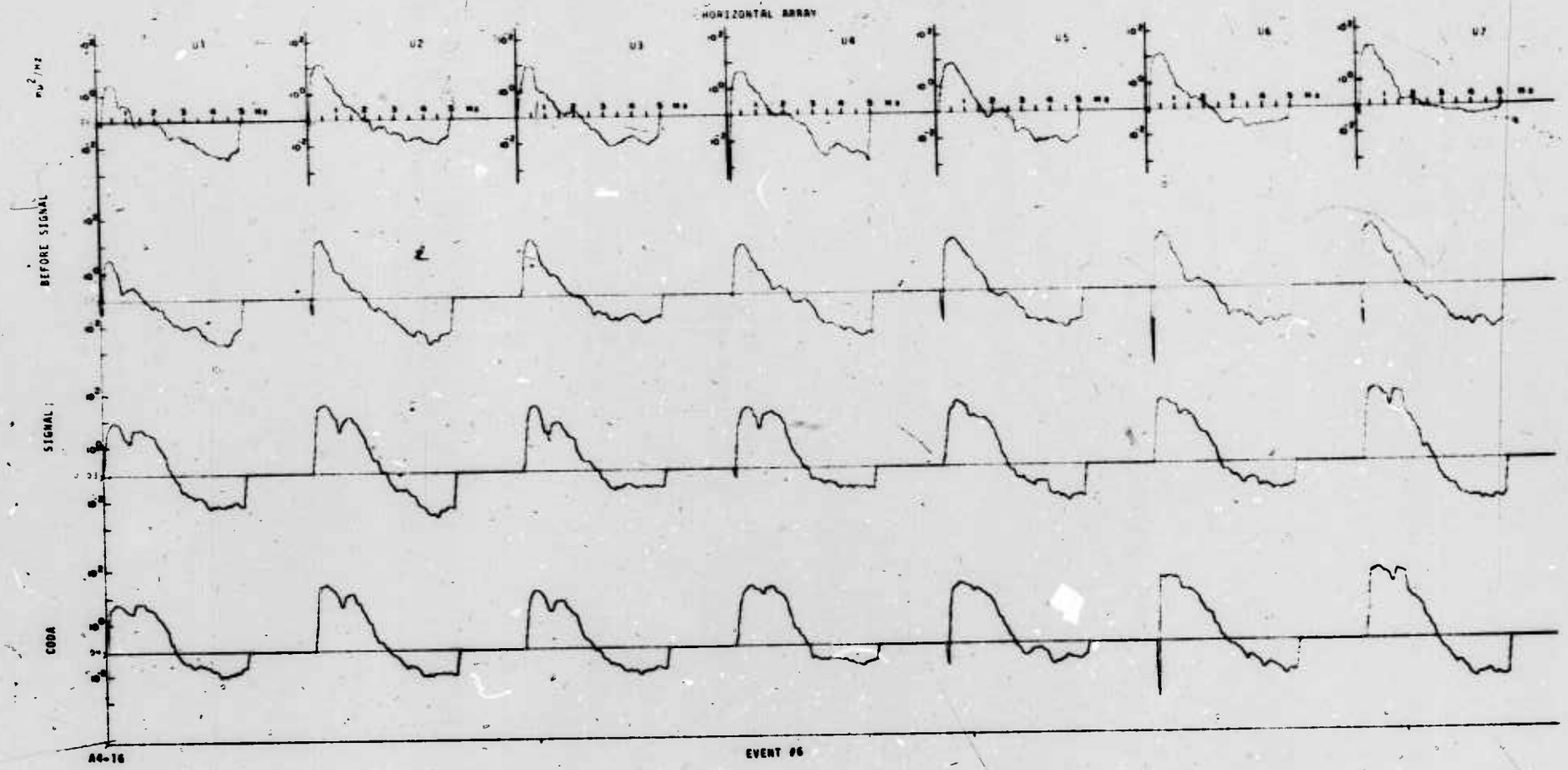
HORIZONTAL ARRAY
U1
U2
U3
U4
U5
U6
U7
BEFORE SIGNAL
SIGNAL
CODA
A0-16
EVENT 06

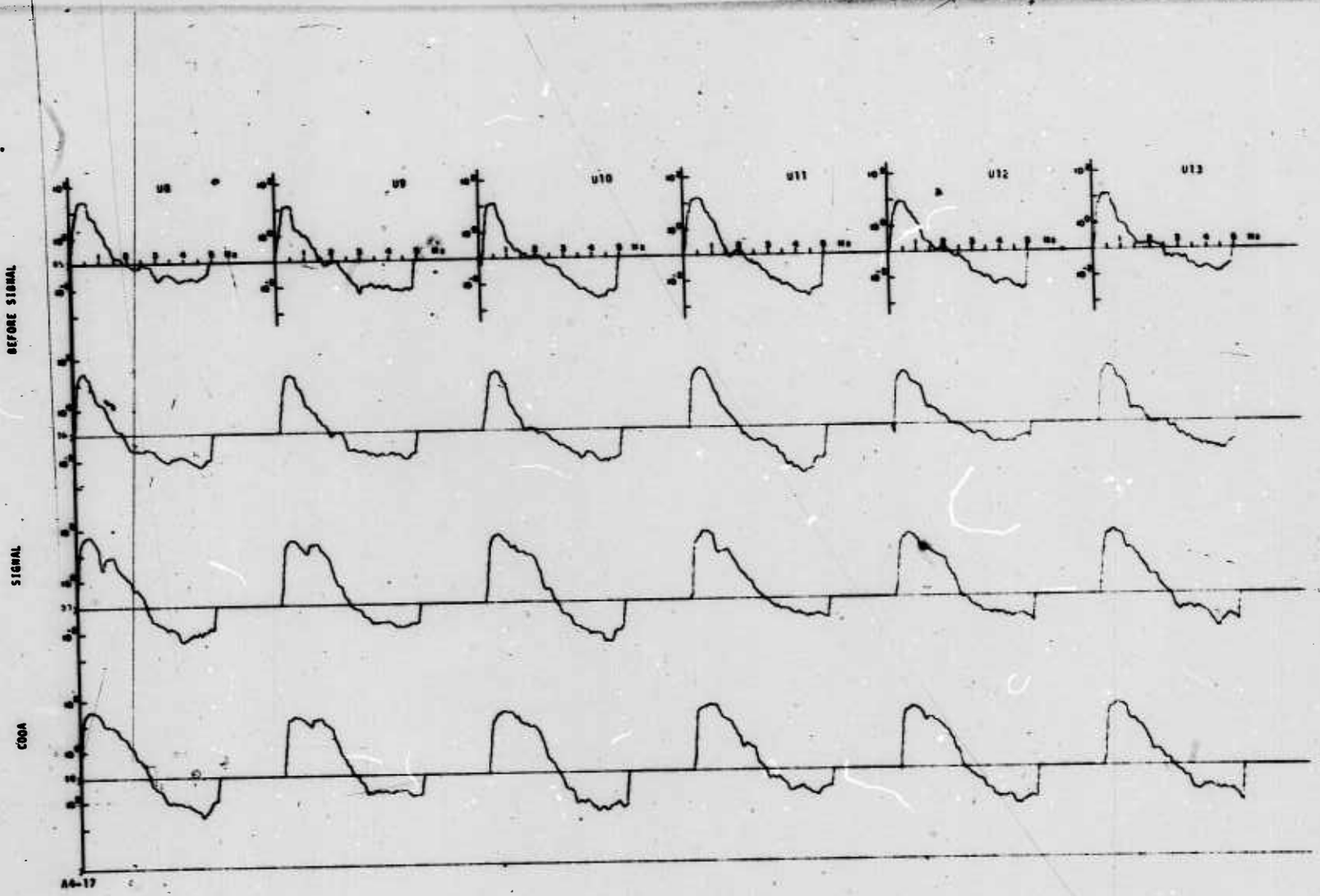
U8
U9
U10
U11
U12
U13
BEFORE SIGNAL
SIGNAL
CODA
A4-17

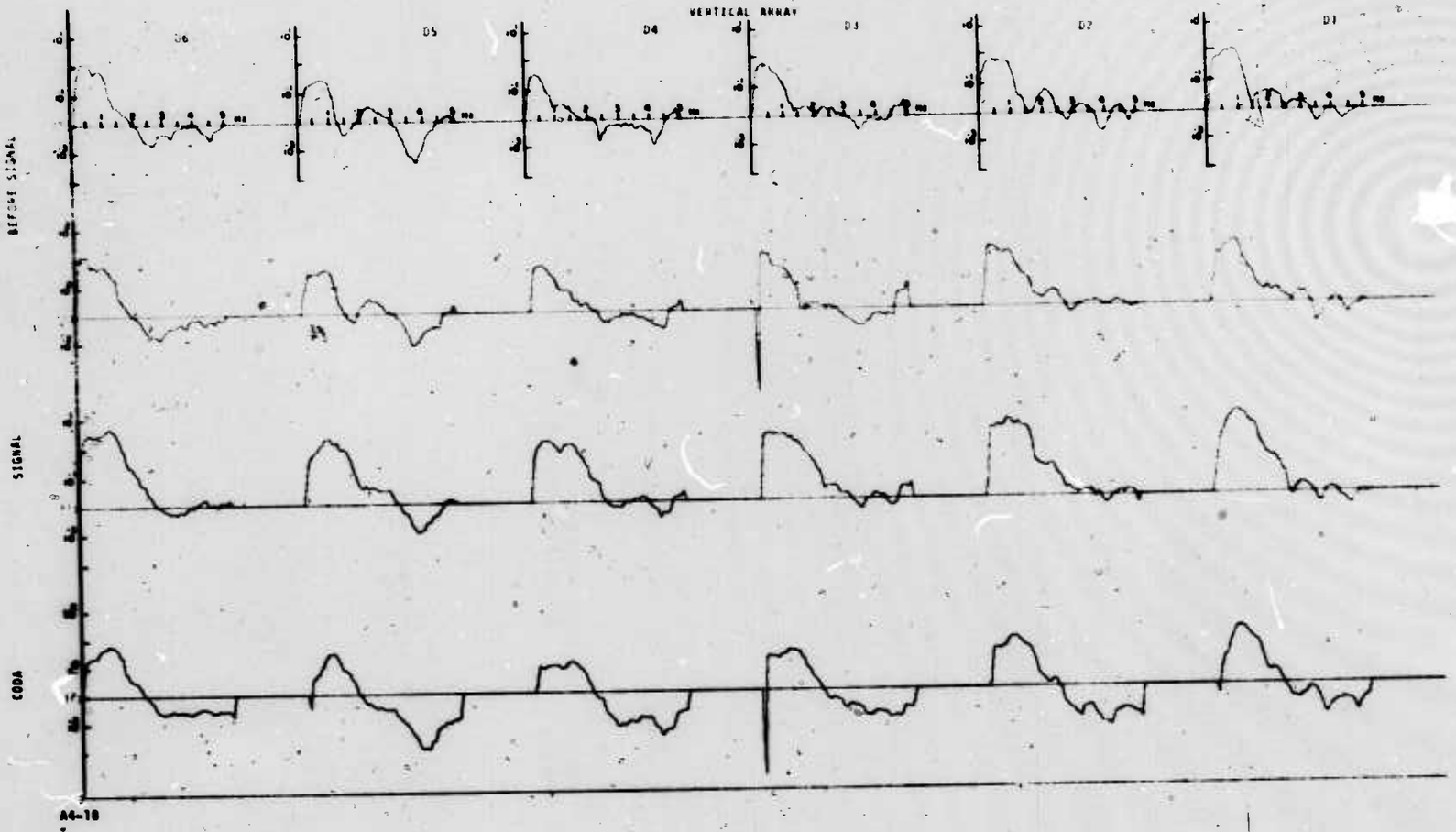
VERTICAL ARRAY
D6
D5
D4
D3
D2
D1
BEFORE SIGNAL
SIGNAL
CODA
A6-18

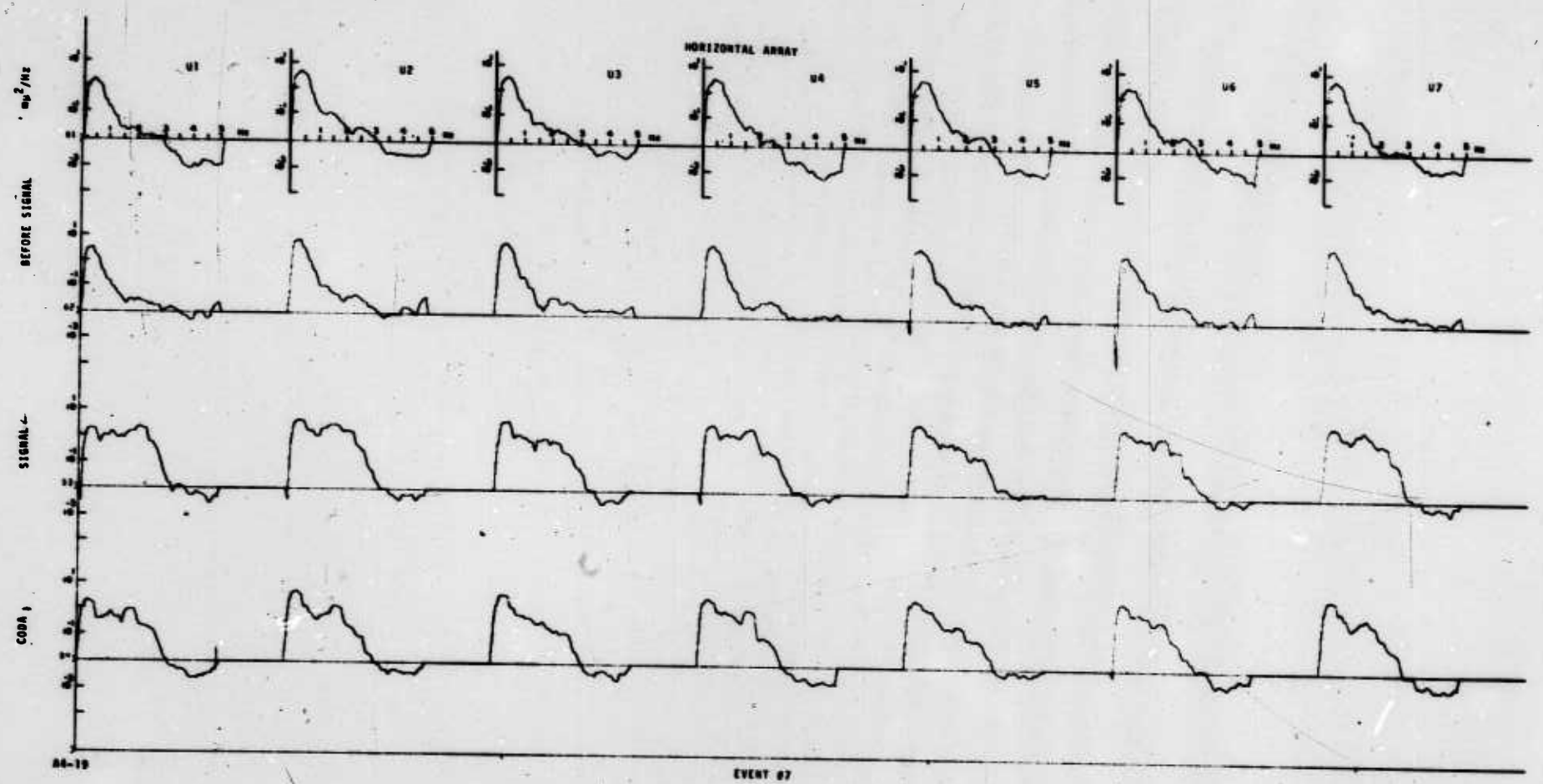
HORIZONTAL ARRAY
U1
U2
U3
U4
U5
U6
U7
BEFORE SIGNAL
SIGNAL
CODA
EVENT #7

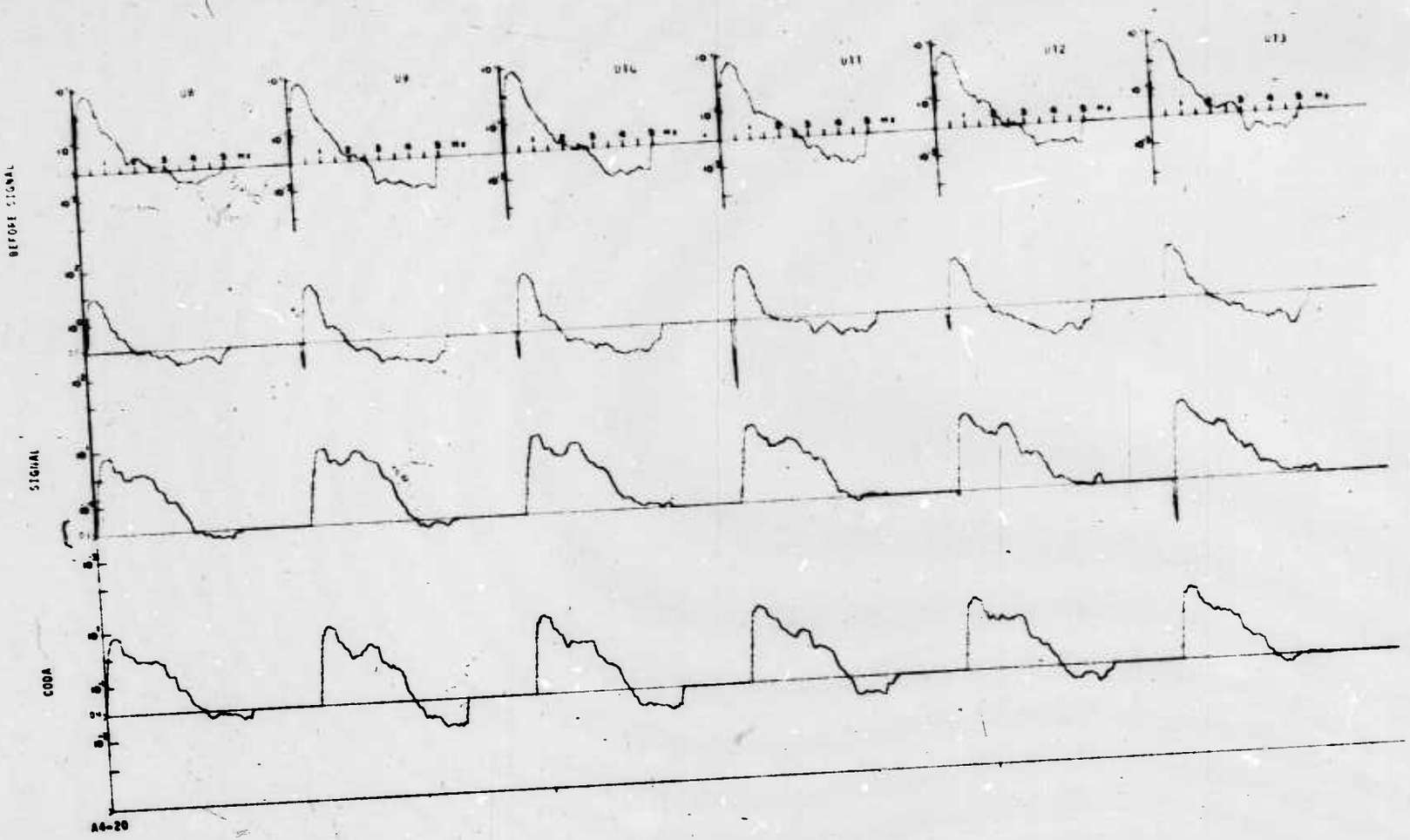
TRANSIT SIGNAL
SIGNAL
CODA

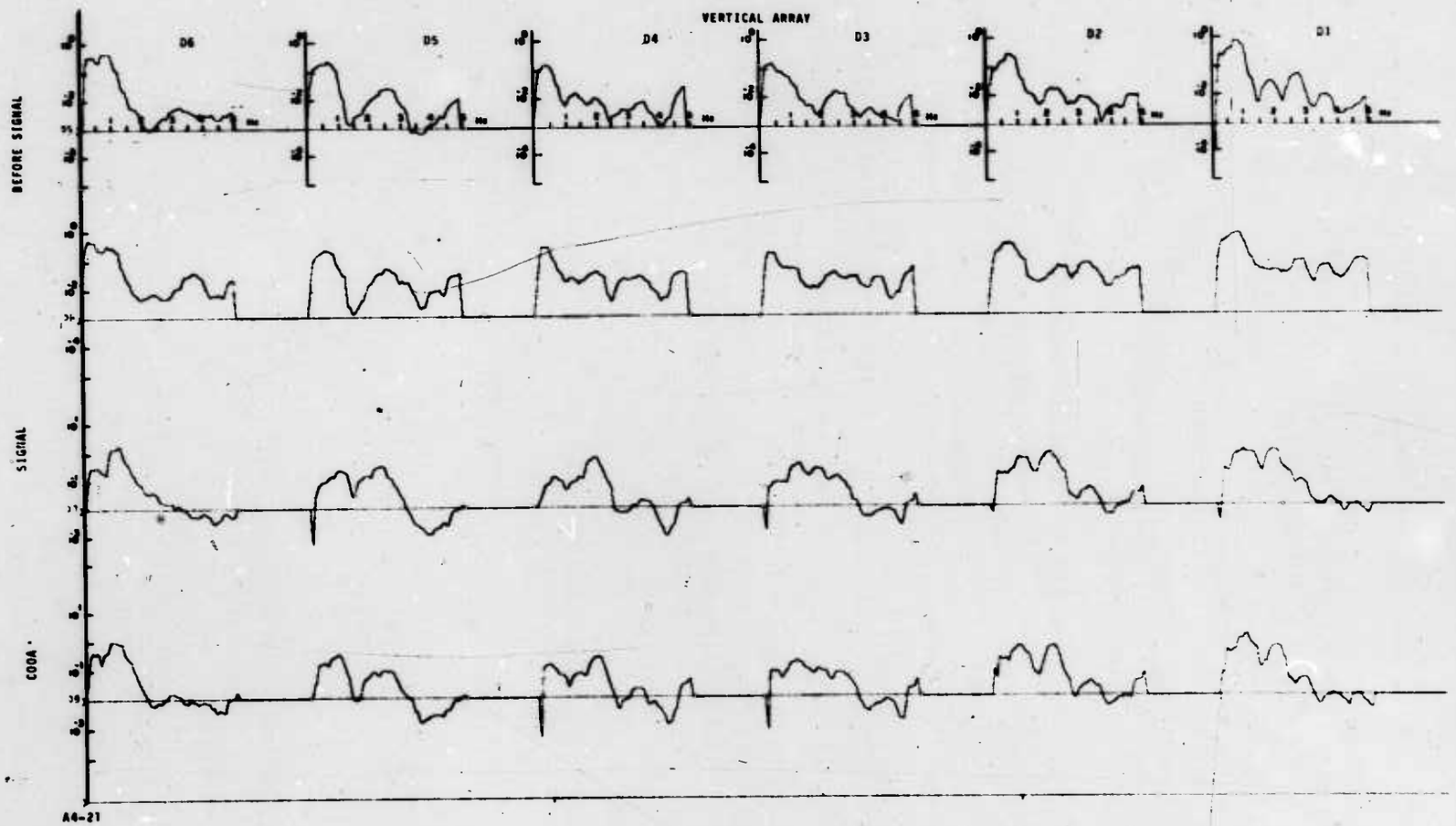
VERTICAL ARRAY
D6
D5
D4
D3
D2
D1
BEFORE SIGNAL
SIGNAL
CODA
A6-21

APPENDIX 5

1. Spectral analysis of signal estimates.

2. Spectral analysis of error in the signal estimates.

3. Two time windows before the signal show the power spectrum of the ambient P-wave under signal estimates; and of the non-P-wave noise under signal error.

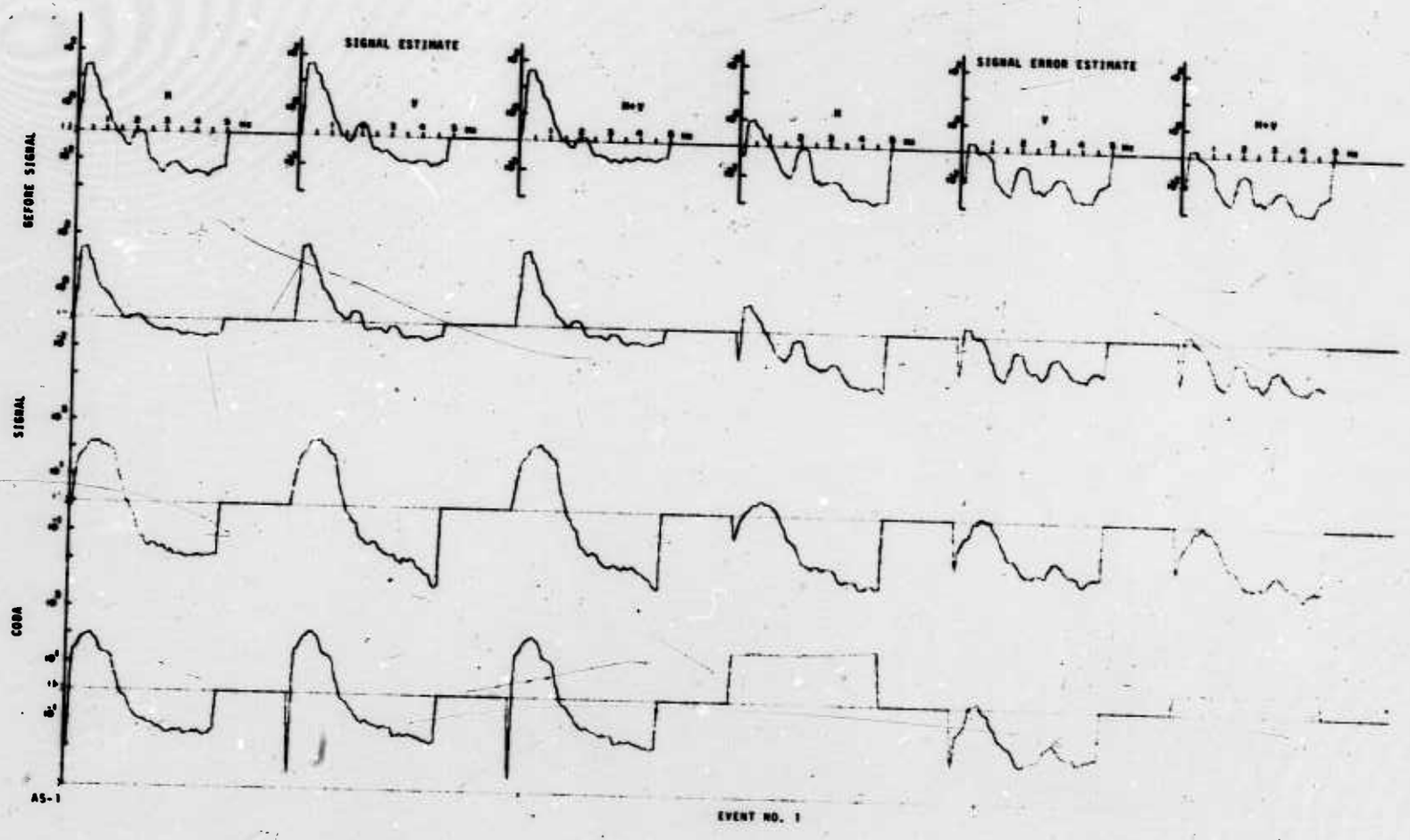
SIGNAL ESTIMATE
SIGNAL ERROR ESTIMATE
BEFORE SIGNAL
SIGNAL
CODA
AS-1
EVENT NO. 1

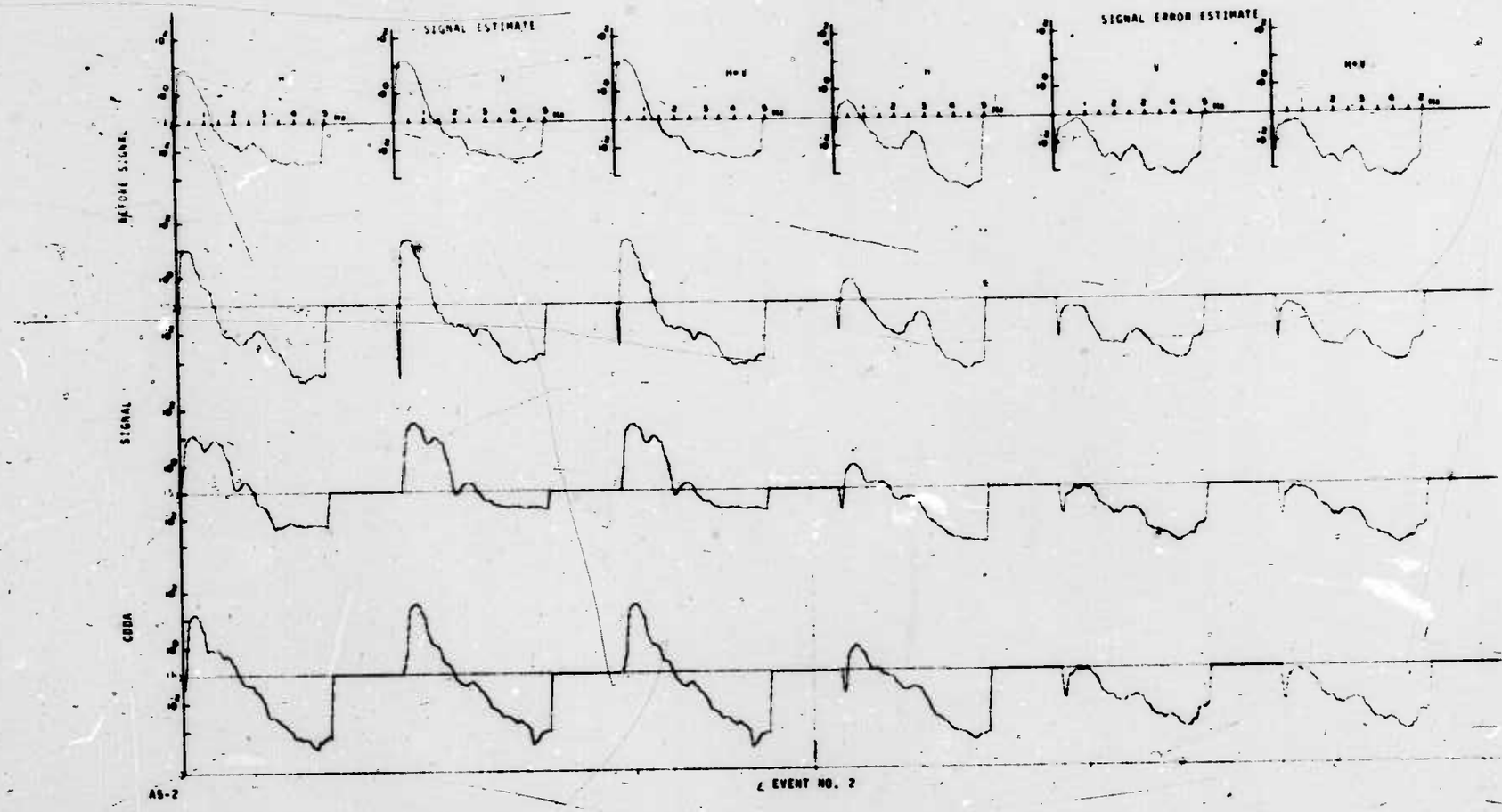
SIGNAL ESTIMATE
SIGNAL ERROR ESTIMATE
BEFORE SIGNAL
SIGNAL
CODA
AS-2
EVENT NO. 2

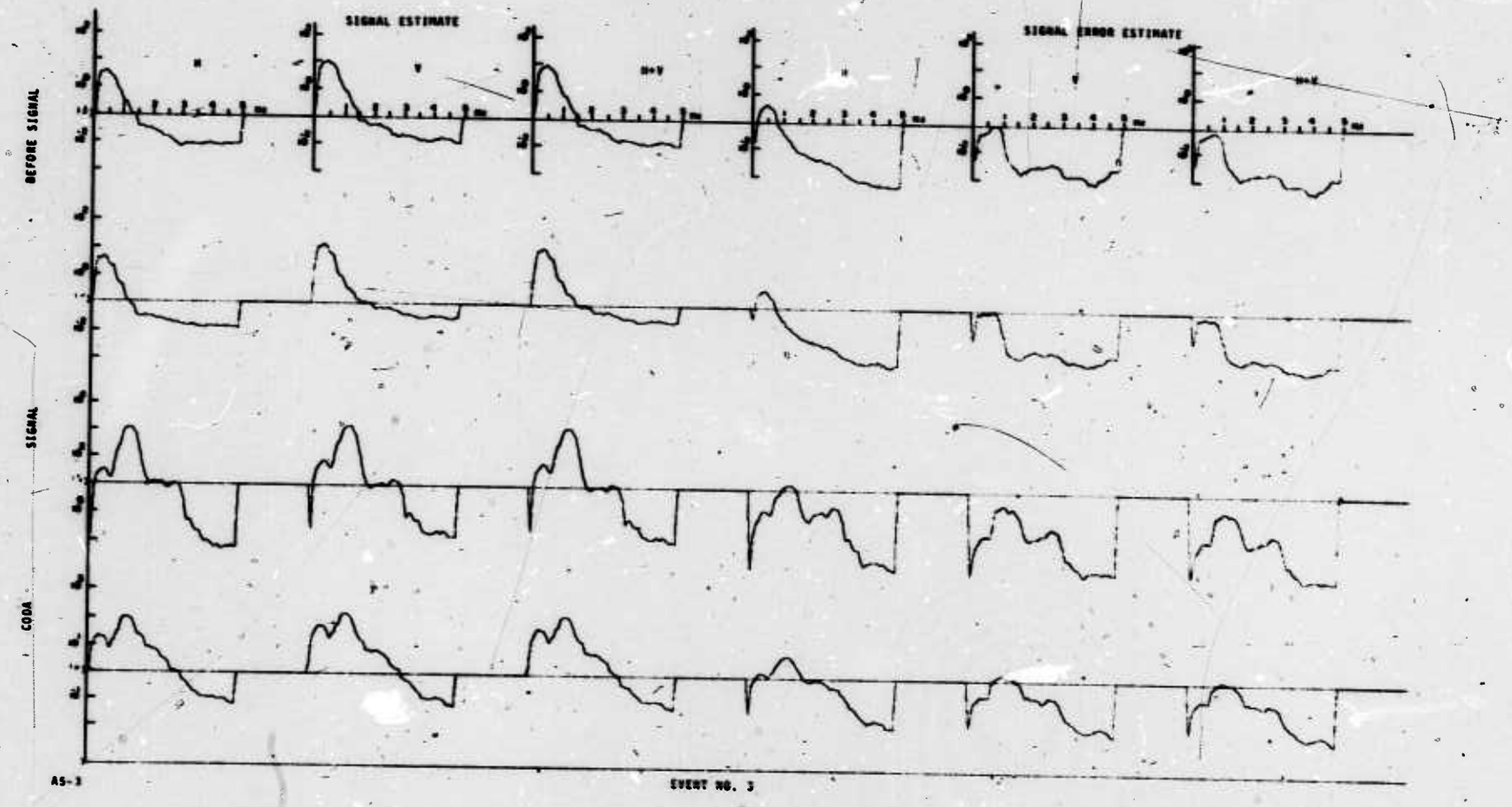
SIGNAL ESTIMATE
SIGNAL ERROR ESTIMATE
BEFORE SIGNAL
SIGNAL
CODA
AS-3
EVENT NO. 3

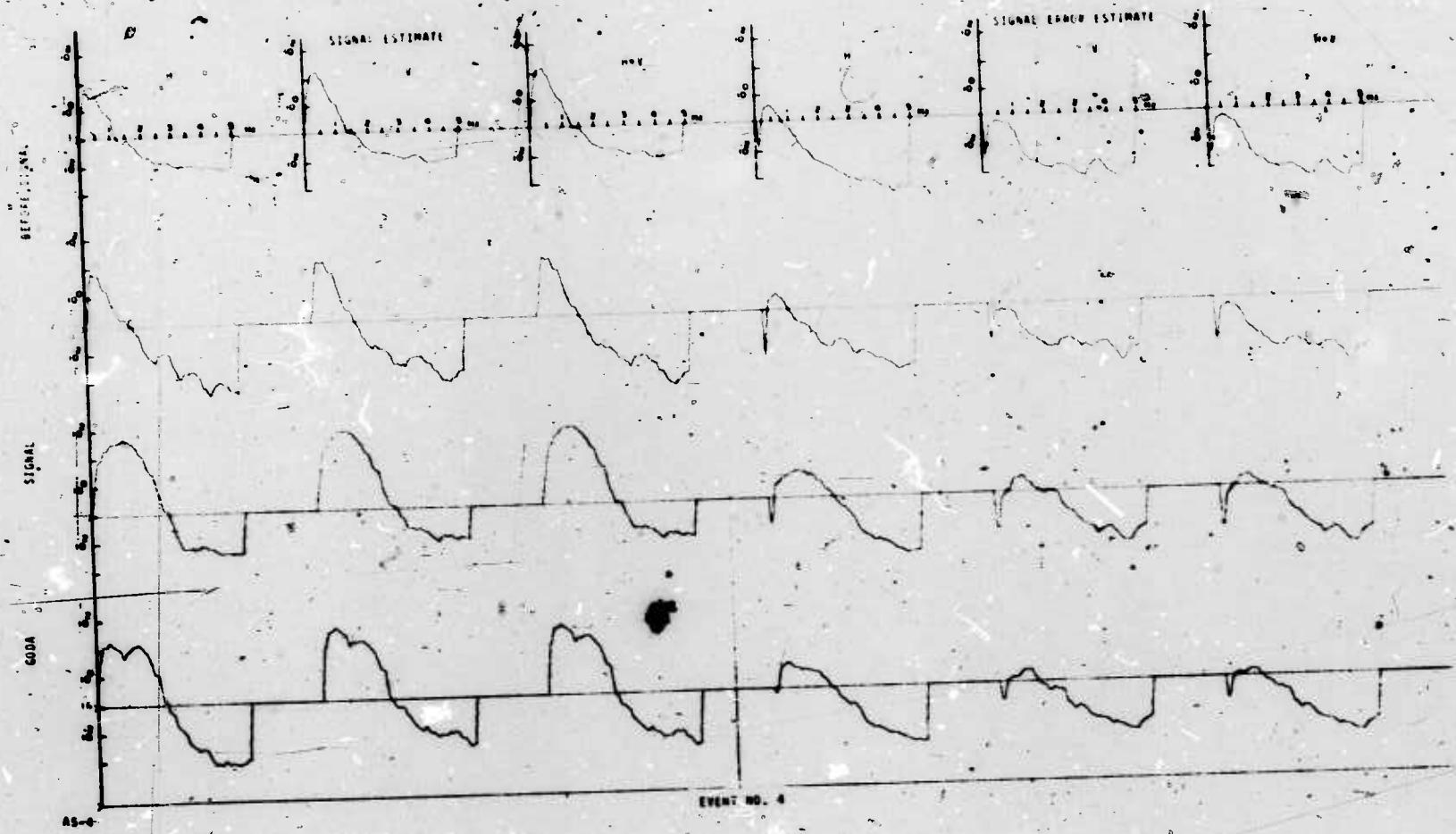
SIGNAL ESTIMATE
SIGNAL ERROR ESTIMATE
SIGNAL
CODA
EVENT NO. 4

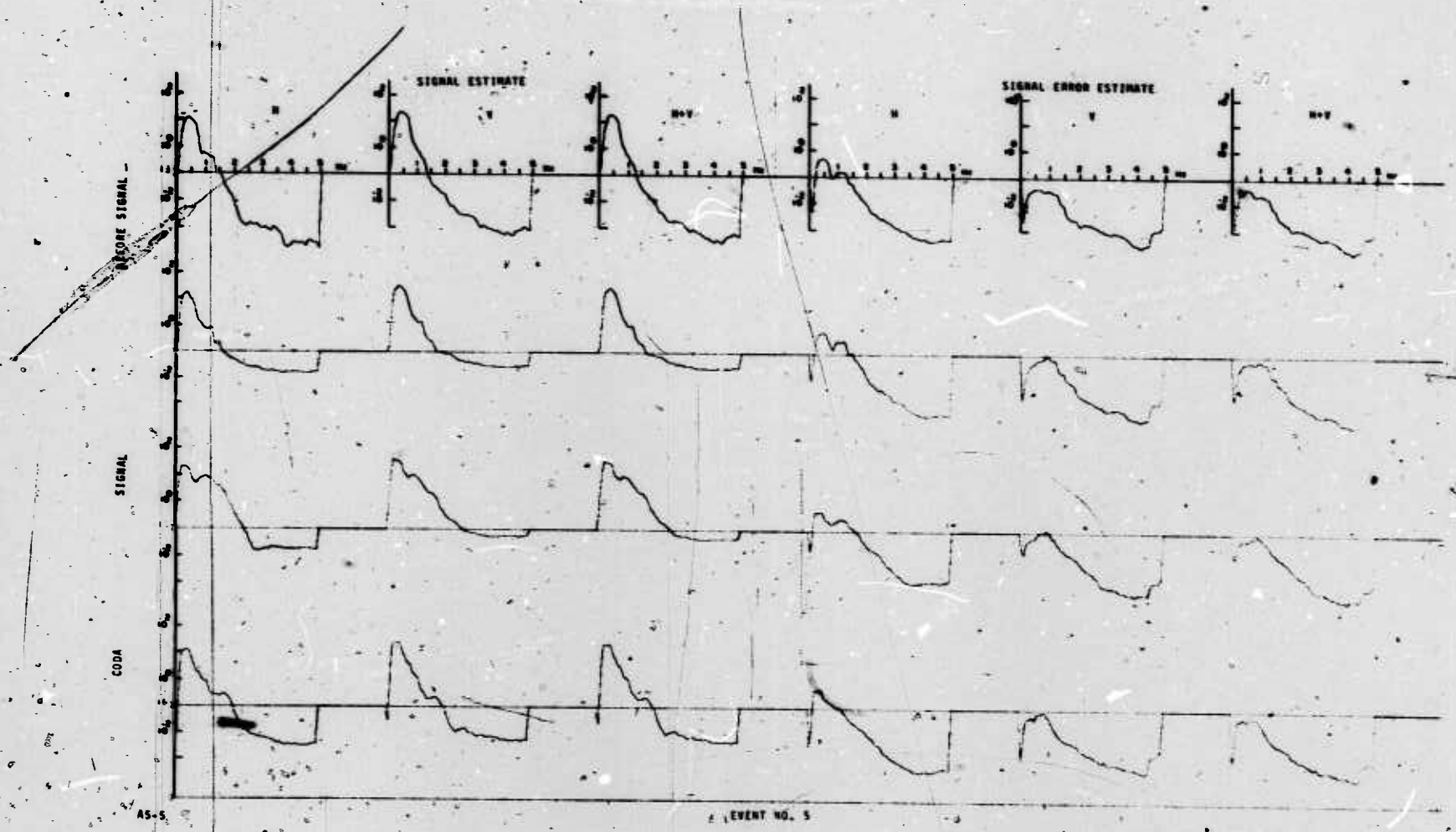
SIGNAL ESTIMATE
SIGNAL ERROR ESTIMATE
H
V
H+V
H
V
H+V
BEFORE SIGNAL
SIGNAL
CODA
AS-5
EVENT NO. 5

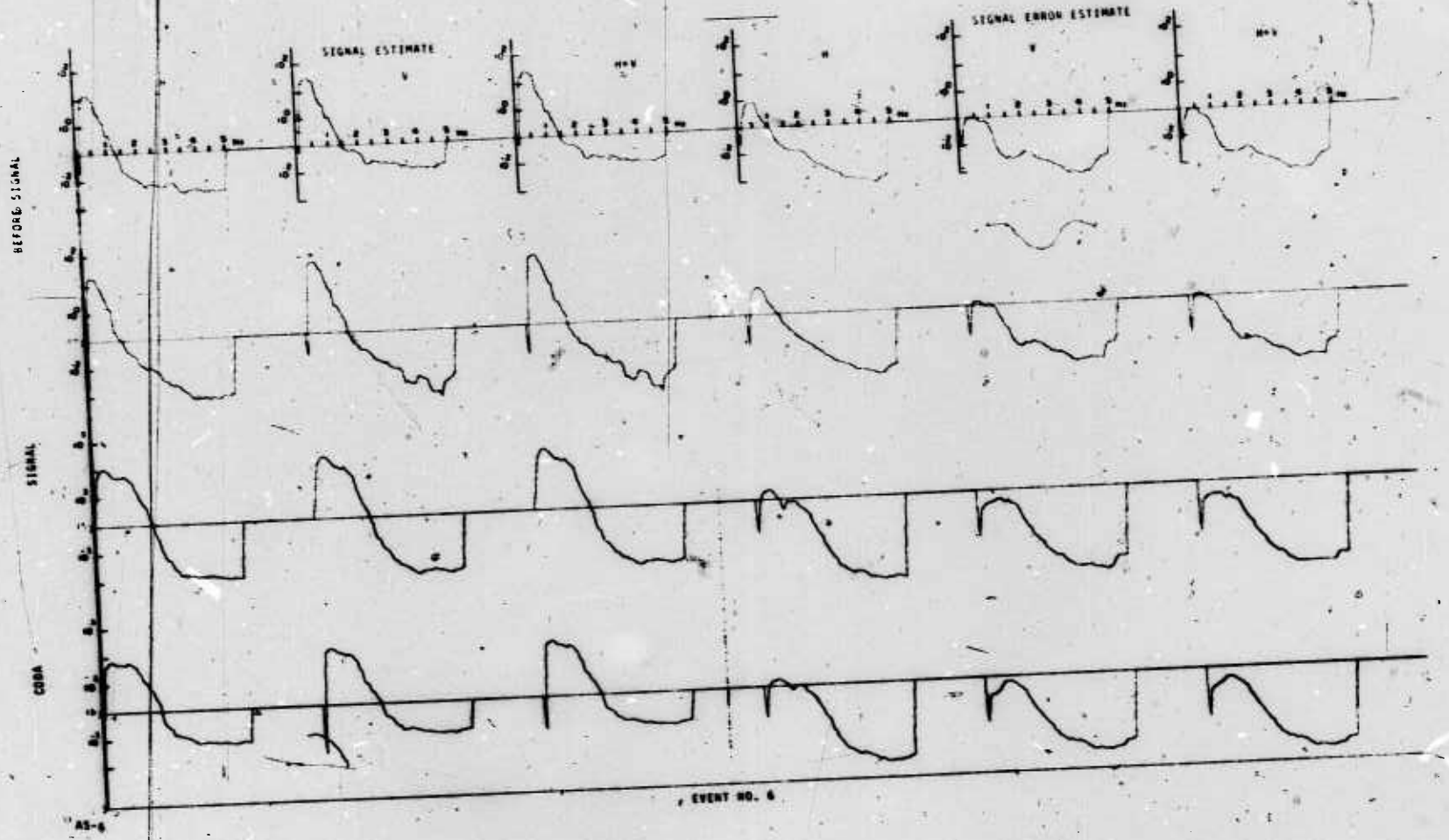
SIGNAL ESTIMATE
SIGNAL ERROR ESTIMATE
BEFORE SIGNAL
SIGNAL
CODA
EVENT NO. 6
AS-6

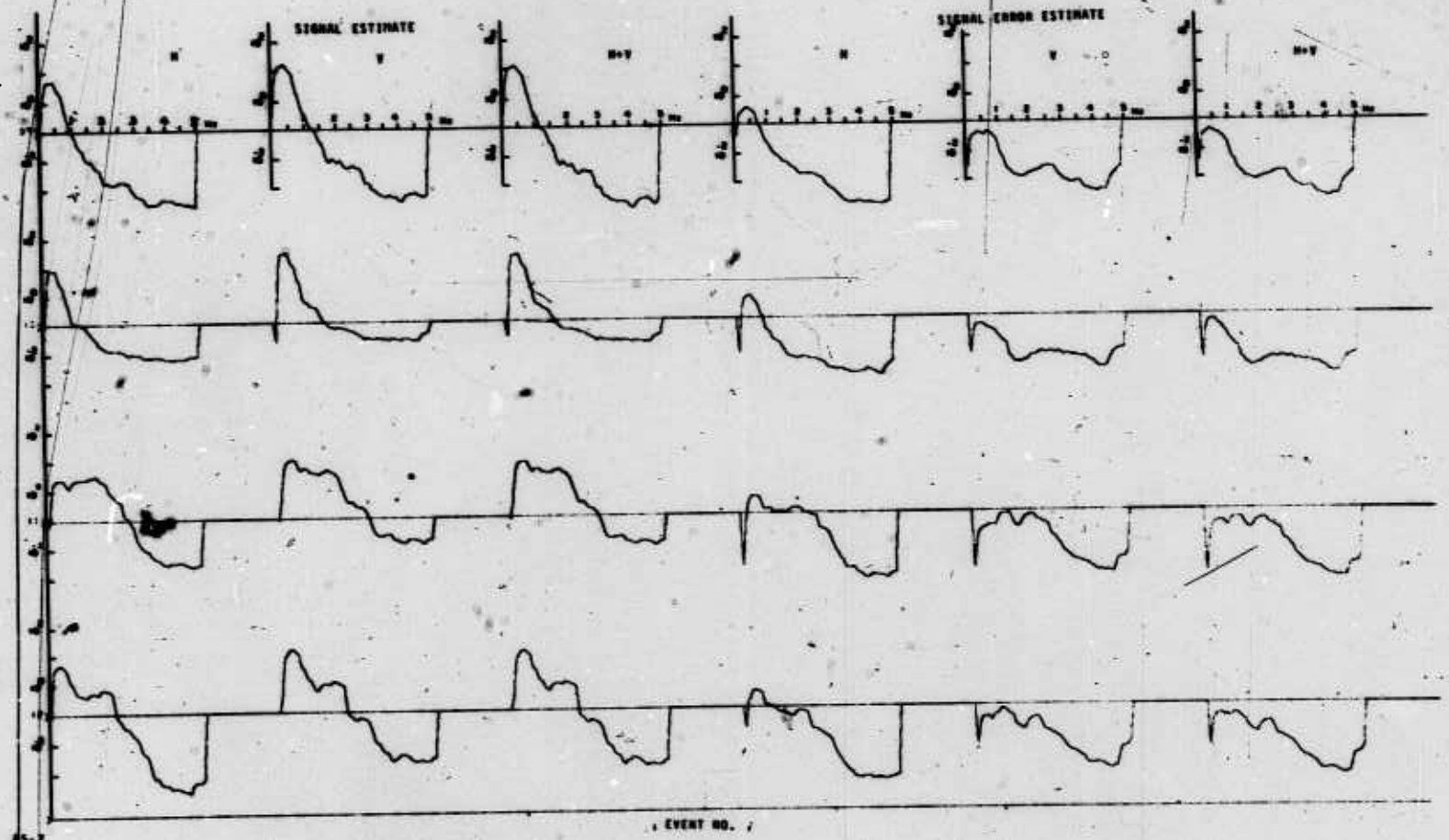
SIGNAL ESTIMATE
SIGNAL ERROR ESTIMATE
N
V
N+V
N
V
N+V
BEFORE SIGNAL
SIGNAL
COOA
EVENT NO.

APPENDIX 6

Statistics pertaining to the detection of teleseismic P-waves on horizontal arrays, vertical arrays and single sensors.

TABLE A-1

Ambient P-wave Noise on the Horizontal Array

Event Number
($m\mu^2$/Hz)

requency (Hz)	1	2	3	4	5	6	7	MEAN	S.D.
.33	27.7	8.46	3.85	6.83	11.9	13.0	5.40	11.0	8.01
.65	4.60	3.61	1.95	1.64	5.36	3.76	1.62	2.96	1.52
.98	.964	.736	.332	.518	.346	.384	.076	.478	.286
.30	.099	.061	.095	.056	.118	.107	.019	.079	.035
.63	.030	.020	.031	.062	.014	.013	.007	.025	.022
.95	.053	.011	.027	.023	.005	.008	.002	.019	.018

TABLE A-2

Ambient P-wave Noise on the Vertical Array

Event Number
($m\mu^2$/Hz)

quency Hz)	1	2	3	4	5	6	7	MEAN	S.D.
33	46.3	17.0	11.0	14.8	21.0	30.9	18.0	23.0	12.1
65	13.8	8.99	6.78	4.30	10.6	6.52	6.79	8.20	3.16
98	1.68	1.16	.998	1.05	.692	.919	.318	.970	.422
30	.270	.117	.299	.223	.140	.327	.104	.211	.089
63	.066	.050	.068	.088	.025	.061	.029	.055	.028
95	.169	.020	.043	.032	.014	.054	.008	.048	.056

TABLE A-3

Ambient Noise Using a Single Sensor

Event Number
($m\mu^2$/Hz)

Frequency (Hz)	1	2	3	4	5	6	7	MEAN	S.D.
.33	50.4	18.8	12.8	16.3	22.7	34.0	20.3	25.0	13.0
.65	15.0	10.0	8.6	4.9	11.3	7.0	7.8	9.23	3.27
.98	2.13	1.79	1.33	1.34	1.82	1.43	.77	1.52	.400
1.30	.380	.203	.397	.375	1.32	.404	.139	.290	.120
1.63	.105	.134	.124	.141	.207	.169	.055	.139	.045
1.95	.336	.088	.084	.065	.103	.149	.033	.122	.100

TABLE B-1

Teleseismic P-wave on the Horizontal Array

Frequency	Event Number ($m\mu^2$/Hz)						
(Hz)	1	2	3	4	5	6	7
.33	55.3	11.2	28.2	10.9	19.8	111.	2.26
.65	151.	6.84	16.0	36.4	5.47	56.5	1.42
.98	147.	4.98	188.	43.4	8.05	51.5	2.33
1.30	88.3	6.86	1160.	36.3	5.74	34.4	2.53
1.63	13.4	1.69	595.	13.8	3.32	6.98	3.17
1.95	.652	.065	17.3	3.20	.617	1.29	1.65

TABLE B-2

Teleseismic P-wave on the Vertical Array

Event Number

(m^2/Hz)

Frequency (Hz)	1	2	3	4	5	6	7
.33	76.4	26.8	61.3	20.8	36.5	171.	9.64
.65	231.	19.3	43.7	63.3	10.9	80.1	5.88
.98	240.	5.04	385.	69.1	9.50	56.9	4.62
1.30	87.0	6.80	1490.	36.7	3.94	31.0	3.19
1.63	7.95	1.24	645.	11.0	2.30	4.00	4.61
1.95	.457	.066	15.8	2.57	.517	.665	2.70

TABLE B-3

Teleseismic P-wave Using a Single Sensor

Frequency	Event Number ($m\mu^2$/Hz)						
(Hz)	1	2	3	4	5	6	7
.33	81.7	29.6	68.5	22.7	38.9	182.	11.5
.65	240.	20.6	49.9	67.2	11.9	85.0	6.80
.98	259.	6.46	427.	75.0	10.4	59.7	5.66
1.30	105.	8.41	1584.	40.9	5.62	36.8	4.23
1.63	18.5	2.41	719.	13.5	3.23	7.63	5.44
1.95	1.53	1.19	27.2	4.33	.998	2.09	4.28

TABLE C-1

(Spectrum After Signal)/(Spectrum Before Signal)

S/N Ratio - Horizontal Array

Event Number

Frequency (Hz)	1	2	3	4	5	6	7
.33	2.00	1.32	7.32	1.60	1.66	8.53	0.42
.65	32.8	1.89	8.21	22.2	1.02	15.0	0.88
.98	154.	6.77	566.	83.8	23.3	134.	30.7
1.30	892.	113.	12200.	648.	48.6	321.	133.
1.63	447.	84.5	19200.	223.	237.1	536.	452.
1.95	123.	5.91	[illegible]	139.	123.4	161.	825.

TABLE C-2

(Spectrum After Signal)/(Spectrum Before Signal)

S/N Ratio - Vertical Array

Frequency	Event Number						
(Hz)	1	2	3	4	5	6	7
.33	1.65	1.58	5.57	1.41	1.74	5.53	0.57
.65	16.7	2.15	6.45	14.7	1.03	12.3	0.87
.98	142.9	4.34	385.	65.8	13.7	61.9	14.5
1.30	322.2	58.1	4980.	165.	28.1	94.8	30.7
1.63	120.5	24.8	9480.	125.	92.0	65.6	159.
1.95	2.70	3.3	367.	80.3	36.9	12.3	337.

TABLE C-3

S/N Ratio Single Sensor Using Noise Before Signal

Frequency	Event Number						
(Hz)	1	2	3	4	5	6	7
.33	1.62	1.57	5.35	1.39	1.71	5.35	0.55
.65	16.0	2.06	5.80	13.7	1.05	12.1	0.87
.98	121.6	3.61	321.	56.0	5.71	41.7	7.35
1.30	276.3	41.4	3990.	109.	4.26	91.1	30.4
1.63	176.2	18.0	5800.	95.7	15.6	45.1	98.9
1.95	4.55	13.5	323.	66.6	9.69	14.0	129.

TABLE D-1

(Ambient P-wave/Mean Ambient P-wave)-Horizontal Array

Event Number

Frequency (Hz)	1	2	3	4	5	6	7	S.D.
.33	2.52	0.77	0.35	0.62	1.08	1.18	0.49	0.72
.65	1.55	1.22	0.66	0.55	1.81	1.27	0.55	0.51
.98	2.00	1.54	0.69	1.08	.723	.803	.158	0.60
1.30	1.25	0.77	1.20	0.70	1.49	1.35	0.24	0.44
1.63	1.20	0.80	1.24	2.48	0.56	0.52	0.28	0.88
1.95	2.78	0.58	1.42	1.21	0.28	0.42	0.11	0.95

TABLE D-2

(Ambient P-wave/Mean Ambient P-wave)-Vertical Array

Freuqency	Event Number							
(Hz)	1	2	3	4	5	6	7	S.D.
.33	2.01	0.74	0.48	0.64	0.91	1.34	0.78	0.53
.65	1.68	1.10	0.83	0.52	1.29	0.80	0.83	0.39
.98	1.73	1.20	1.03	1.08	0.71	0.95	0.33	0.43
1.30	1.28	0.56	1.42	1.06	0.66	1.55	0.49	0.42
1.63	1.20	0.91	1.24	0.63	0.45	1.11	0.53	0.51
1.95	3.52	0.41	0.90	0.67	0.29	1.12	0.17	1.17

TABLE D-3

(Noise Before Signal/Mean Noise)-Single Sensor

Frequency	Event Number							
(Hz)	1	2	3	4	5	6	7	S.D.
.33	2.02	0.75	0.51	0.65	0.91	1.36	0.81	0.52
.65	1.63	1.08	0.92	0.53	1.22	0.76	0.84	0.35
.98	1.40	1.18	0.88	0.88	1.20	0.94	0.51	0.26
1.30	1.31	0.70	1.37	1.29	0.46	1.39	0.48	0.41
1.63	0.78	0.96	0.80	1.01	1.49	1.22	0.40	0.32
1.95	2.75	0.72	0.69	0.53	0.84	1.22	0.27	0.82

TABLE E-1

(S/N of Array)/(S/N of Single Sensor)

Power Gain of H Array vs Single Sensor

Freuqency	Event Number							
(Hz)	1	2	3	4	5	6	7	MEAN
.33	1.23	0.84	1.37	1.15	0.97	1.59	.74	1.13
.65	2.05	0.92	1.42	1.62	0.97	1.24	1.01	1.32
.98	1.27	1.88	1.76	1.50	4.08	3.21	4.18	2.55
1.30	3.23	2.72	3.06	5.94	11.4	3.52	4.38	4.89
1.63	2.54	4.69	3.31	2.33	15.2	11.9	4.57	6.36
1.95	2.70	0.44	1.98	2.09	12.7	11.5	6.40	5.40

TABLE E-2

(S/N of Array)/(S/N of Single Sensor)

Power Gain of V Array vs Single Sensor

Frequency	Event Number							
(Hz)	1	2	3	4	5	6	7	MEAN
.33	1.02	1.01	1.04	1.01	1.05	1.03	1.04	1.03
.65	1.04	1.04	1.11	1.07	0.98	1.02	1.00	1.04
.98	1.17	1.20	1.20	1.18	2.40	1.48	1.97	1.51
1.30	1.17	1.40	1.25	1.51	1.80	1.04	1.01	1.31
1.63	0.68	1.38	1.63	1.31	5.89	1.45	1.61	2.00
1.95	0.59	0.24	1.14	1.21	3.81	0.88	2.61	1.49

TABLE F-1

F - Statistics (Vertical Array)

Ratio Ambient P-wave to Estimation Error

Frequency	Event Number						
(Hz)	1	2	3	4	5	6	7
.33	333.	401.	218.	272.	603.	289.	425.
.65	140.	138.	70.4	87.9	268.	92.5	152.
.98	35.2	24.3	20.2	44.0	23.5	18.8	14.2
1.30	93.4	9.37	70.0	44.5	7.76	51.3	40.5
1.63	65:2	14.4	41.8	41.4	7.91	20.3	22.3
1.95	10.4	7.1	15.6	25.0	6.78	17.8	7.41

TABLE F-2

F - Statistics (Vertical Array)

Ratio Teleseismic P-wave to Estimation Error

Frequency	Event Number						
(Hz)	1	2	3	4	5	6	7
.33	434.	510.	327.	256.	665.	496.	369.
.65	323.	272.	160.	208.	116.	333.	186.
.98	205.	65.8	146.	183.	87.1	151	64.3
1.30	132.	224.	545.	289.	101.	119.	76.4
1.63	59.7	80.0	332.	141.	145.	59.2	106.
1.95	13.3	7.97	53.8	29.3	49.4	34.2	39.2

Unclassified

Security Classification

DOCUMENT CONTROL DATA - R&D

(Security classification of title, body of abstract and indexing annotation must be entered when the overall report is classified)

1 ORIGINATING ACTIVITY (Corporate author)

TELEDYNE GEOTECH
ALEXANDRIA, VIRGINIA

2a REPORT SECURITY CLASSIFICATION

Unclassified

2b GROUP

3 REPORT TITLE

ESTIMATION OF P-WAVES USING VERTICAL AND SMALL APERTURE HORIZONTAL ARRAYS

4 DESCRIPTIVE NOTES (Type of report and inclusive dates)

Scientific

5 AUTHOR(S) (Last name, first name, initial)

Sax, R.L.

6. REPORT DATE	7a TOTAL NO OF PAGES	7b NO OF REFS
	137	13

8a CONTRACT OR GRANT NO	9a ORIGINATOR'S REPORT NUMBER(S)
F33657-70-C-0941	257
b PROJECT NO VELA T/0706	
c ARPA Order No.: 624	9b OTHER REPORT NO(S) (Any other numbers that may be assigned this report)
dARPA Program Code No.: 9F10	

10 AVAILABILITY/LIMITATION NOTICES

nis document is subject to special export controls and each transittal to foreign governments or foreign nationals may be made only with prior approval of Chief, AFTAC.

11 SUPPLEMENTARY NOTES	12 SPONSORING MILITARY ACTIVITY
	ADVANCED RESEARCH PROJECTS AGENCY NUCLEAR MONITORING RESEARCH OFFICE WASHINGTON, D. C.

13 ABSTRACT

In estimating signals as P-waves, with at regard to discrimination of the P-waves in ambient noise from those which are added by a teleseismic signal, the comparative performance of a fifteen element small aperture horizontal array and a seven element vertical array favors the vertical array. As much as 3 db of the gain of the vertical array results in a signal estimation error which is 3 db down on the vertical array estimate of signal and 15 db down on the horizontal array. Some preliminary indications, using the estimate of signal on the horizontal array to compute residuals on the horizontal array and using estimates of signal on the vertical array to compute residuals on the vertical array, are 3 db or the vertical array and 10 db on the horizontal array. Most of this difference in the two arrays is in the low frequency noise (less than 0.6 hz) as tight zero filtering tends to remove the difference in estimation error between the two arrays.

From the point of view of using the arrays to remove ambient noise, the results of a single P-wave signal estimation favors the horizontal array over the vertical array, 4.1 db to 1.8 db. This results in that the ambient noise at this site can be characterized as a single dominant P-wave plus uncorrelated noise. As a horizontal array element is displaced from a reference element, the relative amount of uncorrelated noise increases much more rapidly than on a vertical array. This suggests a Markovian P-wave noise model for quiet sites such as the one considered here. That small horizontal arrays can be expected to contain substantially more uncorrelated noise despite the much larger timeout aperture of the vertical array.

The processor used here is iterative and allows for amplitude anomalies in the teleseismic P-wave model and allows for variable uncorrelated noise under each channel. Both the amount of uncorrelated noise and the amplitude anomalies differ significantly for events from different regions. It is conceivable that a processor can be designed which distinguishes the ambient P-wave model from the teleseismic P-wave model with amplitude anomalies. Such a processor would involve a double P-wave estimation with the two P-wave models distinguishable by their amplitude anomalies. This contrasts with the single P-wave estimation considered in this report.

14 KEY WORDS

Array Processing
Horizontal Arrays
Vertical Arrays
Short Period P Waves
Amplitude Anomalies

Unclassified

Security Classification